UNIVERSITY
OF MICHIGAN
MAY 3 - 1956
PHYSICS
LIBRARY

Journal of Research

of the

National Bureau of Standards

FEBRUARY 1956

VOLUME 56 NUMBER 2

U. S. DEPARTMENT OF COMMERCE
Sinclair Weeks, Secretary
NATIONAL BUREAU OF STANDARDS
A. V. Astin, Director

FEBRUARY • 1956
VOLUME • 56
NUMBER • 2

JOURNAL OF RESEARCH

of the

NATIONAL BUREAU OF STANDARDS

PERIODICALS OF THE NATIONAL BUREAU OF STANDARDS

(Published monthly)

The National Bureau of Standards is engaged in fundamental and applied research in physics, chemistry, mathematics, and engineering. Projects are conducted in fifteen fields: electricity and electronics, optics and metrology, heat and power, atomic and radiation physics, chemistry, mechanics, organic and fibrous materials, metallurgy, mineral products, building technology, applied mathematics, data processing systems, cryogenic engineering, radio propagation, and radio standards. The Bureau has custody of the national standards of measurement and conducts research leading to the improvement of scientific and engineering standards and of techniques and methods of measurement. Testing methods and instruments are developed; physical constants and properties of materials are determined; and technical processes are investigated.

JOURNAL OF RESEARCH

The Journal presents research papers by authorities in the specialized fields of physics, mathematics, chemistry, and engineering. Complete details of the work are presented, including laboratory data, experimental procedures, and theoretical and mathematical analyses. Annual subscription: domestic, $4.00; $1.25 additional for foreign mailing.

TECHNICAL NEWS BULLETIN

Summaries of current research at the National Bureau of Standards are published each month in the Technical News Bulletin. The articles are brief, with emphasis on the results of research, chosen on the basis of their scientific or technologic importance. Lists of all Bureau publications during the preceding month are given, including Research Papers, Handbooks, Applied Mathematics Series, Building Materials and Structures Reports, Miscellaneous Publications, and Circulars. Each issue contains 12 or more two-column pages; illustrated. Annual subscription: domestic, $1.00; 35 cents additional for foreign mailing.

BASIC RADIO PROPAGATION PREDICTIONS

The Predictions provide the information necessary for calculating the best frequencies for communication between any two points in the world at any time during the given month. The data are important to all users of long-range radio communications and navigation, including broadcasting, airline, steamship, and wireless services, as well as to investigators of radio propagation and ionosphere. Each issue, covering a period of one month, is released three months in advance and contains 16 large pages, including pertinent charts, drawings, and tables. Annual subscription: domestic, $1.00; 25 cents additional for foreign mailing.

Order all publications from the Superintendent of Documents
U. S. Government Printing Office, Washington 25, D. C.

The printing of this publication has been approved by the Director of the Bureau of the Budget, May 12, 1953.

Journal of Research of the National Bureau of Standards Vol. 56, No. 2, February 1956 Research Paper 2648

Residual Entropy of Linear Polymers

H. N. V. Temperley

The question whether it is possible to assign a finite entropy to a polymer, bearing in mind the fact that it may not be a well-defined substance in thermodynamic equilibrium, is considered. It is shown that the entropy of chain configurations is the only contribution that will be important at low temperatures. Existing knowledge of the thermodynamics of hydrocarbons enables one to arrive at a generalization of the well-known "flexible chain" model of a polymer molecule. The new model is in good accord with experimental facts on the specific heat of polymers, and enables a finite entropy to be defined and to be reasonably accurately calculated. These findings are then compared with certain experimental results throwing light on the length of the "effective segment" of polymer chains of various types, this quantity being defined in the text. The experimental facts come from studies of polymer solutions, solid polymers, solid and liquid paraffins, and related compounds, and are remarkably consistent with the theoretical expectations. A few apparent inconsistencies and a few instances of alternative possible interpretations for the same facts are noted.

1. Introduction

In attempting to predict heats of polymerization from thermochemical data on long-chain hydrocarbons and the monomer, it is not unusual to meet discrepancies between calculated and observed values of the order of 1 to 10 kcal/mole, Flory [5, ch. 6; p. 254].[1] After a careful survey of the evidence, Flory concluded that: "The pattern presented by heats of polymerization of various monomers appears to be very well explained by two dominant factors: elimination of resonance energy of conjugation, and steric interaction between substituents." In other words, the discrepancies can be explained purely on chemical considerations; the necessary readjustments of electronic configurations associated with the joining together of monomers can be much more important in some types of chain than in other types.

However, it is sometimes pointed out that errors might be caused by treating a polymer as a well-defined chemical substance in true thermodynamic equilibrium. This question may also be of interest in the study of other polymer reactions such as degradation, in which the main chain is broken up into fragments or greatly modified. (For reactions in which the main chain remains practically intact, errors in calculations of the configurational entropy will tend to balance out, since they affect both reactants and products.) The present study was undertaken in an effort to estimate numerical values for the residual entropy of a typical linear polymer, bearing in mind the four facts: first, that it is inevitably a mixture of chains of many different lengths; second, that because of "freedom at the joints" any one chain may assume a wide variety of configurations in space; third, that in a copolymer, the number of ways in which two sets of monomers can be lined up to form a chain can be enormously great; finally, that at least some of any polymer is in an amorphous or disordered state. It is known that crystallization of a polymer is never complete, and some polymers cannot crystallize at all. Moreover, polymers undergo a "glass-like" transition at temperatures at which thermal agitation is still considerable, so that some "frozen-in disorder" is to be expected. We are interpreting the glass-like transition as being essentially the same as that of an inorganic glass, certain degrees of freedom being put out of action as a result of a rapid rise in their time-constants with falling temperature. Some workers have claimed that there is a true phase transition, but a discussion of this point is hardly relevant in the present context. See Kauzmann [12], Powell and Eyring [25], Boyer and Spencer [2]. It might seem a hopeless task to identify the separate contributions to the residual entropy associated with each of the four factors listed above, but the task is very much simplified when it is realized that contributions of less than about R per mole of monomer are unlikely to be of practical interest. At ordinary temperatures such an entropy calls for a correction to the free energy of ½ to 1 kcal/mole. It can very quickly be shown that the contributions due to 2 of the 4 causes listed above are negligibly small, while the entropy associated with copolymerization can probably be estimated fairly accurately in any given case. We are thus left only with the problem of estimating the number of different configurations in which a real molecule of polymer type can exist in a solid or liquid. It is this study that forms the subject of the present paper, but the other three possible contributions to the residual entropy will be considered first.

2. Contributions From Causes Other Than Chain Configurations

2.1. Communal Entropy

We shall consider the effect of chain configurations in detail, but must first discuss a different effect, namely, that in a crystalline solid it is sufficient to think of each molecule as never straying very far from a given lattice point, but in a liquid, gas, or amorphous solid, it may be necessary to allow a typical molecule "effective access" to an appreciable function of the whole volume. For

[1] Figures in brackets indicate the literature references at the end of this paper.

ordinary liquids this leads to the tiresome "communal entropy" problem that is still unsolved. For polymers, however, it is readily shown that as a consequence of the great size of the molecules, any contribution to the entropy resulting from the bodily transport of a whole molecule around the assembly is quite negligible compared with the contributions due to configuration effects. Physically, the coordinates of the center of gravity of a chain represent just three out of the hundreds of coordinates that would have to be known in order to specify the positions of all the elements of a chain. More quantitatively, if we permitted the center of gravity of a chain to wander over the entire volume V of an assembly of N chains instead of restricting it to its own "share" V/N of that volume, the gain in entropy would be $k \ln N$ per chain or $Nk \ln N$ for the assembly. However, this count includes changes of configuration that amount to exchanging the positions of two or more similar chains, which does not lead to a physically distinguishable configuration. The number of permutations of N chains among themselves is $N!$, so the proper contribution to the entropy, if the chains are all alike, is not more than

$$Nk \ln N - k \ln (N!) \approx Nk$$

or k per chain. It is readily shown that any interaction between the chains, whether it is an attraction or repulsion, can only result in some departure from complete randomness, thus making the contribution to the entropy smaller. Even if one argued that two polymer chains could be made physically distinguishable, e. g., by some slight differences in the substituents, so that it became physically proper to drop the $N!$ term, the communal entropy would still only be $k \ln N$ per chain. For an assembly of ordinary size $N \approx 10^{20}$ this would amount to something of the order of 50 k per chain of perhaps 1,000 monomers, whereas, as already shown above, we are looking for effects of the order of k per monomer molecule. Moreover, a preparation in which the number of distinguishable species of linear molecules approached the number of molecules present could only be described as an extremely bad one chemically. We can conclude, therefore, that the contribution due to communal entropy is always negligible. Besides effects associated with the translation of entire molecules, one also should consider possible contributions due to the orientation of the molecule as a whole, the relative positions of all the segments being held fixed. The number of such possible orientations is certainly no greater than the number of physically distinguishable ways in which one single segment of the molecule, for example, the end segment, can be oriented relative to its immediate surroundings. The order or magnitude of this number is readily estimated from entropy data on ordinary liquids and solids.

The total entropy of an ordinary liquid or solid at ordinary temperatures is of the order of a few times R. Even if it were assumed that all of this entropy is associated with the communal effect, together with possible orientations and "rattling around" of a molecule of liquid relative to its immediate surroundings, this would still mean that the number of physically distinguishable states of a typical molecule effectively excited at ordinary temperatures is no more than e^3 to e^5 (about 10 to 100). From this it can be quite safely concluded that the translations and orientations of entire molecules of polymer of fixed configurations can contribute no more than 3 to 5 times k per polymer chain.

2.2. Differing Molecular Weights

It is well known that any linear polymer preparation contains molecules of all possible lengths from the monomer upwards, and it is proper to regard chains of two different lengths as "physically distinguishable." Since chains of more than a few thousand units long seldom occur in practice, the number of species effectively present will be small compared with the total number of chains. Consequently, any contribution to the entropy from this cause should be small. For branched as distinct from nearly linear polymers this argument does not hold. The number of paraffin isomers (C_nH_{2n+2}) is known, G. Polya [24] to be of the order of 2.8^n, so the number of possible species of branched polymer with $n=100$ to 1,000 is much greater than the number of molecules present in an ordinary assembly, in which case the omission of the $N!$ term in the communal entropy would be correct. Even so, as shown earlier, this still leads to an upper limit that is too small to be of significance in practice.

The following argument from Beckett (private communication) enables us to set a more stringent upper limit in the linear case. We may suppose that the chain lengths are distributed about the mean value on the basis of the so-called "most probable" law of Flory [5, ch. 8, p. 319]. This may be regarded as the "worst possible" case, leading to the highest entropy of all possible distribution laws. It is equivalent to the assumption that chains of all lengths are present in proportions corresponding to thermodynamic equilibrium at the polymerization temperature. By certain methods of preparation the much narrower Poisson-type distribution can be obtained, or, by fractionation in solution, a very narrow spread can also be obtained. The entropy associated with a completely random mixture of chains of different species, where N_x is the number of "x-mers" is

$$S_0 = k \ln \left\{ N! / \prod_x N_x! \right\} \text{ with } \sum N_x = N, \sum_x x N_x = M \quad (1)$$

where N is the total number of chains and M the total number of monomer units making up the assembly. Then the law of the most probable distribution is, Flory [5, p. 319]

$$N_x = N(1-p)p^{x-1} \quad (2)$$

with

$$N=M(1-p) \tag{3}$$

as the equation determining p. Substituting from (2) and (3) into (1), approximating to the factorials by means of Stirling's theorem, we find, after performing the summations called for by (1),

$$S_0 \approx -M[(1-p)\ln(1-p)+p\ln p] \tag{4}$$

where p is related to the average length of a chain by (3). Thus, for a degree of polymerization resulting in a chain of an average length of t units, we arrive at an entropy of $\approx k \ln t$ per chain, or $\frac{k \ln t}{t}$ per link, which again is negligible for $t \sim 1{,}000$.

2.3. Entropy Associated with Copolymerization

If two monomers A and B are present in equal numbers they may be arranged in completely random fashion along each chain, unless the chemical kinetics of the reaction are such that A attaches itself easily to B but only with difficulty to another A. For example, a condensation polymerization might be like this. In the first (random) case a residual entropy of $k \ln 2$ per monomer can be expected; in the second the chain would be almost completely ordered and the entropy practically zero. It should be noticed here that the argument must be based on kinetic rather than equilibrium considerations because a chain, once formed, is not likely to break up again in order to assume a slightly more probable configuration. (This excludes conditions where polymer degradation is rapid.) The work is readily extended to the case where the two monomers are present in the proportions $g:(1-g)$, the corresponding maximum entropy being, per link,

$$k(-g\ln g-[1-g]\ln[1-g]) \leq k \ln 2 \tag{5}$$

the question whether or not it is attained again being outside the province of thermodynamics alone.

3. Chain Configuration Problem

We have now shown that with the possible exception of the "copolymerization entropy," which cannot be predicted solely on the basis of equilibrium considerations, the possible other contributions to the entropy are too small to be of significance. This study of the chain configuration problem falls into a number of parts.

(a) What can be said, a priori, about a paraffin-like polymer in the light of existing knowledge of the paraffin chain and of the random-walk problem?

(b) What can be reduced from a study of solid polymers?

(c) What can be deduced from studies of polymers in solution?

(d) What can be deduced from a study of related compounds such as solid and liquid long-chain paraffins?

All of these studies have contributed something to the solution of the problem, and it has been possible to draw the following conclusions with a fair degree of certainty:

(a) For a hydrocarbon-like polymer the entropy associated with chain configurations is no more than $1/5\ k$ per link.

(b) For a rubber-like polymer the experimental and theoretical information is less abundant and less definite, but it seems safe to say that the configuration entropy is no more than k per monomer.

We shall begin by asking what would be expected for a paraffin chain without side substituents, then consider briefly the possible effects of such substitutions and the presence of double bonds in the main chain. We shall then analyze the available experimental evidence in the light of these expectations.

3.1. A priori Expectations

A large number of studies have been made of the expected behavior of statistical assemblies of various types of jointed chains, beginning with the simplest possible case in which the "joints" are supposed to be entirely flexible, and in which complications due to the fact that a chain may not cross itself are ignored. For a survey of this work the reader is referred to Flory [5, ch. 10]. The idea that a long chain molecule can be represented in this way has proved extremely valuable in correlating a large number of experimental facts, but needs to be refined and generalized before it can be applied to the problem of calculating entropies.

It has been pointed out by a number of writers that the freely jointed chain model is in many ways analogous to both the Langevin model of a paramagnetic and to the perfect gas. The analogous thermodynamic variables are listed in table 1.

TABLE 1.

Perfect gas	Pressure	Volume	Compressibility.	Entropy.
Langevin model.	Magnetic field.	Mean magnetic moment.	Susceptibility	Entropy.
Freely jointed chain.	Tension	Mean length of chain.	Young's modulus.	Entropy.

The analogy may be carried even further in that all three models obey Joule's law, the internal energy being entirely kinetic and independent of the extension, volume or magnetic moment, as the case may be. It can also be shown without difficulty that none of these models permits the use of Boltzmann's principle to enable *absolute* calculations of entropy to be made. The physical reason for this is obvious; all three models admit of an infinite number of distinguishable configurations unless the chains are completely stretched out, the magnetic material magnetized to saturation, or the gas compressed to zero volume. Differences of entropy can, however, be defined, e. g., in terms of ratios of volume. Some of the more refined models (e. g., van der Waals model of a gas and Weiss model of a magnetic material) which attempt to take interactions between

atoms into account still possess this same objectionable feature although they do succeed in correlating a large amount of experimental material. As in analogous problems, for which an explicit specification of the entropy itself is required, such as the discussion of vapor pressures, it becomes clear that quantum considerations must be introduced in order to get a model in which the number of distinguishable configurations is finite, and to obtain sensible physical results. It is, however, not difficult to see how such refinements must proceed. We are guided in the first place by analogy with the Brillouin treatment of paramagnetism, in which each atomic magnet is only allowed a finite number of orientations, and we begin by looking for some similar feature in a polymer chain.

For the pure paraffin chain it is possible to state fairly accurately what the model must be like, Pitzer [20], Taylor [28]. For ethane the following model is consistent with both thermodynamic and spectroscopic evidence: the two methyl groups can rotate about the common single bond, but there are three possible energy minima separated by potential barriers of the order of 3 kcal/mole, so that the coordinate ϕ, measuring the angle of twist, is associated with a contribution to the energy of the form

$$E=E_0(1-\cos 3\phi). \qquad (6)$$

It is natural to ask whether an energy function of the form (6) can be applied to each link in longer chain paraffins. If it can, then it becomes plain that the difficulty in assigning a finite entropy to the hydrocarbon chain disappears. For, at a sufficiently low temperature, a chain in equilibrium will be near one of the positions of minimum energy called for by (6). The effect of thermal agitation can then be described accurately enough as leading to a contribution to the potential energy of the order of $E_0 \sum_r \frac{(3\phi_r)^2}{2}$, where ϕ_r is the "twisting coordinate" associated with the r^{th} link in the chain. The discussion of the problem is then that of a set of simple harmonic oscillators, which can be carried out exactly on a quantum mechanical basis. If it were correct to discuss a long paraffin chain in this way, it could be concluded that the entropy associated with thermal agitation should approach zero as $T\to 0$, leaving only the term $k \ln 3$ per link as the maximum possible residual entropy, associated with the fact that, according to an energy-function such as (6), each carbon atom can be linked to the next in three geometrically distinguishable ways. This argument holds equally well even if we take account of degrees of freedom associated with bond lengths as well as bond orientations. For, at a low enough temperature, bond lengths must also be near their equilibrium values, and the effect of departures can also be expressed by means of a quadratic energy function. If we suppose further that these various degrees of freedom are coupled, we should obtain the energy that will contain product terms as well as squares. It is always possible, however, to find a linear transformation of coordinates that reduces such a quadratic form to a sum of squares, at the same time avoiding the introduction of product terms into the kinetic energy. This means that the low temperature behavior of the "stretching", "bending", and "twisting" modes of a hydrocarbon chain is equivalent to that of a set of simple harmonic oscillators, which contributes nothing to the residual entropy.

On this basis it is possible to give a satisfactory qualitative account of the specific heats of polymers. The degrees of freedom of independent chains should be described with reasonable accuracy by a "one-dimensional" spectrum of Debye type, containing both transverse and longitudinal modes, which would lead to a specific heat proportional to T at low temperatures. The interactions between chains can be described by adding to this a three-dimensional Debye spectrum, leading to a contribution to the specific heat proportional to T^3 at low temperatures, and the phenomena of crystallization and the melting of crystals would also be consequences of this interaction. Finally, the "glass-like transition region" marks the range of temperature at which the jumps over the potential barriers occurring in expression (6) become frequent enough for the twisting modes of the chain to come into action. At lower temperatures each chain would be "stiff at the joints" but the stretching modes would remain in operation. In other words, the glass-like transition ought to correspond to the appearance of rubber-like properties and to a rapid rise in the specific heat connecting low and high temperature portions of roughly one-dimensional Debye type, the high temperature part having a lower characteristic Debye temperature. These features seem to agree well with what is observed in practice for the specific heats of various polymers, e. g., Furukawa et al. [6], but only preliminary quantitative analysis on this basis seems to have been carried out. It may well be that too many adjustable constants are involved. The model will not be discussed further from this angle, but the above considerations suggest strongly that it must be a reasonable first approximation.

If an energy function such as (6) were applicable to each link of a very long chain, one could say that the three configurations at any given joint should occur with very nearly equal frequency, and that this leads to a residual entropy of the order of k per "link". (The crude value k in 3 has to be reduced somewhat to allow for steric effects.) Later on we shall assemble some experimental evidence showing that a smaller value is, in fact, more likely to be correct. We are therefore prompted to ask the following two questions:

(a) To what extent is an energy function such as (6) an adequate description of a long chain molecule?

(b) How much is the entropy affected by the deletion of sterically impossible chain configurations?

Since a residual entropy of k per unit would still be noticeable thermochemically, an attempt to set a more precise upper limit is justified. Partial answers to both questions have been obtained by Pitzer [20] and Taylor [28]. From a study of the thermodynamic properties of various hydrocarbons Pitzer con-

cluded that expression (6) was an oversimplification, and that the *trans* configuration in which any three successive bonds in the main chain lie in one plane is, energetically, somewhat more favorable than any other one, involving one or more *gauche* linkages. For brevity we shall hereafter refer to *trans* configuration of bonds as "straight", and to any departure from it as a "kink", although the straight configuration is the well-known zigzag pattern. Pitzer [20] and Taylor [28] propose to replace expression (6) by something like

$$E = E_0\ (1\text{-cos } 3\phi) + E_1\ (1\text{-cos } \phi) \qquad (7)$$

and they estimate that E_0 and E_1 should be so chosen that if a straight or *trans* configuration is taken as having an energy of zero, a kinked or *gauche* configuration should have a minimum energy of about +0.8 kcal/mole, and that the maxima separating the three minima should have peaks of about +4.1 kcal/mole. These figures have been shown to be nearly right by studies of a large number of related hydrocarbons; see, for example, Pitzer [20], [21]; Pitzer and Kilpatrick [23]; Beckett, Pitzer, and Spitzer [1]; Pitzer and Beckett [22]; Person and Pimentel [19]. Confirmation that the steric energy difference is of this order of magnitude for butane, pentane, and hexane is provided by the spectroscopic studies of Sheppard and Szasz [26]. Such a modification in the energy function has some important consequences. It means, in the first place, that the probability that any three successive bonds lie in one plane is not now the simple factor ⅓ but the significantly larger value $\frac{1}{1+2e^{-E_2/kT}}$, where E_2 corresponds to the figure of 0.8 kcal/mole just mentioned. Secondly, such a chain should tend to "straighten out" as it cooled, an effect that is not predicted at all by the simpler model, but for which there is a little experimental evidence. Of course, the glass-like transition intervenes before the straightening-out is complete, otherwise the straight configuration would be the only one that would have to be considered at all at absolute zero, and the configurational entropy would be zero.

The necessity of working with the function (7) instead of (6) appears to be a consequence of interactions between noncontiguous methyl and —CH_2C— groups, and it seems necessary to ask whether one is likely to have any success in applying the same type of function to more complicated cases. Two complicating factors are the presence of side substituents and the possible occurrence of double bonds or other types of linkage in the main chain. The former factor is discussed by Flory [5, ch. 6]. His conclusions are, in effect, equivalent to saying that a function such as (7) should still be adequate, but that the chain configuration of lowest energy is, in general, no longer a simple zigzag. Steric considerations imply that some other more complicated configuration may have to be chosen as the "reference" one, departures from which determine the energy as given by function (7). For the present purposes this is not serious, but it does have to be borne in mind if one is attempting to compute e. g., the effective "spread" of a chain. In the extreme case of polyisobutylene only one configuration could be found that seemed to be sterically possible at all. In cases like this, the energy differences occurring in (7) would presumably be greater than they are for paraffins with a correspondingly smaller entropy at any given temperature. On the other hand, the higher potential barriers would also tend to lead to a higher glass-like transition temperature, so that it does not follow that introducing side substituents will automatically lower the residual entropy. Very little seems to be known about the theoretical effect of double bonds in the main chain, though it is generally considered that they should facilitate rotations of single bonds adjacent to them.

The effect of introducing a triple bond has been examined by Osborne, Garner, and Yost [18] who studied the thermodynamic properties of dimethylacetylene $CH_3-C\equiv C-CH_3$. They concluded that the potential barriers restricting relative rotation of the methyl groups were probably not higher than 0.5 kcal/mole, and gave reasons for thinking that the main effect of the triple bond is simply that the methyl groups are much further apart than they are in ethane. They argue that a double bond ought to have similar consequences in reducing the height of the barrier. The barrier in olefin hydrocarbons for groups adjacent to the double bond is about 1 to 2 kcal/mole. See Kilpatrick and Pitzer [13], who studied ethylene, propylene, and the butenes. This is significantly smaller than for paraffins, but there does not seem to be any information available about the existence or nonexistence of an effect analogous to the energy difference between *trans* and *gauche* configurations that were noted for paraffins. The indirect experimental evidence is certainly consistent with the idea that, in rubber-like polymers, the potential barriers between different chain configurations are lower than in paraffins, and that the bias in favor of straight configurations may be small or nonexistent. If we could neglect other steric effects such as the fact that a chain may not cross itself our present problem would be solved. We could say that, as the relative probabilities of a given C—C bond corresponding to a straight or kinked configuration should be in the ratio $1:2e^{-E_2/Tk}$, the partition function must contain a factor $(1+2e^{-E_2/kT})$ per link, the corresponding entropy per link being

$$k\left[ln\ (1+2e^{-E_2/kT}) + \frac{E_2}{kT}\cdot\frac{2}{e^{E_2/kT}+2}\right], \qquad (8)$$

which falls steadily from k ln 3 to zero as E_2/kT rises from zero to infinity. For the discussion of any particular type of polymer chain, it would only be necessary to insert the appropriate values of E_2 and of the glass-like transition temperature into (8) in order to arrive at the expected residual entropy.

We must now examine the effect of removing from the partition function terms corresponding to self-

crossing configurations which are implicitly included in the calculations leading to (8). Such problems are of considerable mathematical and physical interest, and although only a very few highly idealized ones can be solved analytically (for example, we do not yet know the equation of state of a perfect gas of rigid spheres), it seems possible to get an answer that is sufficiently good for present purposes. It is known [7, 8] that the problem of an actual chain cannot be treated merely as a small perturbation of the "unrestricted" random walk problem. The effect of introducing any realistic type of constraint always results in a significant reduction in the entropy per link. Stated otherwise, the number of possible configurations of the restricted chain is only a very small fraction of that for the unrestricted one. Some writers have introduced the concept of the "equivalent random walk". They suppose that for sufficiently large N, the behavior of a real chain N links long is analytically equivalent to that of a random walk of N/n steps, with a suitable choice of n and of the length of step. Unfortunately, recent work, Wall et al. [32, 33], Temperley [29] indicates that this concept is not strictly valid in two dimensions, nor in three dimensions for values of N small enough to be of physical interest, at least not if we wish to treat n as independent of N. Nevertheless, the concept is of value and will be used again later. If, for example, we had to do with an extremely rigid chain, strongly biased in favor of straight configurations, it would be possible to define some number, m, that measures the average distance between two kinks. We should expect this to be of the same order as the n just introduced, though the concepts of length of step of equivalent random walk and length of link of equivalent flexible chain are logically distinct.

A start was made on the steric problem by Taylor [28] and a very similar process was used by Montroll [16] for the idealized case in which the links of the chain are constrained to lie along a plane square lattice. These authors show that the effect of removing from the partition function terms corresponding to self-crossing paths of a certain type can be established rigorously and very simply. The type of path deleted is, for the plane square lattice, any path containing one or more closed loops consisting of single squares, for example, a path passing in succession through the points (1,2), (2,2), (2,1), (1,1), (1,2). Paths containing longer loops are retained for the present. We summarize Montroll's argument for the plane square lattice, each link being constrained to be at right angles to those that precede and follow it. The first link can take any one of four directions. We can then proceed to the next link by means of either a left or a right turn, which we shall denote symbolically by E or F. The passage from the second to the third link also involves either a left or right turn, and so on. If we retained self-crossing paths, our generating function for a path $n+1$ links long would be simply

$$4(E+F)^n \tag{9}$$

each term in this product, with the factors E and F written in their proper order, corresponding to a possible path. We shall now show how expression (9) is modified if we delete terms containing either of the successions EEE or FFF, as either of these combinations corresponds to the enclosure of a single square. By induction, we can determine the generating function S_n that replaces (9) for a path n units long if we know it for all shorter paths. Let $S_n(E)$ and $S_n(F)$ be those parts of S_n whose final factors are E or F respectively. Now $S_n(E)$ may end in one of the two ways FE or FEE, but in no others, since three E's in a row are forbidden. Thus we have the relation

$$S_n(E)=S_{n-1}(F)\cdot E+S_{n-2}(F)\cdot E\cdot E \tag{10}$$

and a similar one for $S_n(F)$. If we are concerned, as we are here, simply with the counting of configurations in which left and right turns are equally weighted, E and F can be replaced in equations such as (9) and (10) by a single variable x, so we find that $S_n(x)$ is determined by the difference equation

$$S_n(x)=xS_{n-1}(x)+x^2S_{n-2}(x) \tag{11}$$

which can be solved by a process quite analogous to that for linear differential equations, that is, by looking for solutions of the type $S_n=Ap^n$, where A and p are independent of n, but may depend on x. Such a solution will satisfy (11) provided that

$$p^2-xp-x^2=0 \text{ or } \frac{p_1}{p_2}=x\left(\frac{1\pm\sqrt{5}}{2}\right) \tag{12}$$

giving us two independent solutions, each of which can be multiplied by an arbitrary function of x and the two can then be added. It is readily verified that this is the most general solution possible, and the two arbitrary functions are completely determined from the known forms of S_1 and S_2. For the purpose of determining the entropy of a chain n steps long, as n becomes large, the answer can be read off directly from (12), because the complete solution is $A_1p_1^n+A_2p_2^n=S_n$ and the term involving p_2^n can contribute only an insignificant amount to the entropy compared with that in p_1^n. We have, in fact, the result that the entropy per link is reduced from the value k ln 2 that would follow from (9) to the distinctly smaller value $k \ln\left(\frac{\sqrt{5}+1}{2}\right)$, as a result of deleting a certain type of impossible path. This method can readily be generalized to other types of lattice. For example, Taylor [28] showed that the removal of "pentane configurations" reduced the configurational entropy of a linear paraffin from the value k ln 3 per link that we calculate on the basis that successive links must be inclined at the tetrahedral angle to the value $k \ln (1+\sqrt{2})$. His result is equivalent to replacing equation (11) by

$$p^2-2px-x^2=0 \text{ or } p=x(1\pm\sqrt{2}). \tag{12a}$$

By pentane configuration is meant any configuration that nearly closes upon itself in four successive steps, which cannot occur for any paraffin shorter than pentane. The fact that in such cases sizable reduction in the entropy occurs when we remove a particular type of sterically impossible path enables us to understand the failure of past attempts to treat the effect of steric obstruction simply as a small perturbation of the random walk problem. For a long chain, any significant reduction in the entropy per link means that only a very small fraction of the random walks gives permissible chain configurations.

There is no particular difficulty in extending the above work to other types of lattice, including cases in which certain configurations of successive bonds are, a priori, more probable than others. Thus, in Montroll's discussion of the square lattice [16] two adjacent links were not permitted to be in the same straight line, but it is quite possible to extend the discussion to a more general case in which right-angles and straights have different initial probabilities. It becomes much more difficult if we now attempt to remove paths involving longer loops. This question has been studied by the writer elsewhere [29] for the plane square lattice by methods differing from those outlined above, and, while the problem of writing down the generating function for all noncrossing paths is still unsolved, it is believed that enough is known about the properties of this function to enable the entropy to be determined. We quote the result here:

$$S=k\left[\ln\left(1+\sqrt{2}\epsilon^{-E_2/kT}\right)+\frac{E_2}{kT}\cdot\frac{\sqrt{2}}{\epsilon^{E_2/kT}+\sqrt{2}}\right], \quad (13)$$

which, it will be observed, is of precisely the form (7) with 2 replaced by $\sqrt{2}$. E_2 here has the meaning of the gain in energy involved in replacing a right-angle between two successive links by a straight. If we put $E_2=0$ and compare (13) with (12) we arrive at the remarkable conclusion that removing just pentane configurations from random paths, the links inclined at the tetrahedral angle, has precisely the same numerical effect on the entropy as has removing loops of all sizes from random paths disposed along the square lattice, the steric effects being at least as severe in the paraffin chain as they are in the square lattice one. A removal of loops larger than those corresponding to pentane configurations will certainly diminish the paraffin entropy further. We wish to take account of the effect of a finite E_2, as well as of steric effects, in the paraffin chain, and it seems safe to regard (13) as an upper limit for these purposes. With the value of E_2 of 800 cal/mole and a glass transition temperature of the order of 200° K, we should have $\epsilon^{E_2/kT}\approx 7$, so that we estimate $0.5k$ per link as an upper limit for the configurational entropy of a paraffin-like chain. The corresponding length of effective segment is six C—C links. For a rubber, E_2 may be negligible, and our estimate becomes about k per link for the upper limit, and the corresponding effective segment is 1.7 monomer units.

There is still one factor, not negligible, to consider, but there are no accurate means of estimating its numerical importance; this is that the occurrence of crystallization in polymers (in some cases up to high temperatures) shows that the interaction between chains is not negligible, and it can be foreseen that any steric effects between neighboring chains will have the effect of lowering the configurational entropy still further. This is probably true in a liquid paraffin as well as in a solid. If this effect is significant it would mean that the entropies actually occurring would be appreciably below the above estimates, and there is experimental evidence that this is sometimes the case. Various independent attempts to estimate the length of the effective segment give values for this quantity running appreciably higher than those that would be calculated for an isolated chain by the method outlined above. In this way the influence of the neglected factor of interaction between chains seems to be about comparable with that of interaction between distant parts of the same chain. There is some evidence that this neglected factor has a stronger influence in solids than it has in liquids or solutions, and this is to be expected.

3.2. Analysis of Certain Experimental Results

The preceding theoretical considerations suggest that the configurational entropy of a polymer chain may be significantly below the value k log 3 per link that one estimates from "elementary" considerations. The two possible causes for this are: (a) The intrinsic properties of the linkages themselves, e. g., straight configurations may be favored by the nature of the interactions between neighboring links, as in the paraffin chain. (b) Steric effects tend to reduce the number of "coiled-up" configurations. This includes both interactions between neighboring chains and between distant parts of the same chain, while (a) is the result of short-range interactions within chains. What we shall try to estimate from experimental data is the effective length of segment or "average length of chain between kinks." For the paraffin chain, all the C—C bonds in such a segment lie in one plane and assume the zigzag pattern. For other types of chains the geometry of the configuration of lowest energy may be more complicated, but we shall still refer to it as straight, to a departure from it as a kink, and to the mean distance between two kinks as an effective segment. Strictly speaking, the last concept is logically not quite equivalent to that of length of step of equivalent random walk but the ratio of the two is not likely to be far from unity. It is, in principle, possible to distinguish experimentally whether (b) is the dominant consideration or whether (a) is also significant. In the latter case, the effective length of segment should increase as the temperature falls and kinks become less likely, and there does seem to be some evidence that this occurs.

The evidence may be roughly divided as follows, one subsection devoted to each topic:

1. Studies on solid polymers. Apart from the thermodynamic properties already referred to, as being in reasonable accord with the model we are using, there is a little further evidence giving direct information on the segment length in a few cases.

2. Studies on polymer solutions. The information here is mainly indirect, and is usually equivalent to studying the effective size of the coiled up polymer molecule of known molecular weight. For a completely flexible chain, the effective linear dimension of a coiled up molecule is proportional to $N^{1/2}l$, where N is the number of links of end-to-end length l. If straight configurations are so much favored that there is on an average only one kink per m links, such a chain should behave, to a first approximation, like a flexible one of $\frac{N}{m}$ links, each of length Am, (where A is a constant, of the order of unity, depending on the geometry of the straight configuration) and its mean dimension should be increased by a factor $Am^{1/2}$. We can deduce the value of m by comparing the dimensions of the molecule, as inferred from experiment, with that calculated from bond lengths and angles on a random walk basis. Effects (a) and (b) both tend to increase m, and it is only possible to separate them in a few cases.

3. Studies on solid and liquid paraffins and related compounds. There is quite a variety of evidence pointing to the conclusion that such molecules, (up to about 30 carbon atoms), behave roughly like nearly rigid rods. Such a conclusion is in good agreement with the thermodynamic properties of the paraffin chain discussed above.

a. Studies on Solid Polymers

It has been noted (and perhaps this is the most suggestive point) that the tensile strength of a typical polymer remains practically zero until a degree of polymerization of about 50 is reached, after which it begins to increase rather suddenly. It is easy to assume that the real distinction between a "wax" and a "fiber" is that the molecules of a fiber cannot be sheared over one another indefinitely because the kinks become entangled while the molecules of paraffin wax are nearly straight and can slide smoothly past one another. One arrives at an effective distance between kinks of the order of 15 to 20 units, on the basis of the rather crude assumption that molecules would have to have at least two kinks before they could serve as "double-hook" units, which could theoretically form a structure capable of resisting tension.

The fact that above about a two-fold extension, the tension in rubber rises much more rapidly with the extension than the simple "random-chain" theory predicts, indicates that the maximum obtainable extensions, (of the order of 5 to 10 fold) really do represent a situation in which an appreciable fraction of the chains are pulled into configurations approaching maximum extension. This conclusion holds equally well whether, with Treloar [30], we regard the observed stress-strain curves as qualitatively explained by James and Guth's [11] treatment of highly extended chains, which does predict just such a rapid increase in elastic modulus as full extension is approached, or whether, with Flory, [4] we attribute this increase in elastic modulus mainly to the effect of crystallization. Crystallization is facilitated by stretching out the chains thus making the configurations of neighboring chains more nearly alike. If a 5 to 10 fold extension is really the maximum that can be obtained without rupture of an appreciable fraction of the chains, this would mean that

$$\left(\frac{N}{m}\right)\cdot m \approx 5 \text{ to } 10\left(\frac{N}{m}\right)^{1/2}\cdot m$$

or $\frac{N}{m} \approx 30$ to 100, whereas, in an actual lightly vulcanized rubber, the distances between cross-linkages probably correspond to chains at least several hundred units long. Thus it seems difficult to reconcile the observed elasticity of rubber with a value of $m=1$, but postulating a value of the order of 2 to 5 would improve matters considerably. Treloar [30, ch. 8] concluded, on the basis of studies of the double refraction of solid rubber under stress, that $m \approx 2$, the precise numerical value depending on the exact way in which we define m.

A very recent study, Honnold, McCaffrey, and Mrowca [10] has been made using proton resonance methods. It is difficult to obtain actual estimates of segment length directly by this means, but their studies of silicones, and their comparison of polypropylene and polypropylene oxide do indicate that the introduction of oxygen linkages into the main chain makes it more flexible. This is in agreement with the conclusions of Kuhn and Kuhn, [14] obtained from the birefringence of solutions.

b. Analysis of Data on Solutions of Polymers

There are two basic ways to determine the length of the effective segment. The most direct is to treat the large polymer molecule as if it were an aggregate of effective segments, each free to move short distances in the solution, and to assume various orientations. These changes in the position and orientation of the segments correspond to movement of the kinks up and down the long polymer molecules, the average number of kinks remaining constant. This movement of segments as a result of thermal agitation will resemble that of a solute molecule in an ordinary solution, except that the segment is not free to wander very far from the center of gravity of the polymer molecule. This situation is described by the so-called lattice model of a polymer solution, as amended by Flory to cover the case of extremely dilute solutions. See Flory [5, ch. 12] for a summary.

Using this treatment, we can estimate the size of the effective segment in several ways.

(a) From the osmotic pressure. Since this is an equilibrium property, we can use solution theory directly. The limitation is set by the availability of data. The solutions have to be very dilute for

existing theory to be acceptable, whereupon the pressures to be measured become rather low for accurate measurement.

(b) From the viscosity. The idea here is that any motion of a segment through the solvent is associated with the displacement of an equivalent volume of solvent molecules. These molecules have to be removed from the liquid, leaving a "hole" big enough to contain the segment. The segment then enters this hole and the space it leaves vacant in the liquid is filled by the displaced molecules. Independently of any particular model of the liquid, we can argue that the energy barrier associated with such a process must be of the order of magnitude $l\rho v$, where l is the latent heat of evaporation, ρ is the density of the solvent and v the volume of the effective segment. Thus the probability of such a process may be expected to be proportional to $\exp(-l\rho v/kT)$, and the viscosity of the solution should contain a factor that is the inverse of this. If so, the activation energy $l\rho v$ can be estimated by means of the customary plot of log (viscosity) against $1/T$. For a survey of the conclusions from these two methods we quote Powell and Eyring [25, p. 191]. "It is worth noting that the segment lengths estimated from osmotic pressure data (18 to 33 atoms for polystyrene and polyethylene oxide) and from melting point data (20 to 25 atoms for hydrocarbons) are in agreement with the segment lengths from viscosity data (20 to 25 atoms for hydrocarbons, 28 to 34 atoms for polyesters)." The reader is referred to this review article for a survey of the work leading to these conclusions.

Eyring and his collaborators have attempted an alternative estimate of segment length from viscosity data, based on a viscosity formula of the type

$$\eta = A \exp(u/kT),$$

in which attempts are made to estimate A, as well as u, from the experimental results, and to compute a theoretical value of A in terms of segment length. In practice, this method fails to give useful results, but this failure does not mean that the estimates of u are invalid also. Suppose, for example, that u is varying slightly with temperature, say according to the law $u = u_0(1+\alpha T)$. The customary logarithmic plot of the viscosity data against $1/T$ would now yield u_0 and $Ae^{\alpha u_0/k}$ in place of u and A, and a value of α of no more than a few tenths of one percent per degree could lead to a completely false experimental estimate of A. A similar difficulty occurs in the analysis of thermionic data in metals.

(c) A third method of estimating segment lengths, due to Kuhn and Kuhn [14], rests on the study of the double refraction of a polymer solution that is being steadily sheared, the shearing flow tending to orient the typical segment and stretch out the polymer molecule in a manner that depends essentially on the length of the typical segment. By a rather complicated method of analysis, these authors arrive at results ranging from segment lengths of the order of 30 carbon-carbon links for paraffin-like polymers ranging down to 1 to 3 monomer units for rubber, hydrogenated rubber, and polymers which contain C—O linkages in the main chain. Such linkages, by increasing the spatial separation of the $-CH_2C-$ groups, no doubt make the chain more flexible, as already suggested above.

The second basic method of attack on this question is based on an attempt to determine the linear dimensions of the molecules in solution, and to examine how these differ from the values to be expected on the completely random-walk basis. This should give a measure of m, since we have pointed out that the ratio, actual dimension to calculated dimension, should be approximately equal to $m^{1/2}$. The actual dimension is obtained by an ingenious analysis of data on the viscosity of dilute solutions, due to Flory [5, ch. 14]. This new method of analysis of viscosity bears no relation to the method we have already described, but is not inconsistent with it.

The very dilute polymer solution can be regarded as a mixture of roughly spherical aggregates representing the molecules of polymer, separated by fairly large regions of pure solvent. Flory's idea is to suppose each molecule of polymer replaced by an equivalent solid sphere, and to attribute the excess of the viscosity of the solution over that of the pure solvent to the fact that the solvent cannot flow freely through the polymer molecules, but is partly diverted around them. One can then apply Einstein's well-known treatment of the viscosity of a liquid containing a random distribution of solid spheres. Thus, according to this approach, we consider that a whole polymer molecule obstructs the flow of the solvent to an extent that depends on its spread in space, and the motion of individual segments is not considered.

Flory shows that, if the temperature is properly chosen in relation to the solvent and concentration, the spatial distribution of polymer molecules in the solution is indeed random; and further, that the extension of the molecule in space is then very nearly the same as what we should calculate on the assumption that the interactions of solvent molecules and polymer segments with one another and among themselves are equivalent. At this temperature, called by Flory the Θ point, the solvent becomes, so to speak, "neutral", any actual differences in these interaction energies being approximately balanced by the effect of thermal agitation. Various other definitions of the Θ point are possible; for example, it can be shown that it should correspond to the limit of solubility of a sample of polymer of extremely high molecular weight. A solution at its Θ point should then contain a practically random spatial distribution of molecules in the solvent, and the average chain configuration of these molecules should be that which we should predict on the basis of neglect of long-range interactions between segments (apart from steric effects).

Flory's analysis [5, ch. 14, p. 618] leads him to conclude that "the observed end-to-end distances, unperturbed by long-range interactions, are consistently greater than would hold if bond rotation were completely unrestricted. Steric effects of one sort or another probably are responsible." The

factor measuring the "expansion of linear dimensions", which should be a measure of $m^{1/2}$, ranges from 1.60 for gutta-percha to 4.9 for cellulose tributyrate, in satisfactory qualitative agreement with figures for m already calculated for paraffin-like and rubber-like polymers by other means.

It is of some interest to ask what is likely to be the relative importance in causing this expansion of the molecule of the two distinct factors met in discussing the hydrocarbon chain, the fact that two carbon atoms may not be in the same place, and the fact that there may be correlation between the directions of e. g., neighboring C—C bonds. The first of these factors should lead to an expansion that remains the same at all temperatures, while the second should lead to an expansion that increases as the temperature falls. Calculations on a paraffin-like chain, Taylor [28], Kuhn [15] indicate that the end-to-end length should increase by a factor of 1.2 as the temperature falls from +100° C to 0° C. Flory [5] finds evidence of just such an effect for various solutions of cellulose tributyrate, each one studied at its Θ point. This is also the very molecule that shows the biggest departure from the random-walk configuration.

On the basis of all this evidence, we seem justified in concluding that:

a. The absence of configurations in which two carbon atoms coincide increases the linear dimensions by a factor of the order of 1 to 5 above what they would be on a random-walk treatment. This effect seems to be the only important one in rubber-like materials. It implies that only about half the linkages between isoprene units can be regarded as uncorrelated with one another, and leads to a residual entropy of $\frac{1}{2}\,k$ ln 3 per isoprene unit.

b. For a paraffin-like chain there is often an additional effect, due to correlations between neighboring links probably attributable to interactions between the CH_2—C groups in the main chain. This seems to be capable of raising the effective value of m from a value of the order of 2 that seems to follow on the basis of factor (a) alone to a value of the order of 20 or more. The corresponding residual entropy is then of the order of 0.1 to 0.2 k per monomer molecule. It would not be correct to quote a figure as low as 0.05 k corresponding to an effective segment 20 units long, because of the presence of the second term in eq (8).

These values agree remarkably well with those based on the purely theoretical study, bearing in mind that one factor, the interaction of the chains in a solid with one another, was not considered. It is satisfactory that the apparent values of the length of the effective segment are, for both rubber and the paraffin-like polymers, a factor of 2 or so greater than we estimate theoretically for an isolated chain. These experimental studies are almost all based on dubious assumptions, or depend on numerical constants that have been evaluated very tentatively. Any one of them, taken alone, would not be very impressive, as comparatively small errors in some of the numerical constants might make a considerable difference to the calculated values of m. The results of a number of quite independent investigations all give calculated values of the same order of magnitude, and their cumulative value as evidence is very considerable.

We shall close with a survey of the properties of liquid and solid paraffins and similar bodies of chain lengths between about 10 and 60, which seems to confirm the above conclusions obtained directly from polymer studies.

c. Analysis of Data on Paraffins and Allied Series

Convincing evidence that paraffin molecules up to about 40 units long pack like rods in the solid state is provided by the X-ray work of A. Müller. For an account of his work the reader is referred to a review article by Daniel [3]. In addition to determining the structure of the ordinary solids, Müller was able to elucidate the nature of a transition that occurs a little below the melting point for paraffins of lengths between 16 and 32 C atoms. He was able to show that this transition is associated with a change in crystal structure, the packing changing from a type natural for flat ribbons to one appropriate to practically symmetric round rods.

The following evidence that in the high temperature state the molecules really are rotating as rigid rods rather than twisting is available. In the first place, the entropy change associated with the transition has been found to be practically independent of chain length, which is what we should expect if the entropy change is mainly associated with a change in the two-dimensional packing of rigid rods. But if only short segments of the chain were rotating at any one time and some of the bonds were being twisted, one would expect the entropy of transition to be proportional to the number of segments, and thus to the length of the chain. Also, the transition temperature is a linear function of the chain length y, of the form $A+By$. This, combined with the result that the entropy of the transition is practically independent of chain length, implies that the energy change associated with the transition must be a similar linear function. This is just what would be expected if the chains are behaving as rigid rods, one contribution to the energy coming from the interaction between any chain and those lying alongside it, which should be proportional to the length of the chain, y. A second contribution might be expected from the interactions of methyl groups belonging to end-to-end neighbors, which should be practically independent of chain length.

This type of transition occurs only over a limited range of chain lengths simply because, at the top and bottom of this range, the paraffin melts before undergoing the transition. The melting temperatures of various homologous series are well represented by the empirical relation

$$T_m=(C+Dy)/(E+Fy) \tag{14}$$

in contrast with the linear relation for the transition temperature just mentioned. It is now natural to ask whether eq (14) is also to be regarded as evidence

that paraffin chains are behaving as practically rigid rods. In view of the tentative nature of present theories of liquid structure, any attempt to be dogmatic on this point would be out of place. It does, however, seem worth while to mention two possible interpretations of (14), which, although incompatible with one another, are both in agreement with the picture of a fairly long effective segment. It could be argued that since for all homologous aliphatic series, a relation such as (14) seems to hold, and that the melting temperature settles down to a practically constant value for $m \approx 30$, that this represents the length of the effective segment; that lower hydrocarbons are behaving like rigid rods in both solid and liquid states, while higher ones are behaving as if they were composed of effective segments of about 20 to 30 links long, each of which is capable of moving around in the liquid as a unit, corresponding to the motion of individual kinks up and down the chains. We have already met this picture in discussing polymer solutions. On the other hand, an interpretation of relation (14) can be given on the basis that the chains behave like nearly rigid rods for all values of y for which reasonably pure preparations can be made. The energy change associated with melting should be the sum of interactions between side-to-side and end-to-end neighboring chains, and this should be a linear function of y, as before. In the liquid near its freezing point it may be supposed that the chains are still packing in a roughly two-dimensional fashion, but somewhat more loosely than in the solid, and that each chain also acquires some freedom to move lengthways as well as sideways. Such a picture leads to an entropy change consisting of a constant term, associated with the possibility of sideways movement and rotation, that we have already met in the solid-solid transition, with the addition of a term, roughly proportional to chain length, associated with a possible lengthways sliding of the chains, which would be absent in the solid transition. Such behavior of the entropy and energy of transition leads directly to a relation like (14). For a review of the experimental material on which these considerations are based, and also for some extremely interesting material on esters, which is also in reasonable accord with the "rigid-rod" picture, the reader is referred to Daniel's review article [3]. Simanouti and Mizushima, [27] from a spectroscopic study of liquid cetane ($C_{17}H_{36}$), concluded that this liquid was probably a mixture of the various possible forms of molecule containing just one kink or *gauche* configuration, all the remaining linkages being in the *trans* configuration but the molecules in the solid being entirely of the all *trans* (coplanar) type. Thus, the effect of the interactions between neighboring molecules seems to be somewhat stronger in the solid, a result that would be expected and this is also in keeping with the idea of an effective segment of $\sim$20 units.

We conclude by a brief reference to the work of Moore, Gibbs, and Eyring [17], who succeed in interpreting the temperature dependence of the viscosity of liquid paraffins on this same basis of approximately two-dimensional packing, so that the flow of such a liquid resembles the distortion of a crystal under stress by the sliding of layers of molecules over one another, rather than the independent motion of spherical molecules characteristic of ordinary liquids. The latter is what we should expect of the paraffins if there were more than 2 or 3 kinks per molecule, because then they would approximate to spheres far better than to rods.

4. Discussion and Conclusions

This enquiry has led into a variety of different fields and provided us with evidence on the chain configuration problem of very varying degrees of relevance and probable reliability, but the over-all consistency of the experimental evidence is surprisingly good, as is the consistency with the theoretical expectations. We have already met a number of cases in which the same data might be interpreted in more than one way, and, in the present state of our knowledge, both ways may well be wrong. Some of the investigations involve numerical constants evaluated by dubious methods, but, for the purposes of the present enquiry, the fact that these investigations were carried out quite independently of one another is a powerful argument in favor of the qualitative conclusions. It is right to mention at this point a few apparent inconsistencies which cannot be explained away so easily. The general picture is that a paraffin-like chain is fairly rigid, and that the introduction of substituents only tends to increase the rigidity, hence a residual entropy of about 0.2 k per link, but that the introduction of a double bond or a C—O linkage into the main chain should introduce flexibility, and thus put up the residual entropy to as much as 0.5 to 1.0 k per link. And yet, (a) according to theory, and also according to Kuhn and Kuhn [14] and Honnold, McCaffrey, and Mrowca [10] the polyethylene oxide chain should be very flexible, whereas the behavior of this solid is not rubber-like, and osmotic pressure data, Powell and Eyring [25], indicate an effective segment of the order of 20 to 30 atoms. (b) Kuhn and Kuhn [14] studied a hydrogenated rubber, in which all the double bonds were saturated. This should behave like a hydrocarbon chain with one substituent methyl group per isoprene unit, and should therefore form a stiff chain, whereas, in solution, it appears to be at least as flexible as ordinary rubber.

5. Possible Further Work

The main conclusions seem confirmed by a number of independent pieces of evidence, but the investigation does suggest possible further lines of enquiry.

(a) The idea of a possible numerical relationship between effective length of segment and fraction of material crystallized seems likely to throw light on the crystallization of rubbers, if it could be made more precise.

(b) It might be worth studying nonsaturated hydrocarbon liquids by X-ray and viscosity methods in order to see whether such molecules pack as approximate spheres, as they should if they contain a number

of fairly flexible bonds, or whether they pack as long rods. One liquid that might be interesting to study in these ways is squalene, since it consists of six isoprene units, and the average molecule should contain 2 or 3 kinks.

6. References

[1] C. W. Beckett, K. S. Pitzer, and R. Spitzer, J. Am. Chem. Soc. **69,** 2488 (1947).
[2] R. F. Boyer and E. Spencer, Advances in Colloid Sci. **I,** 183 (1946).
[3] V. Daniel, Advances in physics, Phil. Mag. Supplement **2,** 450 (1953).
[4] P. J. Flory, Ind. Eng. Chem. **38,** 417 (1946).
[5] P. J. Flory, Principles of polymer chemistry (Cornell University Press, Ithaca, New York, 1953).
[6] George T. Furukawa, Robert E. McCoskey, and Gerard J. King, J. Research NBS **49,** 273 (1952) RP2364.
[7] T. B. Grimley, J. Chem. Phys. **21,** 185 (1953).
[8] T. B. Grimley, J. Chem. Phys. **22,** 1134 (1954).
[9] E. Guth, H. M. James, and H. Mark, Advances in Colloid Sci. **II,** 253 (1946).
[10] V. R. Honnold, F. McCaffrey, and B. A. Mrowca, J. App. Phys. **25,** 1219 (1954).
[11] H. M. James and E. Guth, J. Chem. Phys. **11,** 455, 531 (1943).
[12] W. Kauzmann, Chem. Rev. **43,** 219 (1948).
[13] J. E. Kilpatrick and K. S. Pitzer, J. Research NPS **37,** 163 (1946) RP1738.
[14] W. Kuhn and H. Kuhn, Helv. Chim. Acta **26,** 1394 (1943).
[15] H. Kuhn, J. Chem. Phys. **15,** 843 (1947).
[16] E. W. Montroll, J. Chem. Phys. **18,** 734 (1950).
[17] R. J. Moore, P. Gibbs, and H. Eyring, J. Phys. Chem. **57,** 172 (1953).
[18] D. W. Osborne, C. S. Garner, and D. M. Yost, J. Chem. Phys. **8,** 131 (1940).
[19] W. B. Person and G. C. Pimentel, J. Am. Chem. Soc. **75,** 532 (1953).
[20] K. S. Pitzer, J. Chem. Phys. **8,** 711 (1940).
[21] K. S. Pitzer, Ind. Eng. Chem. **36,** 829 (1944).
[22] K. S. Pitzer and C. W. Beckett, J. Am. Chem. Soc. **69,** 977 (1947).
[23] K. S. Pitzer and J. E. Kilpatrick, Chem. Rev. **39,** 435 (1946).
[24] G. Polya, Acta Math. **68,** 145 (1937).
[25] R. E. Powell and H. Eyring, Advances in Colloid Sci. **I,** 183 (1942).
[26] N. Sheppard and G. J. Szasz, J. Chem. Phys. **17,** 86 (1949).
[27] T. S. Simanouti and S. Mizushima, Sci. Papers Inst. Phys. Chem. Research (Tokyo) **40,** 467 (1943).
[28] W. J. Taylor, J. Chem. Phys. **16,** 257 (1948).
[29] H. N. V. Temperley (to be published in Phys. Rev.).
[30] L. R. G. Treloar, The physics of rubber elasticity (Oxford University Press, 114 5th Ave., New York, N. Y., 1949).
[31] F. T. Wall, L. A. Hiller, and D. J. Wheeler, J. Chem. Phys. **22,** 1036 (1954).
[32] F. T. Wall, L. A. Hiller, and W. F. Atchison, J. Chem. Phys. **23,** 913 (1955).
[33] F. T. Wall, L. A. Hiller, and W. F. Atchison (unpublished data).

WASHINGTON, April 18, 1955.

Journal of Research of the National Bureau of Standards Vol. 56, No. 2, February 1956 Research Paper 2649

Molecular Weights of Thermally Degraded Polymethyl Methacrylate

Victor E. Hart

Molecular weights of polymer residues from the thermal degradation in vacuum of two polymethyl methacrylate samples, one polymerized with benzoyl peroxide and the other without any initiator, have been obtained over wide extents of degradation at various constant temperatures. A linear relation, dependent upon the temperature but independent of rate of volatilization and rate of change of $1/M_w$, is found when log R is plotted against $1/M_w$. (R=ratio of residue weight to original specimen weight, and M_w=weight-average molecular weight.) The results are explained on the basis of a free-radical chain-reaction mechanism in which intermolecular chain transfer (activation energy=29 kilocalories) is the primary, or perhaps the sole, cause of the molecular-weight decrease.

1. Introduction

Polymethyl methacrylate is of particular interest in the study of polymer degradation because the products volatilized as a result of the thermal decomposition in vacuum consist almost entirely of the monomer, and also because the molecular weights of the residues can be conveniently measured.

Relatively little has been reported in the literature [1 to 6] [1] with regard to the degradation of polymethyl methacrylate prepared without the use of any initiator. Madorsky [1] and Straus and Madorsky [2] found such a polymethyl methacrylate to be considerably more stable (in terms of volatilization rates) at elevated temperatures in vacuum than a sample polymerized with the aid of benzoyl peroxide. They also found that in the course of pyrolysis, the residue of the benzoyl peroxide-polymerized polymer eventually achieved a stability (after about 50% of volatilization) comparable to that of the polymer polymerized without any initiator.

The main object of the present work was to determine molecular weights of the above two polymethyl methacrylate samples as functions of extent of volatilization at constant temperature for thermal degradation in vacuum. Also, it was desired to elucidate the nature of the temperature effect. In the case of the benzoyl peroxide-polymerized sample, it was of particular interest to obtain data beyond the first 50 percent of volatilization, where complicating effects of benzoyl peroxide might no longer be present.

2. Polymethyl Methacrylate Samples

Sample A was analyzed and found to contain approximately 0.6 percent of benzoyl peroxide. Its weight-average molecular weight was 146,000.[2] The monomer used in the preparation of sample B was degassed and sealed in an evacuated tube without any initiator. It was allowed to polymerize in bulk at −25° to −35° C. The weight-average molecular weight of the resulting polymer was 5,030,000 (see footnote 2).

[1] Figures in brackets indicate the literature references at the end of this paper.

[2] The molecular weights were determined by Louis Williams of the Bureau, using the light-scattering method.

3. Experimental Methods

The vacuum apparatus used in pyrolysis was that described previously [7] for the study of the rates of volatilization of polytetrafluoroethylene by the gas-pressure method. The specimen was inserted into a weighed Pyrex glass tube, 45 mm long and 6 mm inside diameter with one end closed, and was weighed on a semimicrobalance. The pyrolysis apparatus, with specimen in place, was kept under vacuum overnight to minimize desorption of gases from the walls of the apparatus during pyrolysis. The cylindrical external heater was so constructed that an essentially uniform temperature could be maintained over the entire specimen. The heater, after being kept at the desired temperature overnight, was moved into position in two steps, 10 min apart, during which time the current was increased by a predetermined amount and duration. The specimen reached the desired temperature in about 2 min after the heater was placed in final position. The temperature was kept within ±0.5° C. The volatile products were condensed during pyrolysis in a liquid-nitrogen trap located between the specimen and the mercury-vapor pump.

The polymer residue was dissolved out of the Pyrex glass tube with a minimum amount of distilled ACS-grade chloroform by using the small reflux apparatus shown in figure 1. Moderate reflux rates were used to avoid foaming, and complete solution usually occurred in less than 2 hrs. The Pyrex tube was then weighed to make certain that the residue was completely dissolved. The solution was allowed to stand overnight prior to viscosity measurement.

One milliliter of solution was required for an intrinsic viscosity determination. The semimicro-dilution viscometer and the techniques used have been described by the author in a previous publication [8]. Kinetic-energy corrections and errors due to drainage, surface tension, solvent evaporation, and the effects of shear rate of the polymethyl methacrylate solutions were negligible with this viscometer. The temperature of the water bath was maintained at 27.30 ±0.01° C. The flow time of the solvent was 195.7 sec. The latter was redetermined after each intrinsic-viscosity measurement, and at

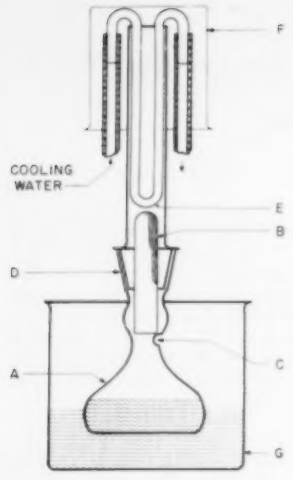

FIGURE 1. *Dissolving fused polymer from a tube.*

A, Weighing bottle containing solvent; B, tube containing fused polymer; C, indentation in the glass; D, tapered ground-glass connection; E, condenser tube; F, beaker for keeping out dust; G, heating bath.

no time was it found to have changed. Average deviation of flow time for solution reruns was less than 0.1 percent, and at least one rerun was always made.

A graphic method described previously by the author [9] was used for accurately calculating intrinsic viscosity from a single specific-viscosity determination. This method is applicable to a wide range of specific viscosities. However, for convenience in measuring the specific viscosity, a value close to 1.0 was generally obtained by adjusting the size of the original polymer specimen and the concentration of the solution according to predictions based upon the trends of the data.

4. Results

The weight-average molecular weight, M_w, was calculated from the intrinsic viscosity, $[\eta]$, using the equation $[\eta]=3.54\times10^{-5}M_w^{0.843}$. The constants in this equation were calculated from intrinsic-viscosity and light-scattering molecular-weight measurements of the original polymethyl methacrylate samples A and B. The above equation agrees satisfactorily with those reported in the literature for polymethyl methacrylate in chloroform [10, 11].

In table 1 are listed molecular weights of residues from pyrolysis of the two polymethyl methacrylate samples. Prior to pyrolysis at 320°, each specimen of sample A was preheated by raising it in a consistent manner from room temperature to 260° in 55 min in the vacuum apparatus. This prevented excessively rapid initial volatilization at 320° C.

In figure 2, weight-average molecular weight is plotted in terms of percentage of the original molecular weight against percentage volatilized at 320° C and at 150° C. Because of a significant temperature effect, it would be incorrect to join the two curves for sample A.

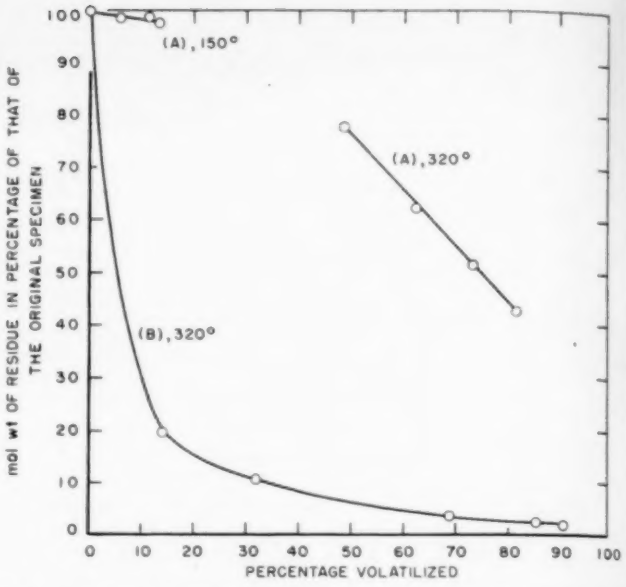

FIGURE 2. *Effect of degradation on the molecular weight of the residue.*

The nature of the molecular-weight change is better illustrated in figure 3, where log R is plotted against $1/M_w$, R being the ratio of the residue weight to the weight of the original specimen. Straight lines result, the slopes of which depend upon the temperature. (The first 48% of the volatilization of sample A in the experiments at 320° C occurred at a high rate, before the temperature of 320° C could

TABLE 1. *Molecular weights of residues from pyrolysis of polymethyl methacrylate*

Pyrolysis				Residue	
Temperature	Specimen weight	Duration	Volatilization	$[\eta]$	M_w
Sample A					
°C	*mg*	*min*	%		
			0	0.801	146,000
150	82.00	40	5.89	.792	144,400
150	78.32	120	11.13	.793	144,800
150	69.22	300	13.25	.785	143,000
320	99.96	10	48.57	.646	113,500
320	196.90	50	62.07	.538	91,300
320	201.14	100	73.16	.459	75,600
320	204.56	180	81.43	.391	62,500
Sample B					
			0	15.8	5,030,000
300	48.75	450	52.70	1.864	398,000
300	147.00	810	68.53	1.302	260,600
320	10.75	10	14.14	4.92	1,000,000
320	28.77	30	31.87	2.41	541,000
320	99.91	136	68.85	0.962	182,000
320	136.90	300	85.30	.680	120,600
320	240.80	420	90.69	.549	93,600
340	79.68	16	41.88	1.734	366,100
340	132.27	40	82.78	0.670	118,400
340	101.77	48	84.74	.608	105,600

be reached. For this reason it was experimentally impracticable to determine the molecular weights within this range of volatilization at this temperature.) From figure 3 it may be inferred that in the type of plot shown in figure 2, the higher the molecular weight, the more abruptly the molecular-weight curve drops, and also the higher the temperature, the more rapid the drop.

5. Theory for Log R as a Function of $1/M_w$

Defining: $R=m/m_o$, where m=weight of specimen remaining at time, t, and m_o=original weight of specimen; $K_2=(-100/R)(dR/dt)=-230.3$ (d log $R)/dt$=rate of volatilization in percentage of the residue per minute; $K_3=d(1/M_w)/dt$=rate of change of reciprocal weight-average molecular weight. As a consequence of the definitions,

$$\frac{K_2}{K_3}=-230.3\,\frac{d\log R}{d(1/M_w)}. \tag{1}$$

The object of the ensuing treatment is to indicate why K_2/K_3 might be expected to be very nearly constant for a given pyrolysis temperature.

A free-radical chain-reaction mechanism (stationary type) is assumed, in which the entire drop in molecular weight during pyrolysis is due to an intermolecular chain-transfer process. The initiation step of the chain reaction may be ignored, as no kinetic expression for this step is required for the present purpose.

The volatilization products of the thermal decomposition of polymethyl methacrylate consist almost entirely of the monomer [2]. As is customary in this case, it is assumed that each polymeric free radical resulting from the initiation process decreases in size by the consecutive splitting off of monomer units from its free-radical end (depropagation). Symbolically, for kinetic analysis

$$P_b \xrightarrow{k_d} P_{b-1}+M\uparrow$$

$$P_{b-1} \xrightarrow{k_d} P_{b-2}+M\uparrow$$

etc.,

where P_b is a polymeric free radical of degree of polymerization, b, and M represents a monomer molecule.

If K_d is the number of monomer units splitting off per gram of residue per minute,

$$K_d=k_d[P\cdot], \tag{2}$$

where $[P\cdot]$ is the number of free radicals per gram of residue, and k_d is the depropagation-rate constant. Since this depropagation step contributes almost the entire amount of the volatilization products, the rate of volatilization, K_2, may be expressed similarly:

$$K_2=k_d[P\cdot]\,\frac{100.1\times 100}{N}, \tag{3}$$

where N is the Avogadro number. (The molecular weight of the monomer is 100.1.)

The chain-transfer mechanism is assumed to be of the usual hydrogen-transfer type, in which a free-radical end acquires a hydrogen atom from a carbon atom in the backbone of another chain and becomes a polymer molecule with a saturated end, S. The molecule attacked splits into two fragments, one of which forms an unsaturated end, U, and the other fragment contains a free-radical end. The latter polymer fragment commences to split off monomer. The transfer process may be represented for kinetic analysis as follows (intermolecular type):

$$P_{b-z}+P_x\mathrm{H}P_y \xrightarrow{k_{tr}} P_{b-z}S+P_{\dot{z}}P_y$$

$$P_{\dot{z}}P_y \rightarrow P_{\dot{z}}+P_yU \text{ (rapid step)},$$

where H is the transfer hydrogen, z is the number of monomer units split off from the free radical prior to the transfer act, and P_x and P_y represent the two polymeric fragments formed from the molecule attacked at random, $P_x\mathrm{H}P_y$.

If K_{tr} is the number of transfer acts occurring per gram of residue per minute, k_{tr} is the transfer-rate constant, and [H] is the number of points at which transfer can occur per gram of residue, which is constant, then

$$K_{tr}=k_{tr}[P\cdot][\mathrm{H}]. \tag{4}$$

Because intermolecular chain transfer is assumed to be the sole cause of the molecular-weight decrease, it follows, as a close approximation within the experimental ranges of volatilization at 300° to 340° C, that

$$\frac{d\left(\frac{N}{M_n}\right)}{dt}=K_{tr}, \tag{5}$$

where M_n is the number-average molecular weight. The following is also assumed as a good approximation within these experimental ranges [12]:

$$\frac{M_n}{M_w}=g=\text{constant}. \tag{6}$$

Substituting for M_n and K_{tr} in eq (5),

$$K_3=\frac{g}{N}\times k_{tr}[P\cdot][\mathrm{H}]. \tag{7}$$

Termination of a reaction chain is assumed to occur merely when a free radical becomes reduced by depropagation to monomer size or to the point where it escapes as a polymeric fragment along with the monomer being evolved. This may be called "termination by free-radical depletion."

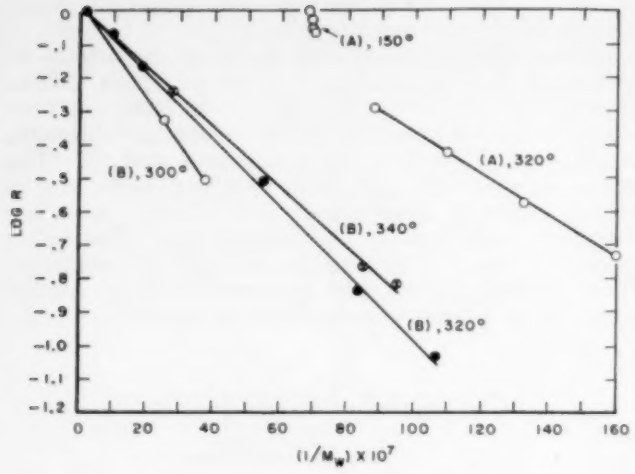

FIGURE 3. *Log R versus* $1/M_w$.

R is the weight of the residue at any given pyrolysis time divided by the original specimen weight.

Eliminating $[P\cdot]$ between eq (3) and (7),

$$\frac{K_2}{K_3}=\frac{k_d\times 1.001\times 10^4}{gk_{tr}[\mathrm{H}]}. \tag{8}$$

It has been assumed that g and [H] are constant. If it is further assumed that the rate constants, k_d and k_{tr}, are indeed constant at a fixed temperature, it follows that K_2/K_3 should be constant, and referring to eq (1), that $(d \log R)/[d(1/M_w)]$ should be constant. It is clear that the theory predicts for a given sample that a plot of log R against $1/M_w$ (as in fig. 3) will be a straight line for pyrolysis at a fixed temperature, independent of change in magnitude of K_2 and K_3, and that the slope of the plot will vary with the temperature, depending on the ratio, k_d/k_{tr}.

For the purpose of testing the freedom of the experimental slopes from dependence upon the magnitude of the rates, K_2 and K_3, it is fortunate that these rates have been found to vary with extent of degradation at 320° C. Both samples A and B showed decreasing rates, and at the end of the experimental ranges of pyrolysis the rates were about a third of the initial values in both cases. These results further support intermolecular chain transfer as the primary, or perhaps the sole, cause of the molecular-weight change. The experimental rate curves covering wide extents of degradation at 320° C, together with studies of the effects of benzoyl peroxide and of inhibitors, are planned for inclusion in a separate publication, in which the initiation mechanism may be elucidated.

In the case of sample A, 48 percent of volatilization occurs before the residue can reach 320°. If the actual values of log R versus $1/M_w$ for those specimens of A for which data were obtained at 320° were plotted for the first 48 percent of volatilization, the curve would reflect the lower temperatures in this range and the corresponding changes in slope. Therefore, the straight line obtained at 320° does not extrapolate back to the initial molecular weight at log $R=0$. Sample B incurs about 8 percent of volatilization before it can reach 320°. However, this amount is quite small for initial curvature to be indicated, and the straight lines do appear in this case to extrapolate to the initial molecular weight at log $R=0$.

The slope for sample B is 1.67 times that for sample A at 320° C. No satisfactory explanation is available at present for this difference. However, some heterogeneity in the molecular structure is suggested in the case of sample A, at least after the temperature of the sample has been raised sufficiently high. A possible reaction of some sort involving benzoyl peroxide and groups along the polymer chain, and resulting in a few points at which the probability of transfer is greatly enhanced, may be considered.

6. Activation Energies

Rearranging eq (8),

$$k_{tr}=\frac{1.001\times 10^4}{g[\mathrm{H}]}\times\frac{K_3k_d}{K_2}.$$

The constants may be combined and replaced with C_1:

$$k_{tr}=C_1\times\frac{K_3k_d}{K_2}. \tag{9}$$

Taking the logarithm of the latter expression and then the derivative with respect to $1/T$, where T is the absolute temperature,

$$\frac{d\log k_{tr}}{d(1/T)}=\frac{d\log K_3}{d(1/T)}-\frac{d\log K_2}{d(1/T)}+\frac{d\log k_d}{d(1/T)}. \tag{10}$$

It follows that

$$E_{tr}=E_3-E_2+E_d, \tag{11}$$

where E_{tr} and E_d are the activation energies for the chain transfer act and the depropagation act, respectively, and E_3 and E_2 are the apparent activation energies corresponding to the initial K_3 and K_2 rates.

If s represents the slope, $(d \log R)/[d(1/M_w)]$, from eq (1)

$$\frac{K_3}{K_2}=\frac{1}{-s230.3}. \tag{12}$$

Taking the common logarithm of this expression, and then the derivative with respect to the reciprocal of the absolute temperature,

$$\frac{d\log K_3}{d(1/T)}-\frac{d\log K_2}{d(1/T)}=-\frac{d\log(-s)}{d(1/T)}. \tag{13}$$

If each term is multiplied by -4.576×10^{-3} (the molar gas constant appearing in the Arrhenius equa-

tion, 1.9872×10^{-3} kcal mole^{-1} degree^{-1}, multiplied by -2.3026), eq. (13) becomes, for initial rates,

$$E_3-E_2=(4.576\times10^{-3})\frac{d\log(-s)}{d(1/T)}, \qquad (14)$$

where E_3 and E_2 are expressed in terms of kilocalories per mole.

From eq (11) one would expect E_3-E_2 to be constant within the experimental temperature range. Equation (14) could then be written as follows, for evaluation between temperatures, T_1 and T_2:

$$E_3-E_2=(4.576\times10^{-3})\frac{\log\frac{s_2}{s_1}}{\frac{1}{T_2}-\frac{1}{T_1}}. \qquad (15)$$

The apparent activation energies, E_3 and E_2, are based upon initial rates, and s should therefore be the initial slope. As s remains constant at constant temperature, however, the accuracy of the value of E_3-E_2 calculated through the use of eq (15) should in the present case be greater than that which might be obtained by the usual method of determining each activation energy separately from the initial rates.

The following experimental values of s are found for sample B: -13.79×10^4 at 300° C; -10.07×10^4 at 320° C; and -9.04×10^4 at 340° C. The resulting values calculated for E_3-E_2 are 10.6 kcal at 300° to 320° C and 3.9 kcal at 320° to 340° C. There seems to be no entirely satisfactory explanation for this difference, but the figure calculated for the 300° to 320° C range may be preferred because the rates of volatilization at 340° C are quite high from the experimental standpoint. It cannot be ascertained from the present data whether a systematic experimental error is actually involved at 340° C or whether a change in mechanism is indicated.

Cowley and Melville estimated the activation energy for depropagation, E_d, to be 18.5 kcal/mole from figures for the heat of polymerization (−13.0 kcal), and for the activation energy of propagation (5.5 kcal) [3]. If this value for E_d and the value for E_3-E_2 in the range 300° to 320° C are substituted in eq (11), a value of 29 kcal/mole is obtained as an estimate of the activation energy for the transfer act in the degradation of sample B.

7. References

[1] S. L. Madorsky, J. Polymer Sci. **11,** 491 (1953).
[2] S. Straus and S. L. Madorsky, J. Research NBS **50,** 165 (1953) RP2405.
[3] P. R. E. J. Cowley and H. W. Melville, Proc. Roy. Soc. (London) [A] **210,** 461 (1951).
[4] P. R. E. J. Cowley and H. W. Melville, Proc. Roy. Soc (London) [A] **211,** 320 (1952).
[5] N. Grassie and H. W. Melville, Proc. Roy. Soc. (London) [A] **199,** 1 (1949).
[6] S. Bywater, J. Phys. Chem. **57,** 879 (1953).
[7] S. L. Madorsky, V. E. Hart, S. Straus, and V. A. Sedlak, J. Research NBS **51,** 327 (1953) RP2461.
[8] V. E. Hart, J. Polymer Sci. **17,** 207 (1955).
[9] V. E. Hart, J. Polymer Sci. **17,** 215 (1955).
[10] J. H. Baxendale, S. Bywater, and M. G. Evans, J. Polymer Sci. **1,** 237 (1946).
[11] B. Baysal and A. V. Tobolsky, J. Polymer Sci. **9,** 171 (1952).
[12] E. W. Montroll and R. Simha, J. Chem. Phys. **8,** 721 (1940).

WASHINGTON, October 10, 1955.

Journal of Research of the National Bureau of Standards Vol. 56, No. 2, February 1956 Research Paper 2650

Thermal Expansion of Binary Alkaline-Earth Borate Glasses

Herman F. Shermer

The thermal expansivity of a number of calcium, strontium, and barium borate glasses are reported. The expansivity of the calcium and strontium borates increases with increasing alkaline-earth oxide concentration. The expansivity of the barium borate glasses is a minimum at about 20 mole percent of barium oxide. The expansivity measurements on the glasses were correlated with the density measurements in the liquid range. The expansivity of any composition is the lowest in the glassy (solid) region and is greater in the liquid region. The expansivity in a third region which was described as "very viscous" was not measured but was indicated to be greater than in either of the measureable regions. The density curves for each alkaline-earth borate series converges with increasing temperature.

1. Introduction

A study of the thermal expansion of the binary alkaline-earth borate glasses was undertaken as part of a comprehensive investigation of various physical properties of simple glass-forming systems. This report is the third of a series on the relationships between chemical composition and physical properties of the binary alkaline-earth borates. The first report [1] [1] was mainly concerned with the properties of the molten compositions, such as viscosity and surface tension, and the second [2] was concerned with the compressibility of the alkaline-earth borate glasses.

The plan of the present work was the determination of the relative effects of varying amounts of calcium, strontium, and barium oxides on the thermal expansion of borate glasses. It was desired to study these relationships over as wide a composition range as possible, but the region of glass formation was limited at low alkaline-earth oxide concentrations by the formation of two immiscible liquids, and at high concentrations by crystallization [4, 5].

2. Preparation of Glasses and Method of Test

The glasses investigated were made by melting the required amounts of reagent-grade chemicals in platinum crucibles at approximately 1,300° C. The alkaline-earth oxides were introduced to the batch in the form of carbonates, and the boric oxide was added as boric acid. The melts, which weighed approximately 500 grams, were stirred with a propellor-type platinum stirrer until they appeared clear (at least 1 hour), and then they were poured into a cold iron mold. These binary glasses were later annealed by holding them at 590° C for 3 hours and then cooling them at 3 deg C per hour for 30 hours, after which the power to the furnace was shut off, and the glasses were allowed to cool to room temperature. Polariscopic examination of the specimens revealed a slight amount of strain in the calcium borate glasses, but this strain was not detected in the expansion curves. The presence of strain is normally indicated by a decrease in the expansion with increase in the temperature in the range just below the point at which rapid expansion begins. The samples used in the determination of thermal expansion were cut from cylinders (approximately ½ in. in diameter and 3 in. long) that had been used for compressibility specimens in previous work [2].

Bridgman and Simon [3] have shown that a compaction of fused B_2O_3 occurs during compression measurements. As the glasses used in this study had been used previously for compressibility measurements and contained 63 to 84 mole percent of B_2O_3, one must consider the possibility that such compactions may have occurred. Weir and Shartsis [2] report a decrease in volume during compression testing on the order of 0.2 percent and also report it as being independent of B_2O_3 concentration. An increase of this magnitude was attributed to experimental error. Even if this compaction were real, it is believed that its magnitude is too small to seriously affect the expansion data. Bridgman and Simon [3] have indicated that time and/or temperature may be employed to restore the specimens to their original densities. In the present investigation it is believed that the period between the compressibility measurements and expansion measurements (approximately 6 months) and the heating of the specimens to 200° C preparatory to measurement minimized any possible effect of the previous compression measurements. An adjacent portion of the specimen was removed and analyzed by triple evaporation with HF and H_2SO_4.[2]

[1] Figures in brackets indicate the literature references at the end of this paper.

[2] The compositions were analyzed by Ernest B. Clark, formerly of the staff of the National Bureau of Standards.

Following the original determination of thermal expansion, an adjacent portion of the four samples of calcium borate glasses that showed strain was reannealed to determine what differences, if any, would be observed in the thermal-expansion curves. These glasses were reannealed by heating them to 655° C for 3 hours. They were then cooled at approximately 3 deg C per hour until they reached 455° C (68 hours), after which they were allowed to cool in the sealed furnace, with no further application of power.

The measurements of thermal expansion were made by the interferometer method of Peters and Cragoe [6] as modified by Saunders [7]. The test specimen was formed into a T-shaped spacer about 5 mm high, which was placed between two optically flat Vycor disks, the lower one of which served as an interference thermometer. This "sandwich" was placed in a metal cup with a fused-silica top to decrease any temperature gradients. This cup was placed within a resistance-type electric furnace, which was heated at 2 deg C per minute from room temperature to above the deformation point. The motion of the two sets of fringes, one set formed within the lower plate, which indicated the temperature, and the other formed between the two plates, which indicated the expansion, was recorded on photographic film, and the results were read from this film.

3. Results and Discussion

3.1. B_2O_3

In the study of the expansivity of the binary alkaline-earth borate glasses, it seemed desirable to know the coefficient of linear expansion and other characteristics of the expansion curve for boric oxide (B_2O_3) glass. Published data on the expansion of this glass are conflicting, as shown in the reviews of the subject by Morey [8] and Karkhanavala [9]. The differences seem to be caused primarily by different melting schedules and heat treatments and, as a result of this, differences in the amount of associated water [10]. Some of this water is retained from the boric acid, and other water may be adsorbed from the atmosphere after the glass is cooled. In order to reduce this water to an amount comparable with the other glasses measured in this investigation, the boric oxide glass was melted on the same schedule as the binary glasses, and all glasses were stored in kerosine. Each sample was cut and dried by heating to 200° C and then allowed to cool in the furnace overnight, and the expansion was determined the following day. The results of the determinations are shown graphically in figure 1 and are included for comparison in table 1. The small hump in the thermal expansion curve for B_2O_3 at about 160° C is indicative of the small amount of water present [9].

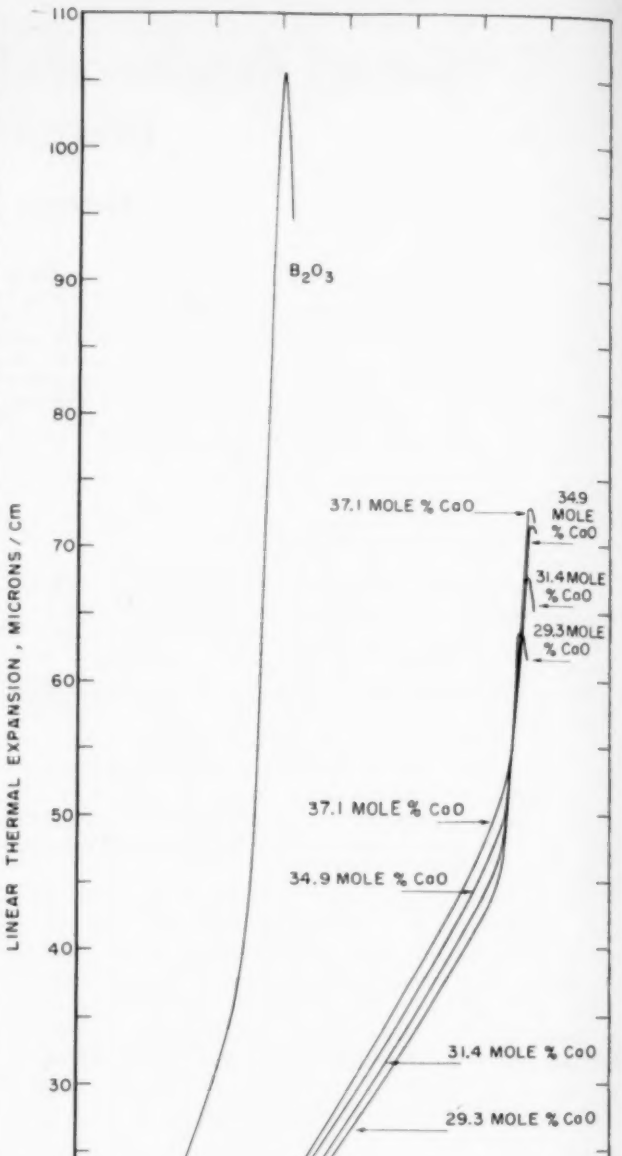

FIGURE 1. *Linear thermal expansion of some binary calcium borate glasses and fused* B_2O_3.

TABLE 1.—*Thermal expansivity of binary alkaline-earth borate glasses*

Chemical composition		Density (room temp)	Critical temp	Deformation temp	Average coefficients of expansion per degree C at—[a]					
RO	RO				Room to 100° C	100° to 200° C	200° to 300° C	300° to 400° C	400° to 500° C	500° to 600° C
Fused B_2O_3										
Mole %	*wt %*	*g/cm³*	*°C*	*°C*						
0.0	0.0	1.859	260	305	16.16×10^{-6}	13.77×10^{-6}	----------	----------	----------	----------
$CaO-B_2O_3$										
29.3	25.0	2.484	633	658	5.64×10^{-6}	6.08×10^{-6}	6.54×10^{-6}	7.16×10^{-6}	7.69×10^{-6}	8.68×10^{-6}
		Reannealed	646	662	5.49	6.02	6.39	7.13	7.71	8.09
31.4	27.0	2.531	647	665	5.73	6.31	6.74	7.67	7.92	8.85
		Reannealed	649	665	5.82	6.35	6.81	7.65	8.10	8.31
34.9	30.2	2.595	648	668	6.01	6.76	7.52	7.78	8.38	9.18
		Reannealed	656	668	6.62	6.75	7.47	7.85	9.50	9.21
37.1	32.3	2.633	643	669	6.40	7.04	7.46	8.22	8.69	9.55
		Reannealed	657	669	6.31	6.84	7.58	8.16	8.76	9.35
$SrO-B_2O_3$										
21.4	29.0	2.649	598	614	5.79×10^{-6}	6.22×10^{-6}	6.66×10^{-6}	7.28×10^{-6}	8.04×10^{-6}	----------
21.8	29.4	2.677	604	621	5.77	6.36	6.76	7.40	7.87	----------
26.0	34.4	2.802	619	635	5.85	6.46	7.03	7.76	8.68	----------
26.9	35.5	2.852	620	638	6.01	6.58	6.86	7.56	8.12	9.04×10^{-6}
		Remeasured	621	638	5.97	6.56	7.12	7.67	8.15	9.08
28.5	37.3	2.931	624	641	6.34	6.76	7.24	7.98	8.42	9.42
30.5	39.6	3.007	628	649	6.71	6.96	7.72	8.28	9.26	9.03
33.3	42.6	3.101	629	649	6.96	7.47	8.32	8.49	8.62	10.16
$BaO-B_2O_3$										
17.3	31.6	2.678	509	540	6.59×10^{-6}	6.69×10^{-6}	7.25×10^{-6}	7.80×10^{-6}	9.77×10^{-6}	----------
20.1	35.8	2.813	561	580	6.19	6.59	7.01	7.67	8.39	----------
23.7	40.6	2.996	575	595	6.43	6.64	7.02	7.71	8.21	----------
27.1	45.1	3.190	589	606	6.59	6.90	6.01	8.14	9.36	----------
29.0	47.5	3.289	587	606	6.82	7.46	7.89	9.48	10.39	----------
31.7	50.6	3.429	598	610	7.37	7.64	8.13	8.86	9.58	----------
36.0	55.4	3.630	594	609	7.86	8.48	8.91	9.68	10.74	----------

[a] The estimated accuracy of values of average coefficient of expansion per degree C is $\pm0.1\times10^{-6}$. The values given contain one additional figure for convenience in intercomparisons and better determination of greater temperature ranges.

3.2. Calcium Borates

The results of the thermal-expansion measurements of the calcium borate glasses are given in table 1 and figure 1. Although the four curves for the calcium borate glasses are similar, certain trends are apparent. The most obvious of these is the increase in expansivity with increasing concentration of calcium oxide. This is true in the region from room temperature to the "critical" temperature and also at the deformation point. The critical temperature is defined here as the approximate temperature at which rapid expansion begins. This is in contrast with the expansion of fused B_2O_3, which may be thought of as having the lowest concentration of calcium oxide, and which has the highest expansion. It may also be noted that the temperature of the deformation point increases with increasing calcium-oxide concentration. The deformation point is the highest point on an expansion curve obtained by the interferometer method and corresponds to the temperature at which viscous flow exactly counteracts thermal expansion.

The values of the coefficients of expansion of the calcium borates are included in table 1. Values for the reannealed samples are also given. In general, the reannealed glass had a slightly lower expansion below the critical temperature. It may also be noted that the height of the curve at the deformation point was greater in the reannealed sample, indicating a higher density at room temperature. The samples used for reannealing were not large enough for accurate density determinations.

The apparent increase in density of the calcium borate glasses when reannealed at 655° C indicated that the original annealing at 590° C was not continued for sufficient time for equilibrium conditions to be established at that lower temperature. It also indicates that the equilibrium condition of the glass before and after the original annealing corresponded to a temperature above the equilibrium condition that was established during the second annealing. The results of the original measurement of thermal expansion are shown in figure 1. The results of the second determination are in table 1 but because of the small differences in expansivity found upon reannealing the curves are not shown.

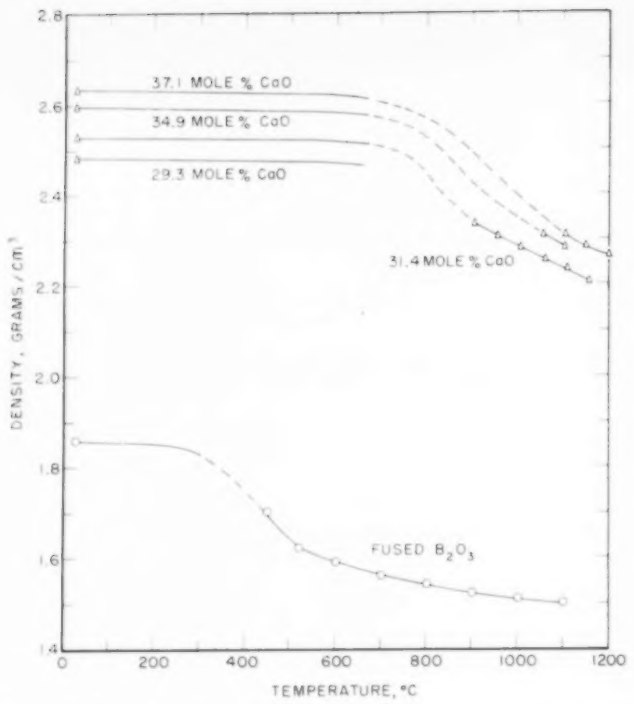

FIGURE 2. *Densities of some binary calcium borate glasses and liquids, with fused and liquid B_2O_3, as a function of temperature.*

Figure 2 shows the thermal-expansion curves for B_2O_3 and the binary calcium borates plotted as change in density with temperature. This method of presenting the data made possible the inclusion of density values in the liquid range that were obtained previously [1]. It has not been possible to obtain density values of the liquids when they are very viscous, but it is hoped that the interpolations are reasonable. Three characteristics of this set of curves are the convergence of the curves with increase in temperature, the greater change in density with temperature in the liquid range than in the solid range, and a middle range in which the glasses have higher coefficients of expansion than in either of the measurable ranges.

3.3. Strontium Borates

The thermal expansivity values for 7 strontium borate glasses are given in table 1 and the curves of 4 of them are shown in figure 3. Most of the characteristics of the calcium borate curves are repeated here. The expansivity from room temperature to the critical temperature and the expansivity and temperature at the deformation point all increased with increasing concentration of strontium oxide. Two determinations of the glass containing 26.9 mole percent of SrO are included in the table to illustrate the reproducibility of the results.

Figure 4 shows the thermal-expansion curves of the strontium borates plotted as part of the density-versus-temperature curves for these compositions.

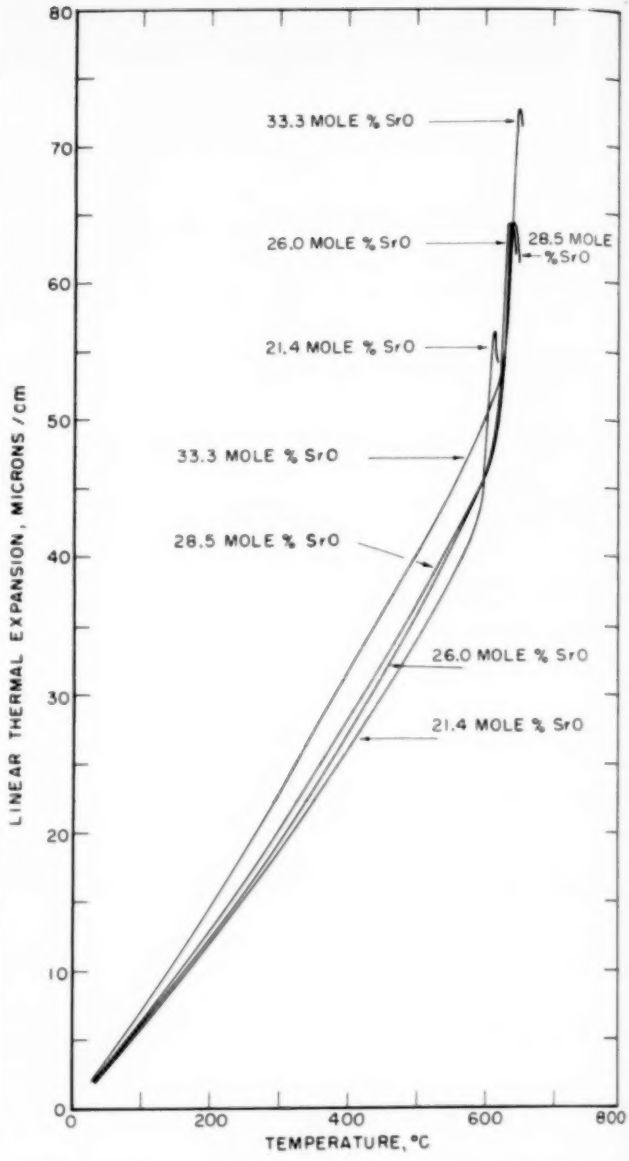
33.3 MOLE % SrO
26.0 MOLE % SrO
28.5 MOLE % SrO
21.4 MOLE % SrO
33.3 MOLE % SrO
28.5 MOLE % SrO
26.0 MOLE % SrO
21.4 MOLE % SrO
LINEAR THERMAL EXPANSION, MICRONS / cm
TEMPERATURE, °C

FIGURE 3. *Linear thermal expansion of four selected binary strontium borate glasses.*

This set of curves shows a behavior similar to that of the calcium borates in its covergence with increasing temperature, higher expansivity in the liquid range, and still higher expansivity in the very viscous range, which was not measured.

3.4. Barium Borates

The results of the measurements of thermal expansion of the barium borates are included in table 1, and the curves of four of them are shown in figure 5. There is one important variation in these results from those found in the calcium and strontium systems. This change is in the relative expansion of the glass containing 20.1 mole percent of BaO below that of the glass containing 17.3 mole percent of BaO. This decrease in expansivity with increase

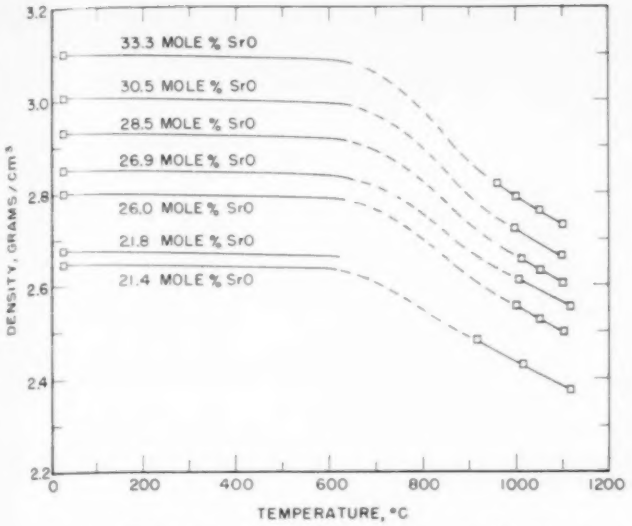

FIGURE 4. *Densities of some binary strontium borate glasses and liquids as a function of temperature.*

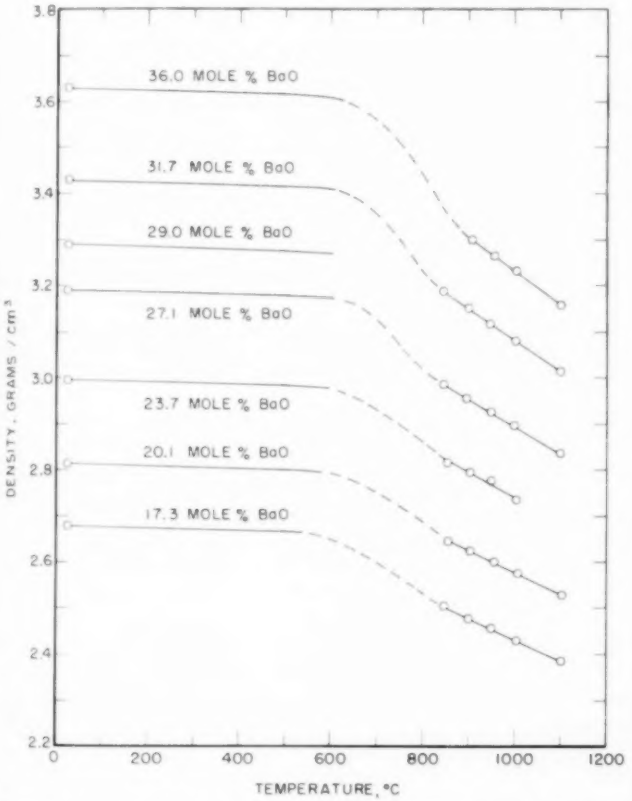

FIGURE 6. *Densities of some binary barium borate glasses and liquids as a function of temperature.*

in alkaline-earth oxide concentration is in the same relative direction as the decrease in expansivity between fused B_2O_3 and the barium borate glass containing the least amount of BaO. The regions of glass formation of the calcium and strontium borates do not contain minima because of their small compositional range. The glass-forming region of the barium borates, however, is longer and contains

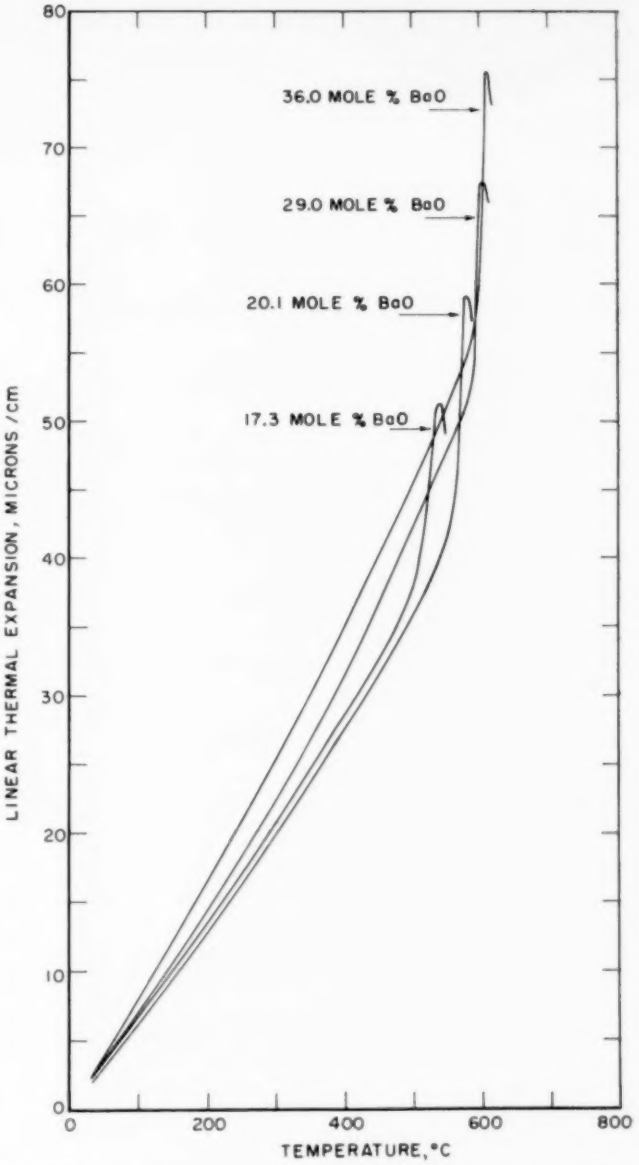

FIGURE 5. *Linear thermal expansion of four selected binary barium borate glasses.*

the minimum. This minimum is better seen in figure 7. Although the expansivity of the barium borate glasses, below the critical temperature, passed through a minimum in respect to composition, the total expansion from room temperature to the deformation point did not. It may be noted here that the minima in the values of the coefficients of expansion with concentration do not occur at the same point in the various temperature ranges. In general, there seems to be a translation of the minimum to higher barium-oxide concentrations with increase in temperature.

Figure 6 shows the relationship between densities, or expansivities, of the binary barium borates with temperature. The characteristics of this set of curves are similar to those discussed previously for the calcium and strontium borates.

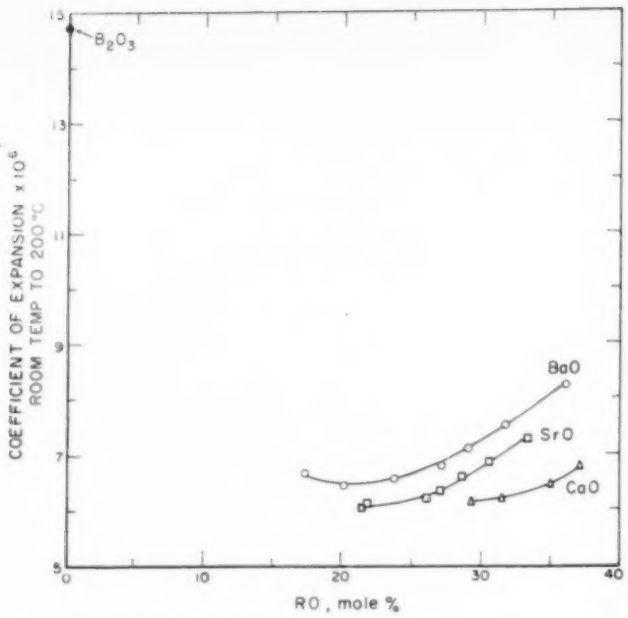

FIGURE 7. *Coefficient of linear thermal expansion as a function of composition of binary alkaline-earth borate glasses and fused* B_2O_3.

(△, calcium borates; □, strontium borates; and ○, barium borates.)

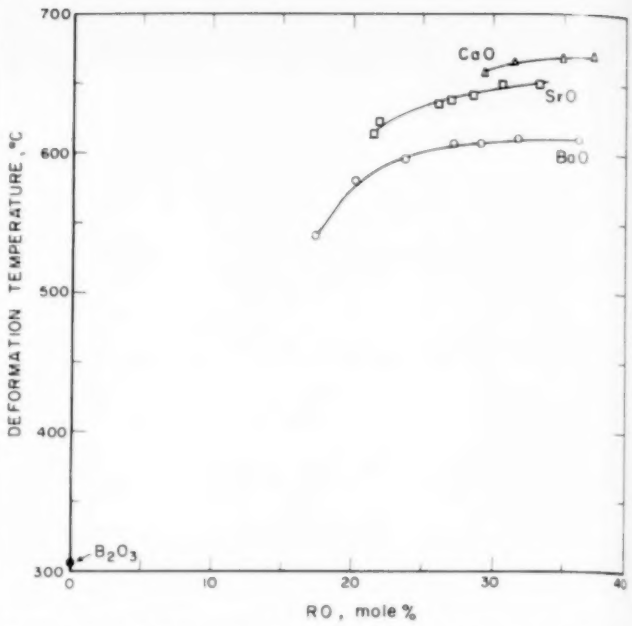

FIGURE 8. *Deformation temperature as a function of composition of binary alkaline-earth borate glasses and fused* B_2O_3.

(△, calcium borates; □, strontium borates; and ○, barium borates.)

3.5. Comparison of Thermal Expansivity of Alkaline-Earth Borates

A comparison of the mean coefficient of expansion over the range from room temperature to 200° C of the binary alkaline-earth borate glasses as a function of concentration of alkaline-earth oxide in mole percent is shown in figure 7. It is apparent that a minimum would have to occur in each of the curves if glasses could be made with lower concentrations of alkaline-earth oxides. There is not sufficient information available to determine the location of the minima in the calcium and strontium curves.

Figure 8 shows a comparison of the deformation temperatures of the binary borate glasses as a function of alkaline-earth oxide concentration in mole percent. These curves show that at comparable compositions the calcium borate glass has the highest temperature at its deformation point, followed by the strontium and then the barium composition. This is in the same order as the melting points of the three alkaline-earth oxides.

4. Calculation of Thermal Expansion From Composition

Much work has been done in the past in an effort to find a series of factors from which thermal expansion could be predicted from the composition of various glasses. Sun and Silverman [11] compiled the results of several of these investigations. Among the oxides included in their compilation are three that are applicable to the present investigation, namely, B_2O_3, CaO, and BaO. The values assigned to these oxides by various investigators leave much to be desired. Figure 7 shows that the expansion-versus-composition curves of the binary alkaline-earth borate glasses are not linear, and, therefore, it would seem that in this case the coefficient of thermal expansion is not an additive property.

5. Coordination of B_2O_3

The thermal expansivities of alkaline-earth borate glasses are of special interest because they exhibit the so-called "boron anomaly"; i. e., they show minima with respect to composition. Warren and Pincus [12] offer an explanation for this anomaly. It concerns the ability of the boron atom to change from triangular to tetrahedral coordination when an oxide such as CaO is present and supplies the necessary oxygen. It is believed that fused B_2O_3 is triangularly coordinated, and that with the addition of CaO, increasing amounts of boron change to tetrahedral coordination. Stegmaier and Dietzel [13] demonstrated that beyond a point determined by the particular oxides present, any additional content of alkali or alkaline-earth oxides will tend to reverse the process, i. e., change the B_2O_3 from fourfold to threefold coordination. A mathematical approach to the problem such as that of Warren and Pincus requires more X-ray data on the particular systems of glasses under study than are now available. An

alternate approach is from the measurements of physical properties. The measurement of thermal expansion seems to be quite useful in this respect. The minima in the thermal-expansion-composition curves shown in figure 7 are interpreted as indicating maxima in the tetrahedral coordination of B_2O_3. This seems to be in accord with the fact that the BO_4 tetrahedra tend to strengthen the structure and therefore have a lower expansion.

6. Summary and Conclusions

The thermal expansivity of glasses formed in the three binary alkaline-earth borate series was measured. The thermal expansivity of the glasses increased with increasing concentration of calcium or strontium oxide. The expansivity of the binary barium borate glasses went through a minimum with changing concentration of barium oxide. A minimum was implied in the other curves by the high relative expansion of fused B_2O_3. It was not found possible to obtain additive factors for the calculation of thermal expansion that would be applicable to these compositions.

The results were correlated with the density values obtained previously in the liquid range in order that the relationship between expansion and temperature could be studied over a greater temperature range. The expansivity of the solid glasses was the lowest, and that of the measurable liquids was much higher. The change in density across the very viscous region was such as to show a still greater expansivity in this range. The density curves were found to converge with increase in temperature.

7. References

[1] Leo Shartsis and H. F. Shermer, Surface tension, density, viscosity, and electrical resistivity of molten binary alkaline-earth borates, J. Am. Ceram. Soc. **37,** 544 (1954).

[2] Charles E. Weir and Leo Shartsis, Compressibility of binary alkaline-earth borate glasses, J. Am. Ceram. Soc. (submitted for publication).

[3] P. W. Bridgman and I. Simon, Effects of very high pressures on glass, J. Appl. Phys. **24,** 405 (1953).

[4] E. P. Flint and L. S. Wells, The system lime-boric oxide-silica, J. Research NBS **17,** 745 (1936) RP941.

[5] Ernest M. Levin and George M. Ugrinic, The system barium oxide-boric oxide-silica, J. Research NBS **51,** 37 (1953) RP2430.

[6] C. G. Peters and C. H. Cragoe, Measurements on the thermal dilation of glass at high temperatures, BS Sci. Pap. **16,** 449 (1920) S393.

[7] James B. Saunders, An apparatus for photographing interference phenomena, J. Research NBS **35,** 157 (1945) RP1668.

[8] G. W. Morey, Properties of glass, 2d ed., p. 273 Am. Chem. Soc. Monograph No. 124 (Reinhold Publishing Corp., New York, N. Y., 1954).

[9] M. D. Karkhanavala, Bibliography of thermal expansion of glasses, Glass Ind. **33,** 404 (1952).

[10] James J. Donoghue and Donald Hubbard, Thermal expansion studies of boric oxide glass and crystalline boric oxide, J. Research NBS **27,** 371 (1941) RP1425.

[11] Kuan-Han-Sun and Alexander Silverman, Additive factors for calculating the coefficient of thermal expansion of glass from its composition, Glass Ind. **22,** 114, 125 (1941).

[12] B. E. Warren and A. G. Pincus, Atomic consideration of immiscibility in glass systems, J. Am. Ceram. Soc. **23,** 301 (1940).

[13] W. Stegmaier and A. Dietzel, Die Bedeutung der Basizität von Glasschmelzen und Versuche zu deren Messung. Teil II, Glastech. Ber. **18,** 353 (1940).

WASHINGTON, November 1, 1955.

Journal of Research of the National Bureau of Standards Vol. 56, No. 2, February 1956 Research Paper 2651

Dielectric Relaxation for a Three-Dimensional Rotator in a Crystalline Field: Theory for a General Six-Site Model

Benjamin M. Axilrod

A theory of dielectric relaxation is presented for a generalized six-site model where the transition probabilities for the turning of dipoles from one orientational site to another are arbitrary. The sites are arranged in three dimensions. The nature of the set of discrete relaxation times generated by this model is examined in a general manner. It is found that the relaxation times are all real and positive and the range of the relaxation times is established.

1. Introduction

Previous work [1][1] with two simple models of a rather restricted nature has been sufficient to indicate that a set of discrete dielectric relaxation times can arise in a lattice consisting of dipoles that may occupy orientational sites arranged in three dimensions. As in studies on the single-axis rotator [2, 3], the source of the set of relaxation times was the anisotropy in the crystalline field, which hindered the turning of dipoles from one orientational site to another.

In the present paper the purpose is to extend the treatment of the three-dimensional rotator problem discussed in reference [1] by constructing the rate equations for a six-site model with *arbitrary* transition probabilities in order to examine the general nature of the set of relaxation times.

2. General Six-Site Model

2.1. Model

A model in which a dipole of moment μ on each lattice point can orient in any six directions is considered. These equilibrium orientations are along the Cartesian coordinate axes, x, y, and z (fig. 1 (a)). As in previous work [1, 2, 3], the following conditions are assumed:

(a) There is no correlation in the motion of dipoles on different lattice points.

(b) The barrier system is the same for all molecules in the lattice.

(c) The only elementary process is a reorientation to an adjacent site (single jump hypothesis, *S-J*). It should be noted that the general results obtained do not depend upon the orthogonal site orientations exhibited in figure 1 (a). This model was selected because it serves as well as any other for the general discussion and it was desirable to derive certain explicit expressions useful for polarizability calculations for this special case.

The transition probability for the turning of a dipole from a site i to an adjacent site j is given by

$$k_{ij}=Be^{\frac{-W_{ij}}{kT}} \tag{1}$$

where B is a frequency factor, k is Boltzmann's constant, and T is the absolute temperature. The quantity W_{ij} is the local free energy of activation barrier, which must be surmounted by a dipole in turning from site i to site j (fig. 1 (b)). The transition probability for the jump j to i, k_{ji}, is given by eq (1) with W_{ji} in place of W_{ij}. As transitions are permitted from a site i to four adjacent sites, there are 24 elementary process transition probabilities k_{ij} with $i, j=1, 2, \ldots 6$, and $i\neq j$ in the general model. From physical considerations it is shown in the appendix (section 3.1) that of these 24 constants only 17 are independent, and that relations exist for the k_{ij} corresponding to a closed circuit of transitions and the inverse circuit. Thus, if we consider the series of site-to-site transitions $1\rightarrow2$, $2\rightarrow3$, $3\rightarrow1$, and the inverse circuit $1\rightarrow3$, $3\rightarrow2$, $2\rightarrow1$, we find [2]

$$k_{12}k_{23}k_{31}=k_{13}k_{32}k_{21}. \tag{2a}$$

Other relations such as the above must apply, one for each site triplet for the remaining seven octants:

$$k_{13}k_{34}k_{41}=k_{14}k_{43}k_{31} \tag{2b}$$

$$k_{14}k_{45}k_{51}=k_{15}k_{54}k_{41} \tag{2c}$$

$$k_{15}k_{52}k_{21}=k_{12}k_{25}k_{51}; \tag{2d}$$

the four remaining equations, (2e) through (2h) are obtained from the equations above by substituting the subscript 6 for 1. Any one of the set of eight relations in eq (2) may be derived from the other seven.[3] These are the basic equations which restrict the arbitrary choice of the k_{ij} for the six-site model. Equations (2) are also needed for a mathematical proof noted later.

[1] Figures in brackets indicate the literature references at the end of this paper.

[2] A single relation of this type was given in reference 3 for single-axis rotators (see eq (7) and (25)).

[3] For example, eq (2e), $k_{42}k_{23}k_{34}=k_{43}k_{32}k_{24}$, may be obtained as the quotient [eq (2a)×(2b)×(2c)×(2d)]/[eq (2f)×(2g)×(2h)].

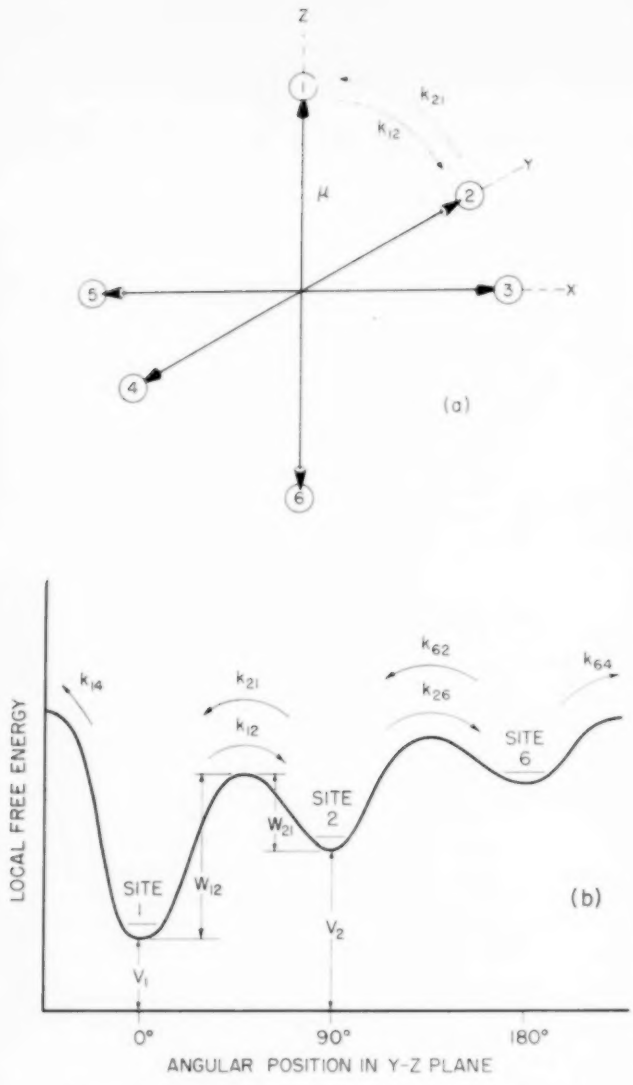

FIGURE 1. *General six-site Cartesian axes model.*

(a) The equilibrium orientations of the dipole moment μ. (b) Local free-energy barrier as a function of angular position in the y–z plane through sites 1, 2, and 6. W_{12} is the barrier for a transition from site 1 to site 2 and W_{21} is the barrier for the reverse transition. V_1 and V_2 are the free energies for sites 1 and 2, respectively, relative to an arbitrary zero.

2.2. Rate Equations

Assume a lattice with a total of N dipoles where the number of dipoles oriented in the ith site at any time t is given by N_i. The summation of the N_i is always N. The number of dipoles turning per unit time from a given site i to an adjacent site j is $k_{ij}N_i$, and the number entering site i from j is $k_{ji}N_j$; the total leaving site i to turn to adjacent sites is $\sum_{j,j\neq i} k_{ij}N_i$. Accordingly, the differential equations for the change in population of each site are [4]

$$\left.\begin{aligned}
\frac{dN_1}{dt} &= -(k_{12}+k_{13}+k_{14}+k_{15})N_1 + k_{21}N_2+k_{31}N_3+k_{41}N_4+k_{51}N_5\\
\frac{dN_2}{dt} &= k_{12}N_1-(k_{21}+k_{23}+k_{25}+k_{26})N_2 + k_{32}N_3+k_{52}N_5+k_{62}N_6\\
\frac{dN_3}{dt} &= k_{13}N_1+k_{23}N_2-(k_{31}+k_{32}+k_{34}+k_{36})N_3 + k_{43}N_4+k_{63}N_6\\
\frac{dN_4}{dt} &= k_{14}N_1+k_{34}N_3-(k_{41}+k_{43}+k_{45}+k_{46})N_4 + k_{54}N_5+k_{64}N_6\\
\frac{dN_5}{dt} &= k_{15}N_1+k_{25}N_2+k_{45}N_4 - (k_{51}+k_{52}+k_{54}+k_{56})N_5+k_{65}N_6\\
\frac{dN_6}{dt} &= k_{26}N_2+k_{36}N_3+k_{46}N_4 + k_{56}N_5-(k_{62}+k_{63}+k_{64}+k_{65})N_6
\end{aligned}\right\} \quad (3)$$

The molecular relaxation times, τ_β, will be included in the solutions of the above equations.

2.3. Characteristic Determinant and Its Properties

Solutions of linear homogeneous differential equations of the type shown in eq (3) are of the form

$$N_i = \sum_{\beta} C_{i\beta} e^{f_\beta(k)t}, \quad (4)$$

where the symbol $f_\beta(k)$ represents a function of some or all of the k_{ij}. The functions $e^{f_\beta(k)t}$ are referred to as decay functions, since the $f_\beta(k)$ are always negative for $\beta \geqq 2$ (see below). The index β refers to the mode of decay. Each decay function indicates the rate at which a particular mode of decay promotes the attainment of equilibrium after the abrupt removal of a disturbance. The $f_\beta(k)$ are obtained by forming the characteristic determinant of eq (3) and solving for its eigenvalues. This characteristic determinant is

$$\Delta(\boldsymbol{D},k_{ij}) = \begin{vmatrix}
A_1 & -k_{21} & -k_{31} & -k_{41} & -k_{51} & 0\\
-k_{12} & A_2 & -k_{32} & 0 & -k_{52} & -k_{62}\\
-k_{13} & -k_{23} & A_3 & -k_{43} & 0 & -k_{63}\\
-k_{14} & 0 & -k_{34} & A_4 & -k_{54} & -k_{64}\\
-k_{15} & -k_{25} & 0 & -k_{45} & A_5 & -k_{65}\\
0 & -k_{26} & -k_{36} & -k_{46} & -k_{56} & A_6
\end{vmatrix}, \quad (5a)$$

[4] By the S-J hypothesis, $k_{16}=k_{61}=k_{21}=\ldots=k_{51}=0$.

where we let $\boldsymbol{D}=d/dt$ and define A_1, A_2, A_3, . . . as

$$\begin{aligned} A_1&=\boldsymbol{D}+k_{12}+k_{13}+k_{14}+k_{15},\\ A_2&=\boldsymbol{D}+k_{21}+k_{23}+k_{25}+k_{26},\\ A_3&=\boldsymbol{D}+k_{31}+k_{32}+k_{34}+k_{36},\\ &\vdots\\ A_6&=\boldsymbol{D}+k_{62}+k_{63}+k_{64}+k_{65}. \end{aligned} \tag{5b}$$

The characteristic determinantal equation, obtained by setting Δ equal to zero in eq (5a), has six roots, or eigenvalues, f_β, for the operator $\boldsymbol{D}$. The nature of the elements in Δ permits one to answer some questions regarding the eigenvalues and, hence, about the relaxation times, τ_β.

The following questions may be raised: Are the eigenvalues real, what is their sign, what is their range, and are they distinct for the most general case, i.e., when the k_{ij} are distinct? The eigenvalues can be shown to be real by applying a theorem due to Goldberg.[5] The line of reasoning is briefly thus: From the theory of matrices the characteristic determinant of a symmetric matrix has real roots. Hence, if a symmetric matrix, S, can be constructed that has the same characteristic determinantal equation as Δ, i.e., $\Delta=0$, then the eigenvalues of Δ will be real. Sufficient conditions for forming such a matrix S with the same roots as Δ are the set of relations given by eq (2) and the inequalities $k_{ij}\geq 0$. Since eq (2) and $k_{ij}\geq 0$ are imposed by physical considerations, it follows that the eigenvalues are always real.

The sign and range of the eigenvalues f_β are specified by applying a theorem derived by Gerschgorin [4] and rediscovered by Brauer [5] regarding the areas in the complex plane in which the roots of a matrix lie; it can be shown (see appendix, section 3.3) that for our particular case, eq (5a), the eigenvalues lie between zero and twice the most negative diagonal element in the matrix (a_{ij}) derived from Δ in eq (5a) by setting $\boldsymbol{D}=0$ and changing the sign. Since, by definition, $k_{ij}\geq 0$, the roots are all negative.

The proof that the eigenvalues are distinct if the k_{ij} are distinct has not been accomplished.

From the theory of matrices we obtain two other properties of the characteristic determinant Δ. In the matrix (a_{ij}), defined above, it is evident (see eq (5b)) that each column sum vanishes. This indicates that one eigenvalue of Δ corresponds to the root $\boldsymbol{D}=0$. Next, the trace or diagonal sum of a matrix (b_{ij}) is equal to the sum of the eigenvalues, $\sum_s \lambda_s$, of the characteristic determinant $|b_{ij}-\lambda\delta_j^i|$, where δ_j^i is the Kronecker delta. From eq (5) it is seen that for the matrix $(-a_{ij})$ the diagonal sum is $\sum_{i,j}' k_{ij}$, where the prime means $i\neq j$. Since the eigenvalues of the characteristic determinant are unchanged if each element is replaced by its negative, the sum of the eigenvalues of Δ is $-\sum_{i,j}' k_{ij}$. The latter property is useful as a check when the eigenvalues are determined in a particular problem.

[5] See appendix, section 3.2.

2.4. Relaxation Times

With the general results obtained in section 2.3, we may write the solutions of the rate equations, noting that f_1 is zero, in the form

$$\begin{aligned} N_i&=C_{i1}+C_{i2}e^{f_2(k)t}+\ \ldots\\ &=C_{i1}+C_{i2}e^{-t/\tau_2}+\ \ldots \end{aligned} \tag{4'}$$

where the τ_β are defined as the molecular relaxation times [1,2,3]

$$\tau_\beta=-1/f_\beta(k). \tag{6}$$

Since we have shown that the f_β are all real and negative, it follows that the τ_β for the general six-site Cartesian axes model are all real and positive. As implied earlier, eq (4′) show how and at what rate a system tends to return to equilibrium after the abrupt removal of a disturbance such as a static electric field. Thus, for any arbitrary choice of the k_{ij}, consistent with eq (2), the return of the system to equilibrium is described by an exponential decay and cannot include any oscillatory modes.

Also, from the application of Gerschgorin's Theorem to the range of the eigenvalues, we find that the shortest relaxation time $\tau_{\min}$ is [6]

$$\tau_{\min}\geqq\frac{1}{2|a_{mm}|}, \tag{7}$$

where a_{mm} is the most negative diagonal element in the matrix (a_{ij}) defined in section 2.3. If k_{pq} is the largest of the k_{ij}, eq (5) and (7) lead to

$$\tau_{\min}\geqq\frac{1}{8k_{pq}}. \tag{8}$$

The above results cover the inferences that may be readily drawn regarding the molecular relaxation times for the general six-site model.

2.5. Dielectric Relaxation Spectrum

If we assume the molecular and macroscopic relaxation times are equal, an approximation used previously [1,2,3,5], the molecular relaxation times τ_β describe the approach to equilibrium of the polarization. The coefficients $C_{i\beta}$ (for $\beta\geqq 2$) in general measure the "strength" of each mode contributing to the relaxation process. In the case where we consider the restoration of equilibrium following the removal of a static electric field, the polarization

[6] In eq (7) the symbol $|a_{mm}|$ represents the absolute value of the a_{mm}.

$P(t)$ decays with time as

$$P(t)=\sum_{\beta}P_{\beta}e^{f_{\beta}(k_{ij})t}=\sum_{\beta}P_{\beta}e^{-t/\tau_{\beta}}. \tag{9}$$

The coefficients P_β, and hence the orientational polarizabilities α_β associated with each mode, may be obtained from the quantities $C_{i\beta}(\beta\geqq 2)$ for a particular model by standard methods [1]. The α_β are calculated assuming a polycrystalline substance.

We note that for sinusoidal fields eq (9) leads to the approximate expression [1,6]

$$\epsilon''(\omega)\cong K\sum_{\beta}\alpha_{\beta}\omega\tau_{\beta}/(1+\omega^2\tau_{\beta}^2), \tag{10}$$

where $\epsilon''(\omega)$ is the dielectric-loss factor as a function of angular frequency ω, K is a constant, and α_β is the orientational polarizability associated with the βth mode. Although the expression is not exact, it is sufficient for an approximate analysis of the general characteristics of the dielectric relaxation spectrum. For the case of a single relaxation time, eq (10) reduces to the form of the Debye equation [7] for $\epsilon''(\omega)$.

The coefficients $C_{i\beta}$ (and hence the P_β and α_β) cannot be obtained explicitly in the general case as they depend (eq (3) and (4)) on the eigenvalues, and the latter cannot be expressed explicitly in terms of the k_{ij}. As a consequence, we have not been able to prove in the general case, where the k_{ij} are distinct, that all relaxation modes are active in the dielectric spectrum. However, the latter situation seems quite possible, since in earlier calculations inactive modes (compensatory reorientation of dipoles to maintain a net dipole moment of zero) were formed only for very simple models, such as those containing two pairs of equivalent sites.

To obtain further information about the dielectric behavior of dipolar systems represented by the general six-site model, it is necessary to examine special models. This is planned for a subsequent paper.

A few useful formulas to apply to special models are given in the appendix, section 3.4.

The author is indebted to John D. Hoffman for numerous helpful discussions regarding the general subject and to Karl Goldberg and Martin Greenspan for assistance with mathematical aspects.

3. Appendix

3.1. Relations Between k_{ij}

Let the free energies relative to an arbitrary zero of energy for two adjacent sites i and j be designated as V_i and V_j, and the free-energy barriers for i to j and j to i transitions be defined as W_{ij} and W_{ji}, respectively. The height of the free-energy barrier between sites i and j, *referred to the zero of energy*, is then

$$W(i,j)=V_i+W_{ij}=V_j+W_{ji}. \tag{11a}$$

Consider a series of transitions i to j, j to l, l to i for a closed circuit of three adjacent sites and write the equations corresponding to eq (11a) for the barrier heights referred to the zero of energy

$$j\rightarrow l \quad W(j,l)=V_j+W_{jl}=V_l+W_{lj} \tag{11b}$$

$$l\rightarrow i \quad W(l,i)=V_l+W_{li}=V_i+W_{il}. \tag{11c}$$

The sum of the eq (11) is

$$W_{ij}+W_{jl}+W_{li}=W_{ji}+W_{lj}+W_{il}. \tag{12}$$

If we recall the definition of k_{ij}, eq (1), inspection shows that eq (12) corresponds to log $(k_{ij}k_{jl}k_{li})$= log $(k_{ji}k_{lj}k_{il})$, and hence

$$k_{ij}k_{jl}k_{li}=k_{il}k_{lj}k_{ji}. \tag{13}$$

The same type of relations, eq (12) and (13), can be obtained for any closed circuit of transitions between adjacent sites with three or more jumps to the circuit.[7] For the six-site model there are seven independent relations, such as eq (13), namely, any seven of the eight eq (2). All others and those involving more sites are derivable from eq (13). Accordingly, of the 24 transition probabilities only 17 are independent. This is plausible on physical grounds. The local free-energy system of the general model is fixed when six minus one site energies and 12 barriers $W(i, j)$ are specified; the "minus one" arises because the zero of energy is arbitrary.

The following geometrical argument illustrates how all product relations of the type in eq (13), but involving more sites, can be constructed from suitable products of the product relations given in eq (2) for three adjacent sites.

The six orientational sites (fig. 1) are located at the corners of an octahedron. Associated with the product relations on the k_{ij}, eq (13), for a closed circuit of transitions between the adjacent sites i, j, l, is the circuit of the perimeter of the face with vertices i, j, l, and the inverse circuit. Consider a closed circuit along the edges of the octahedron connecting the successively adjacent sites $i, j, l, \ldots, m, i$, for example, where there are 4, 5, or 6 sites. This closed circuit divides the octahedron, a simply connected surface, into two parts, each of which is constituted of triangular faces; for convenience, choose the surface with the fewer faces, labeled $T_1, \ldots, T_p$. If we traverse in succession in the same sense [8] as that on the whole perimeter $(i, j, l, \ldots, m, i)$, the perimeters of each of the triangular faces $T_1, \ldots, T_p$ this is the same as traversing the bounding path $i, j, l, \ldots,$

[7] An alternate method of arriving at product relations of the type in eq (13) or eq (2) is to invoke "detailed balancing" for each pair of adjacent sites. This means that at equilibrium the number of dipoles turning in unit time from site i to site j is equal to the number turning from site j to site i, or $k_{ij}C_{i}=k_{ji}C_{j}$; C_i is the equilibrium number of dipoles in the ith site. For a particular case, sites 1, 2, 3, we may then write $k_{12}C_{1}=k_{21}C_{2}$, $k_{23}C_{2}=k_{32}C_{3}$, and $k_{31}C_{3}=k_{13}C_{1}$. The product of the last three equations yields eq (2a), $k_{12}k_{23}k_{31}=k_{21}k_{32}k_{13}$.

[8] That is, if the perimeter of the portion of the surface bounded by the sites $(i, l, \ldots, m, i)$ is traversed in a clockwise sense by the above sequence, then each of the constituent triangles is traversed in the same sense.

m, i. Hence if we multiply the product equations such as (13) for the triangles $T_1, \ldots, T_p$, traversing their edges in the correct sense, we obtain the corresponding product relation for the circuit $(i, j, l, \ldots, m, i)$ and the inverse circuit $(i, m, \ldots, l, j, i)$. In this way the k_{ij} product relation for any sequence of connected sites can be formed by multiplying the product relations for the enclosed triangular circuits.

3.2. Application of Goldberg's Theorem [9] to the Matrix for the Six-Site Model

Theorem: If a real matrix $A=(a_{ij})$ of order n has the properties $a_{ij}\geq 0$ for $i, j=1, \ldots, n$ with $i\neq j$ and

$$a_{i_1 i_2} a_{i_2 i_3} \ldots a_{i_m i_1} = a_{i_2 i_1} a_{i_3 i_2} \ldots a_{i_1 i_m} \qquad (14)$$

for all $(i_1, \ldots, i_m)$ belonging to $(1, \ldots, n)$, $m\geq 3$, then all the characteristic roots of A are real.

We wish to apply the theorem to the matrix $-\Delta_0$ derived from Δ in eq (5a) by letting $\boldsymbol{D}$ be zero and changing the signs of the elements. If we let a_{ij} be the element of $-\Delta_0$ in the ith row and the jth column, the usual order of index notation, we note that for $i\neq j$

$$a_{ij}=k_{ji}, \qquad (15)$$

i. e., the order of indices is reversed on the k's. Hence with eq (15), eq (14) can be written as follows, after interchanging the left and right sides and then reversing the factor order on the right side:

$$k_{i_1 i_2} k_{i_2 i_3} \ldots k_{i_m i_1} = k_{i_2 i_1} k_{i_3 i_2} \ldots k_{i_1 i_m}$$

$$= k_{i_1 i_m} \ldots k_{i_3 i_2} k_{i_2 i_1}. \qquad (14')$$

Equation (14′) now evidently equates the product of k_{ij}'s for the closed circuit of m sites $(3\leq m\leq 6)$ $i_1\rightarrow i_2$, $i_2\rightarrow i_3$, . . . , $i_m\rightarrow i_1$ to the corresponding product for the inverse circuit $i_1\rightarrow i_m$, . . . , $i_2\rightarrow i_1$. There are two types of circuits: (a) circuits in which at least one successive pair i_p, i_q are nonadjacent sites, and (b) circuits in which all successive site pairs are adjacent. Since by the *S-J* hypothesis $k_{i_p i_q}\equiv k_{i_q i_p}\equiv 0$ for all nonadjacent site pairs, eq (14′), and hence eq (14), is valid for case (a). Next we have indicated in section 3.1 that closed-circuit product relations of the type eq (14′) are valid for a sequence of three or more adjacent sites. Hence our matrix $-\Delta_0$ for the general six-site model satisfies the above theorem.

3.3. Range of Eigenvalues

Brauer [5] has derived the following theorem regarding the characteristic roots (eigenvalues) of a matrix.

Theorem: Let $A=(a_{ij})$ be an arbitrary matrix and

$$\sum_{\substack{j=1\\ j\neq i}}^{n} |a_{ij}| = P_i, \quad \sum_{\substack{i=1\\ i\neq j}}^{n} |a_{ij}| = Q_j.$$

Each characteristic root λ lies in at least one of the circles

$$|\boldsymbol{z}-a_{ii}|\leq P_i$$

and in at least one of the circles

$$|\boldsymbol{z}-a_{jj}|\leq Q_j.$$

A is a square matrix of order n over the complex field; $\boldsymbol{z}$ is the complex variable $\boldsymbol{x}+i\boldsymbol{y}$. P_i is the sum of the absolute values of the off-diagonal elements in the ith row; Q_j is a similar sum for the jth column.

In the matrix $-\Delta_0$ derived from the characteristic determinant, eq (5a), by letting $\boldsymbol{D}$ be zero and changing the signs, we know that the off-diagonal elements are all real and positive, and so an off-diagonal column sum is Q_j. Also from eq (5a) we see that the jth diagonal element a_{jj} is $-Q_j$. Hence, for the jth circle $(j=1, \ldots, 6)$ the radius is Q_j, and the center is on the real axis at $-Q_j$. Let $Q_m\geq Q_j$ $(j=1, \ldots, 6)$. Q_m defines the largest circle. Previously all roots were shown to be real. Hence all roots lie on or within the mth circle on the axis of reals, that is between zero and $2a_{mm}$ (a_{mm} being the most negative of the diagonal elements in $-\Delta_0$).

3.4. Useful Formulas

Relation between the equilibrium number of dipoles in each site with and without a static electric field. We refer to the method of solving the rate equations in reference 1. After a "mode analysis" in which for each given mode β the coefficients $C_{i\beta}$ are determined relative to one another, the boundary condition at $t=0$ is introduced. This condition corresponds to the sudden removal of a static electric field. This results in the equations

$$C_{i1}^F = \sum_{\beta} C_{i\beta},$$

where C_{i1}^F is the equilibrium number of dipoles in the ith site in the presence of the field. A general expression for these coefficients in terms of the equilibrium coefficients for zero field is helpful in solving any particular model.

The equations below for the C_{i1}^F are derived in a manner similar to that indicated in section 2.4 of reference 1.

We assume a static electric field $\vec{\boldsymbol{F}}$ defined by the magnitude F and the polar angles ξ and θ, with ξ being the azimuth angle measured from the z-axis. For convenience, let

$$\gamma=\mu F/\boldsymbol{k}T \text{ and } \gamma_x=\gamma \sin\xi\cos\theta$$

$$\gamma_y=\gamma \sin\xi \sin\theta$$

$$\gamma_z=\gamma \cos\xi.$$

[9] K. Goldberg of the Applied Mathematics Division of the Bureau. His proof is published in RP2652 in this Journal. The theorem as stated above is in a slightly different form from that as stated by Goldberg; his condition (2) has been replaced by the condition $a_{ij}\geq 0$ which still permits the construction of an equivalent symmetric matrix, namely, $b_{ij}=(a_{ij}a_{ji})^{1/2}$.

Then

$$\left.\begin{aligned}
C_{11}^{F}&=C_{11}\left[1-\gamma_x(C_{31}-C_{51})/N-\gamma_y(C_{21}-C_{41})/N-\gamma_z\left(\frac{C_{11}-C_{61}}{N}-1\right)\right]\\
C_{21}^{F}&=C_{21}\left[1-\gamma_x(C_{31}-C_{51})/N-\gamma_y\left(\frac{C_{21}-C_{41}}{N}-1\right)-\gamma_z(C_{11}-C_{61})/N\right]\\
C_{31}^{F}&=C_{31}\left[1-\gamma_x\left(\frac{C_{31}-C_{51}}{N}-1\right)-\gamma_y(C_{21}-C_{41})/N-\gamma_z(C_{11}-C_{61})/N\right]\\
C_{41}^{F}&=C_{41}\left[1-\gamma_x(C_{31}-C_{51})/N-\gamma_y\left(\frac{C_{21}-C_{41}}{N}+1\right)-\gamma_z(C_{11}-C_{61})/N\right]\\
C_{51}^{F}&=C_{51}\left[1-\gamma_x\left(\frac{C_{31}-C_{51}}{N}+1\right)-\gamma_y(C_{21}-C_{41})/N-\gamma_z(C_{11}-C_{61})/N\right]\\
C_{61}^{F}&=C_{61}\left[1-\gamma_x(C_{31}-C_{51})/N-\gamma_y(C_{21}-C_{41})/N-\gamma_z\left(\frac{C_{11}-C_{61}}{N}+1\right)\right]
\end{aligned}\right\} \tag{16}$$

The total polarizability, α_{tot}. We assume a polycrystalline substance and follow the procedure outlined in section 2.4, reference 1, for obtaining the polarizability associated with each mode. Here, however, we introduce for each site i the value of N_i at $t=0$, namely, C_{i1}^{F}. With the use of the expressions for the C_{i1}^{F} given in the preceding paragraph, one can obtain

$$\alpha_{tot}=\left[1-\frac{(C_{31}-C_{51})^2+(C_{21}-C_{41})^2+(C_{11}-C_{61})^2}{N^2}\right]\frac{\mu^2}{3kT} \tag{17}$$

4. References

[1] J. D. Hoffman and B. M. Axilrod, J. Research NBS **54,** 357 (1955) RP2598.
[2] J. D. Hoffman and H. G. Pfeiffer, J. Chem. Phys. **22,** 132 (1954).
[3] J. D. Hoffman, J. Chem. Phys. **23,** 1331 (1955).
[4] S. Gerschgorin, Izvest. Akad. Nauk S. S. S. R. Series VII, Otdel. mat. i estest. **4,** 749 (1931).
[5] A. Brauer, Duke Math. J., **13,** 387 (1946).
[6] J. G. Powles, J. Chem. Phys. **21,** 633 (1953).
[7] P. Debye, Polar molecules, p. 94 (Dover Publications, New York, N. Y., 1945).

Washington, October 20, 1955.

Journal of Research of the National Bureau of Standards Vol. 56, No. 2, February 1956 Research Paper 2652

A Matrix with Real Characteristic Roots

Karl Goldberg

It is proved that a certain matrix, which is the coefficient matrix of a differential equation found in the theory of dielectric relaxation, has only real characteristic roots. This is done by finding a real symmetric matrix with the same principal minors and thus the same characteristic roots.

In papers [1, 2, 3][1] by J. D. Hoffman and B. M. Axilrod a certain differential equation has a real, constant coefficient matrix $A=(a_{ij})$ with the properties

$$a_{ii}\geq 0 \qquad \text{for all } i \tag{1}$$

$$a_{ij}\leq 0 \qquad \text{for all } i\neq j \tag{2}$$

$$\sum_i a_{ij}=0 \qquad \text{for all } j \tag{3}$$

$$a_{i_1i_2}a_{i_2i_3}\ldots a_{i_ki_1}=a_{i_2i_1}a_{i_3i_2}\ldots a_{i_1i_k} \qquad \text{for all } i_1,i_2,\ldots,i_k. \tag{4}$$

In this note we prove the conjecture of J. D. Hoffman and B. M. Axilrod that a matrix with these properties has only real characteristic roots and that these characteristic roots lie between zero and twice the maximum diagonal element.

The second statement is a direct consequence of the first and properties (1), (2), and (3) by the theorem of S. Gershgorin [4] and A. Brauer [5]. This theorem states that all the characteristic roots of a matrix $A=(a_{ij})$ lie in the area bounded by the circles $|z-a_{jj}|\leq\sum_i|a_{ij}|-|a_{jj}|$.

Therefore, we may concentrate on proving that all the characteristic roots are real. We shall do this by exhibiting a symmetric matrix with the same characteristic roots as one with properties (2) and (4).

Let $B=(b_{ij})$ be a matrix of the same order as the matrix $A=(a_{ij})$, which has properties (2) and (4), such that

$$b_{ij}=-(a_{ij}a_{ji})^{1/2}$$

with the square root assumed to be positive. Then

$$\begin{aligned}b_{i_1i_2}b_{i_2i_3}\ldots b_{i_ki_1}&=(-1)^k(a_{i_1i_2}a_{i_2i_1}a_{i_2i_3}a_{i_3i_2}\ldots a_{i_ki_1}a_{i_1i_k})^{1/2}\\&=(-1)^k|a_{i_1i_2}a_{i_2i_3}\ldots a_{i_ki_1}|\\&=a_{i_1i_2}a_{i_2i_3}\ldots a_{i_ki_1}\end{aligned}$$

for all $i_1,i_2,\ldots,i_k$

Now consider any principal minor

$$|A(s_1,s_2,\ldots,s_m)|=|a_{ij}|_{i,j=s_1,s_2,\ldots,s_m} \text{ of } A.$$

From the definition of a determinant we have

$$|A(s_1,s_2,\ldots,s_m)|=\sum\pm a_{s_1t_1}a_{s_2t_2}\ldots a_{s_mt_m}$$

where the sum is taken over all permutations

$$\begin{pmatrix}s_1s_2&\ldots&s_m\\t_1t_2&\ldots&t_m\end{pmatrix}$$

of $s_1,s_2,\ldots,s_m$, and the sign is positive if the permutation is even, and negative if it is odd.

Each permutation is the product of cycles. Thus

$$\begin{pmatrix}s_1s_2&\ldots&s_m\\t_1t_2&\ldots&t_m\end{pmatrix}=\begin{pmatrix}i_1i_2&&i_k\\&\ldots&\\i_2i_3&&i_1\end{pmatrix}\ldots,$$

so that

$$\begin{aligned}a_{s_1t_1}a_{s_2t_2}\ldots a_{s_mt_m}&=a_{i_1i_2}a_{i_2i_3}\ldots a_{i_ki_1}\ldots\\&=b_{i_1i_2}b_{i_2i_3}\ldots b_{i_ki_1}\ldots\\&=b_{s_1t_1}b_{s_2t_2}\ldots b_{s_mt_m}.\end{aligned}$$

It follows that

$$|A(s_1,s_2\ldots,s_m)|=|B(s_1,s_2,\ldots,s_m)|,$$

that is, that the corresponding principal minors of A and B are equal.

This implies that A and B have the same characteristic equation and thus have the same characteristic roots.

---

[1] J. D. Hoffman and B. M. Axilrod, Dielectric relaxation for spherical molecules in a crystalline field: Theory for two simple models, J. Research NBS **54,** 375 (1955) RP2598.

[2] J. D. Hoffman, Theory of dielectric relaxation for a single-axis rotator in a crystalline field. II, J. Chem. Phys. **23,** 1331 (1955).

[3] B. M. Axilrod, Dielectric relaxation for a three-dimensional rotator in a crystalline field: Theory for a general six-site model, J. Research NBS **56,** 81 (1956) RP2651.

[4] S. Gershgorin, Über die Abgrenzung Engenwerte einer Matrix, Izvest. Akad. Nauk, S.S.S.R. **7,** 749 (1931).

[5] A. Brauer, Limits for the characteristic roots of a matrix, Duke Math. J. **13,** 387 (1946).

WASHINGTON, October 20, 1955.

[1] Figures in brackets indicate the literature references at the end of this paper.

373918—56——3

Journal of Research of the National Bureau of Standards Vol. 56, No. 2, February 1956 Research Paper 2653

Reflection and Transmission of Gamma Radiation by Barriers: Semianalytic Monte Carlo Calculation [1]

Martin J. Berger and John Doggett

The transport equation for photons which have been Compton-scattered repeatedly with a specified sequence of energy losses and deflections was solved analytically, by an "orders of scattering" approach, to obtain conditional reflection and transmission probabilities. These probabilities were then averaged over all possible intermediate angular and energy configurations in a Monte Carlo calculation carried out on the NBS automatic computer (SEAC). The efficiency of the Monte Carlo calculation was increased by taking advantage of the close correlation between the transmission of radiation through thick barriers and the corresponding penetration problem in an infinite homogeneous medium for which an exact solution was available. The reflected and transmitted energy flux (integrated over all spectral energies and directions) has been calculated for 0.66-, 1- and 4-Mev radiation incident on water barriers, and 1-, 4-, and 10-Mev radiation incident on iron, tin, and lead barriers. Angular and energy spectra were obtained for water at 0.66 Mev. The ratio of the scattered energy flux, transmitted through a barrier to the scattered flux at equal depth in an infinite medium, was found to be constant for distances from the source greater than four mean free paths of the source radiation.

1. Introduction

The theory of the diffusion and penetration of gamma radiation in an infinite homogeneous medium is now well developed, complete solutions being provided by the moment-method [1] [2] and the closely related semiasymptotic Laplace-transform method [2]. A satisfactory theory of boundary effects is still lacking. The "orders of scattering" approach [3] provides formal solutions to boundary problems, which can in practice be evaluated only when few orders of scattering need be considered. The Monte Carlo method [4] is a very effective means for treating boundary effects but is inefficient when applied to the radiation that penetrates very far from the source. This inefficiency can, in principle, be removed by so-called "biased" sampling, but the success of such techniques has not yet been demonstrated conclusively.

This investigation is part of an exploratory Monte Carlo program for the survey of boundary effects in gamma-ray diffusion. The specific aim is to calculate the reflection and transmission of radiation by plane parallel barriers. The approach is eclectic, and a combination of all three of the methods described above is being used. It can be characterized as an "orders of scattering" method in which the multiple integrals, which ordinarily make the evaluation of the solution troublesome, are evaluated numerically by random sampling. Conversely, one could call it a "reinforced" Monte Carlo calculation whose efficiency for dealing with deep penetration has been increased in two ways: by confining the random sampling to the angular and energy variables, while treating the space variable analytically, and through the use of correlated sampling, the correlated problem being the diffusion of γ-radiation in an infinite homogeneous medium.

The reflection and transmission problems differ substantially from the point of view of random sampling, because transmission through thick barriers, being unlikely, tends to require an excessive amount of sampling and thus puts a high premium on analytical help. Nevertheless, the two problems were treated together because they fitted in a single computational scheme.

Two types of questions may be asked in radiation diffusion problems. One concerns the estimation of the radiation intensity at any one position, corresponding to the observable response of some integral detector like an ionization chamber. The other type of question is more detailed and concerns the spectral composition and directional distribution of the radiation at any one point. In the work reported here most of the effort has been devoted to intensity (energy flux) determinations. Exploratory studies of spectral and angular distributions were made only for one source energy (0.66 Mev) and one barrier material (water).

For the deep-penetration problem the attention was focused on the comparison of the radiation intensity behind a finite barrier of thickness t and inside an infinite medium at a depth z (equal to t) from the source plane (see fig. 1,a,b). No quantitative indication was previously available on this comparison. Notice that practical situations are usually intermediate between those schematized in figure 1,a,b, because there is some matter (possibly of different composition) behind the barrier, though often at some distance from it (fig. 1,c).

On the problem of relative intensity a rather definitive answer has been obtained. In the first place, it proved unnecessary to have extended the calculation to very great depths because the intensity ratio no longer varies appreciably beyond about four mean free paths of the incident radiation. It follows that any future investigation may confine itself to moderate depths and may thus utilize less elaborate methods. Data on the values of the

[1] This work was supported by the Office of Naval Research and the Reactor Division of the U. S. Atomic Energy Commission.

[2] Figures in brackets indicate the literature references at the end of this paper

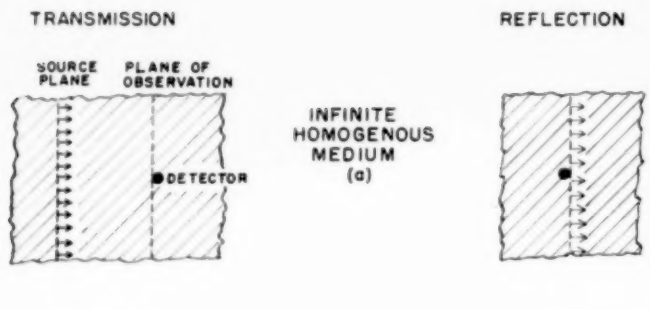

FIGURE 1. *Schematization of the barrier reflection-transmission problem.*

intensity ratio for various depths are given in table 3 for four materials (water, iron, tin, and lead) and four γ-ray energies (0.66, 1, 4, and 10 Mev). Those data may be applied as correction factors to the extensive results of calculations for infinite media [5]. The ratios differ substantially from unity only for low energies and low-Z materials, and also vary smoothly, so that adaptation to other circumstances ought to be easy.

In the treatment of the reflection problem, attention was directed in the first place to the dependence of the reflected intensity on the γ-ray energy, on the material of the barrier, and also on the angle of incidence. The results for a semi-infinite barrier are given in table 2,a. An additional item of interest was the dependence of reflection on the barrier thickness, that is, on how rapidly the reflection approaches the value for a semi-infinite barrier. Some data on this aspect are given in table 2,b.

2. Outline of the Calculation

2.1. Analytical Frame

We consider a homogeneous plane-parallel layer of material located between the planes $z=0$ and $z=t$. Radiation is incident with specified energy and direction on the face $z=0$. What are the characteristics of the radiation reflected through the plane $z=0$ and transmitted through the plane $z=t$?

The state of a photon traversing the barrier is described by three variables: the energy E, the angle θ between the direction of motion and the z-axis, and the depth z in the barrier.

Photons can be scattered and absorbed inside the barrier. Let $\mu_A(E)$ equal the probability of absorption per unit path length; $c(E)$ the probability of scattering per unit path length, and $\Psi(E,\theta;\, E',\theta')$ the probability distribution (normalized to unity) that a scattering will change the state of the photon from (E,θ) to (E',θ'). Consider a photon that, as the result of n scatterings, has successively assumed the energies and directions

$$\begin{Bmatrix} E_0, E_1, \ldots, E_n \\ \theta_0, \theta_1, \ldots, \theta_n \end{Bmatrix} = \text{energy-angle history } h_n.$$

The index n refers to the state of the photon immediately after its nth scattering; $n=0$ pertains to the state in which the photon enters the barrier. The probability distribution of h_n is

$$Q_n = \prod_{m=0}^{n-1} \Psi(E_m,\theta_m;\, E_{m+1},\theta_{m+1}) \tag{1}$$

Let $P_n(z,t,h_n)$ be the probability that a photon with history h_n will cross the plane z $(0 \le z \le t)$ after the nth and prior to an $(n+1)$st scattering. An analytical expression for this crossing-probability is derived in section 3. If a beam of K photons per unit area and unit time is incident on the barrier, the flux per unit time at depth z is

$$F(E,\theta,z,t) = K \sum_{n=0}^{\infty} f_n \int dE_1 \int d\theta_1 \ldots \int dE_n \int d\theta_n P_n Q_n \delta(E-E_n)\delta(\theta-\theta_n), \tag{2}$$

where δ is Dirac's delta function. If the weight factors f_n are unity, the flux represents the number of photons crossing a unit area of the z-plane per unit time. Most radiation detectors do not measure the number flux through a fixed plane; their response depends in various ways on the energy and direction of the radiation and is represented by the f_n's. A few examples are:

Type	f_n	Flux
a	1	Number — Flux (or current) per unit area of surface perpendicular to the z-axis.
b	E_n	Energy — Flux (or current) per unit area of surface perpendicular to the z-axis.
c	$\lvert\sec\theta_n\rvert$	Number — Flux per unit area of surface perpendicular to the direction of motion of the radiation. This is the flux seen by an isotropic detector. It is proportional to the photon density.
d	$\lvert\sec\theta_n\rvert E_n$	Energy — Flux per unit area of surface perpendicular to the direction of motion of the radiation. This is the flux seen by an isotropic detector. It is proportional to the photon density.

The numerical results of this paper pertain to flux type (d). By this choice they become comparable to the results of an extensive set of calculations for infinite media by the moment-method [5].

2.2. Monte Carlo Estimates

In the evaluation of expression (2) for the flux, the sum over collisons must be cut off for $n>N$, and the integration over the intermediate energies and angles is carried out by the Monte Carlo method. A suitable value of the cutoff N depends on the absorbing properties of the medium, the depth of penetration, and the spectral-energy range over which one wants to know the flux. Calculations for an infinite medium show that for all practical purposes the energy flux vanishes below 30 kev in water, below 50 kev in iron, 75 kev in tin, and 100 kev in lead, for source energies between 0.5 and 10 Mev. The photon energy histories were therefore terminated at these limits. Trial calculations indicated that under these circumstances, for a barrier thickness up to 16 mean free paths ($\mu_0 t=16$), it was sufficient to let N=25 for water, 12 for iron, 9 for tin, and 6 for lead.

Energy-angle histories of length N were sampled according to the distribution function Q_N. The detailed equations for doing this are well known. They are presented elsewhere, together with the adaptations required or desirable for computations on an automatic computer [6].

Let h_{nj} be an initial portion of length $n\leq N$ of the jth sample history h_{Nj}, and let $P_{nj}(z,t)$ be the corresponding crossing-probability. If a sample of J histories is available, the flux of radiation in a specified spectral interval R_E and angular interval R_θ can be estimated as follows:

$$\int_{R_E} dE \int_{R_\theta} d\theta F(E,\theta,z,t)=\frac{K}{J}\sum_{j=1}^{J}\sum_{n=0}^{N} f_{nj}P_{nj}(z,t)\Delta_1(E_{nj})\Delta_2(\theta_{nj}), \quad (3)$$

where

$$\Delta_1(E_{nj})\begin{cases}=1, \text{ if } E_{nj} \text{ is in the interval } R_E\\ =0, \text{ if } E_{nj} \text{ is outside the interval } R_E\end{cases}$$

$$\Delta_2(\theta_{nj})\begin{cases}=1, \text{ if } \theta_{nj} \text{ is in the interval } R_\theta\\ =0, \text{ if } \theta_{nj} \text{ is outside the interval } R_\theta.\end{cases}$$

If one wants to know the value of the flux for fixed values of E and θ rather than in intervals, the sampling procedure must be modified so as to be conditional not only on the initial photon state but also on the final state $E_n=E$ and $\theta_n=\theta$. For this purpose one replaces P_n by $P_n^*(h_n^*)\Psi(E_{n-1},\theta_{n-1};\, E,\,\theta)$, where

$$h_n^*=\begin{Bmatrix} E_0, E_1, \ldots, E_{n-1}, E \\ \theta_0, \theta_1, \ldots, \theta_{n-1}, \theta \end{Bmatrix}.$$

We have been content to obtain the flux in energy and angular intervals because the main body of calculations was done in any case for the total intensity integrated over all spectral energies and directions.

In conformity with the usage that has become common in shielding work, the results for the intensity are presented in the form of buildup factors $B(z,t)$, which are equal to the ratio of the total to the unscattered energy flux:

$$B(z,t)=\frac{\int_0^{E_0} dE \int_0^{\pi} d\theta F(E,\theta,z,t)}{Kf_0P_0}. \quad (4)$$

The Monte Carlo estimates of the buildup factors are the mean values

$$\overline{B}(z,t)=(1/J)\sum_{j=1}^{J} B_j(z,t), \quad (5)$$

where

$$B_j(z,t)=(E_0|\sec\theta_0|P_0)^{-1}\sum_{n=0}^{N} E_{nj}|\sec\theta_{nj}|P_{nj}(z,t).$$

The standard deviation of the buildup factor estimate is $J^{-1/2}\sigma(z,t)$ where

$$\sigma(z,t)=\left\{\frac{1}{J}\sum_{j=1}^{J}[B_j(z,t)-\overline{B}(z,t)]^2\right\}^{1/2}. \quad (6)$$

The buildup factors (and their standard deviations) were estimated from the same set of energy-angle histories for three specific situations:

(i) $\overline{B}(0,t)$ = energy reflection buildup factor [3]

(ii) $\overline{B}(t,t)$ = energy transmission buildup factor

(iii) $\overline{B}(t,\infty)$ = energy buildup factor for the flux at depth t within a semi-infinite medium.

2.3. Correlation

The difference between $\overline{B}(t,t)$ and $\overline{B}(t,\infty)$ is predominantly due to photons with histories such that in an infinite medium they would cross the plane $z=t$, have their directions reversed as the result of one or a few collisions in the vicinity of t, and would then make another crossing. Thus $\overline{B}(t,\infty)$ is—loosely speaking—a function of two factors: a probability $p_1(t)$ of penetration to depth t, and a probability p_2 of being turned around in the vicinity of the t-plane. On the other hand, $\overline{B}(t,t)$ only contains the factor $p_1(t)$. The greatest statistical fluctuations in a Monte Carlo calculation are found in the estimate of $p_1(t)$, because only a small part of the sampled histories provides information concerning deep penetration. If the same set of energy-angle histories is used for the estimate of $\overline{B}(t,\infty)$ and $\overline{B}(t,t)$, it is to be expected that the estimate of the ratio of these two quantities will have a much smaller statistical dispersion than the estimates of the individual buildup factors because the ratio no longer contains the troublesome factor $p_1(t)$. Unscattered radiation should be excluded from the comparison because it

[3] The energy reflection buildup factor has the following physical significance. Consider an isotropic detector placed in the path of a broad beam of radiation, and denote the energy flow through the detector by F_0. Then place a barrier of thickness t immediately behind the detector. This increases the energy flow through the detector to F. Then $\overline{B}(0,t)=F/F_0$. The quantity $\overline{B}(0,t)-1$ is related to but not identical with the energy albedo, which as commonly defined pertains to an energy current.

i

s not affected by the boundaries. We therefore subtract 1 from both buildup factors and introduce the ratio

$$k(t)=\frac{\overline{B}(t,t)-1}{\overline{B}(t,\infty)-1}. \tag{7}$$

A Monte Carlo estimate of k has an estimated standard deviation $J^{-1/2}\sigma_k$, where

$$\sigma_k=k\left\{\left[\frac{\sigma(t,t)}{\overline{B}(t,t)-1}\right]^2+\left[\frac{\sigma(t,\infty)}{\overline{B}(t,\infty)-1}\right]^2-2\rho\,\frac{\sigma(t,t)}{\overline{B}(t,t)-1}\,\frac{\sigma(t,\infty)}{\overline{B}(t,\infty)-1}\right\}^{1/2}, \tag{8}$$

and

$$\rho(t)=\frac{(1/J)\sum_{j=1}^{J}[B_j(t,t)-\overline{B}(t,t)]\,[B_j(t,\infty)-\overline{B}(t,\infty)]}{\sigma(t,t)\,\sigma(t,\infty)} \tag{9}$$

is the correlation coefficient of $\overline{B}(t,t)$ and $\overline{B}(t,\infty)$. The two buildup factors have a strong positive correlation so that $\rho\approx 1$ and the value of σ_k/k is small. For moderate and deep penetrations, $\overline{B}(t,\infty)$ is practically identical with the buildup factor for an infinite medium which can be obtained by a reliable moment-calculation. These known results, together with an estimate of the ratio $k(t)$, provide an accurate indirect method for determining the transmission buildup factor which requires much smaller sample sizes than a direct estimate. Thus the Monte Carlo and moment-methods complement each other: one provides knowledge of the boundary effect, the other knowledge of deep penetration of radiation. In section 5 the advantage of this correlation technique is demonstrated.

3. Solution of the Transport Equation for the Crossing-Probabilities

The crossing-probabilities obey the following integral equations:

$$P_{n+1}(z)=\frac{c(E_n)}{|\cos\theta_n|}\int_0^z dz' P_n(z')e^{-[\mu_A(E_{n+1})+c(E_{n+1})](z-z')/\cos\theta_{n+1}} \tag{10a}$$

if $\cos\theta_{n+1}>0$.

$$P_{n+1}(z)=\frac{c(E_n)}{|\cos\theta_n|}\int_z^t dz' P_n(z')e^{-[\mu_A(E_{n+1})+c(E_{n+1})](z-z')/\cos\theta_{n+1}} \tag{10b}$$

if $\cos\theta_{n+1}<0$.

$$P_0(z)=e^{-[\mu_A(E_0)+c(E_0)]z/\cos\theta_0}. \tag{10c}$$

These equations express the fact that the probability of passage through the z-plane after $n+1$ collisions is equal to the probability of passage through the plane z' after n collisions, times the probability of a collision between z' and $z'+dz'$, times the probability of passage from z' to z without further scattering or absorption, the triple product being averaged over all values of z' compatible with the boundary conditions.

We shall find it convenient to introduce in place of the probabilities P_n the related quantities

$$G_n(z)=|\sec\theta_n|P_n(z) \tag{11}$$

which already incorporate the trigonometrical factor required for the type of flux which we want to determine. The following abbreviated notation will be adopted:

$$\left.\begin{aligned}&\mu_n=\mu_A(E_n)+c(E_n)\\&c_n=c(E_n)\\&\eta_n=\cos\theta_n\\&u_n=0 \text{ if } \cos\theta_n>0\\&u_n=t \text{ if } \cos\theta_n<0\end{aligned}\right\} \tag{12}$$

Equations (10a, b, and c) can then be rewritten in the form

$$G_{n+1}(z)=\frac{c_n}{\eta_{n+1}}\int_{u_{n+1}}^{z} dz' G_n(z')e^{-\frac{\mu_{n+1}}{\eta_{n+1}}(z-z')} \tag{13a}$$

$$G_0(z)=\frac{1}{\eta_0}e^{-\frac{\mu_0}{\eta_0}z} \tag{13b}$$

To solve these equations, assume that G_n can be expressed in the form

$$G_n(z)=\sum_{m=0}^{n} A_m^n e^{-\frac{\mu_m}{\eta_m}(z-u_m)}. \tag{14}$$

Substitution of eq (14) into (13a) yields the equation

$$G_{n+1}(z)=\frac{c_n}{\eta_{n+1}}\sum_{m=0}^{n}\frac{A_m^n\eta_m}{\eta_{n+1}\mu_m-\eta_m\mu_{n+1}}\left\{e^{-\frac{\mu_m}{\eta_m}(u_{n+1}-u_m)}e^{-\frac{\mu_{n+1}}{\eta_{n+1}}(z-u_{n+1})}-e^{-\frac{\mu_m}{\eta_m}(z-u_m)}\right\} \tag{15}$$

so that the functional form of G_{n+1} is the same as that of G_n. The expansion coefficients are

$$A_m^{n+1}=\frac{c_n}{\eta_{n+1}}\,\frac{1}{\frac{\mu_{n+1}}{\eta_{n+1}}-\frac{\mu_m}{\eta_m}}A_m^n \text{ for } 0\le m\le n \tag{16a}$$

$$A_{n+1}^{n+1}=-\sum_{m=0}^{n}A_m^{n+1}e^{-\frac{\mu_m}{\eta_m}(u_{n+1}-u_m)}. \tag{16b}$$

We have thus obtained inductively the general solution for $G_n(z)$. Although the solution is rather formal and not readily surveyed, it is convenient for numerical evaluation with an automatic computer because of its recursive nature.

It is possible that $\eta_m\mu_{n+1}-\eta_{n+1}\mu_m=0$, so that singularities occur in the recursion relations (16a, b). But this difficulty is apparent rather than real, because upon substitution of the coefficients A_m^{n+1} into the expression for G_{n+1} the singularities occur pairwise and cancel each other. This can be seen by a reexamination of (15). Note that the existence of the singularity implies that $\eta_{n+1}\eta_m>0$, because both μ_m and μ_{n+1} are positive. It follows that u_m is equal to u_{n+1}. Therefore, the factor multiplying A_m^n in eq (15) is

$$\alpha_m^n=\frac{c_n e^{-\frac{\mu_{n+1}}{\eta_{n+1}}(z-u_{n+1})}}{\frac{\mu_{n+1}}{\eta_{n+1}}-\frac{\mu_m}{\eta_m}}\left\{e^{\left(\frac{\mu_{n+1}}{\eta_{n+1}}-\frac{\mu_m}{\eta_m}\right)(z-u_{n+1})}-1\right\}. \quad (17)$$

As $\eta_m\mu_{n+1}-\eta_{n+1}\mu_m\to 0$

$$\alpha_m^n\to c_n(z-u_m)e^{-\frac{\mu_m}{\eta_m}(z-u_m)}. \quad (18)$$

If the singularities are removed by a limiting procedure, the functional form of G_{n+1} is thus changed. For the numerical computation on an automatic computer we have found it simplest not to use the limiting procedure, but to stick to the unmodified formal solution, while eliminating singular cases by introducing a cutoff for the quantity $\alpha=(\mu_{n+1}/\eta_{n+1})-(\mu_m/\eta_m)$ in the denominator of eq (16a). Every $\alpha<10^{-3}$ was replaced by 10^{-3}. The error incurred by this approximation increases with $|z-u_m|$. But even for deep penetration it is quite small. For example, when $\alpha(z-u_m)=20$, $[\exp(-0.001\times 20)-1]/10^{-3}=20.201$, so that the error is only 1 percent.

4. Machine Computation

The calculation was programed for the NBS automatic computer (SEAC). It was carried out in two stages. First, energy-angle histories (in groups of approximately 100) were generated by random sampling and stored on magnetic wire or tape. These histories were then used as input data for the second stage, in which the quantities G_n (proportional to the crossing-probabilities P_n) were calculated. Any desired type of flux or buildup factor can be obtained by a suitable linear combination of the G_n's, the selection being made by an appropriate output code.

The buildup factor code provides for the computation of $\overline{B}(0,t)$, $\overline{B}(t,t)$, and $\overline{B}(t,\infty)$, for $\mu_0 t=2^n d$ $(n=0,1,\ldots,5)$, d being a disposable parameter. Either all 18 or any subgroup of these buildup factors can be computed in an integrated operation. The standard deviations $\sigma(0,t)$, $\sigma(t,t)$, and $\sigma(t,\infty)$, as well as the correlation coefficient $\rho(t)$ are also contained in the output.

Most of the computational effort was devoted to the buildup factors, but limited use was also made of output codes for energy spectra and angular distributions.

The amount of SEAC computing time depends on the number N of collisions through which one follows the photon histories. As has been mentioned, it was found sufficient to let $N=25$ for water, 12 for iron, 9 for tin, and 6 for lead. The amount of machine time (seconds per history) required for the generation and storage of photon energy-angle histories was

$$t_1=0.4\ N. \quad (19)$$

For the joint computation of 18 buildup factors, the machine time (seconds per history and buildup factor)

$$t_2=0.18\ N+0.0205\ N^2 \quad (20)$$

for $6\le N\le 25$. For the computation of an individual buildup factor, the machine time (seconds per history)

$$t_3=1.3\ N. \quad (21)$$

It can be seen that the joint computation of several buildup factors was more economical.

A major difficulty in setting up the machine program was the scaling problem. SEAC operates only on numbers less than 4 in absolute value. But the coefficients A_m^n in the expansion for G_n can occasionally become extremely large because of sampling accidents. This difficulty was aggravated by the fact that singularities were not removed analytically from the recursion relations (16a, b) but by a numerical cutoff procedure. This resulted in the occurrence of pairs of coefficients with approximately the same large absolute value, but opposite sign, whose weighted difference must be calculated with great accuracy. This required the use of floating-decimal-point routines, which, although they were specially adapted to the problem, proved to be costly in computation time.

The occurrence of large terms with alternating signs in the series for G_n provided a convenient check on the code and the computer operation. Clearly G_n, being a positive multiple of a probability, must be a positive quantity. It was found by experience that because of the alternating character of the series for G_n, almost any sort of code or machine trouble quickly led to the occurrence of negative G_n's. The machine was instructed to interrupt the computation whenever this happened. As many G_n's are computed per second, the absence of such interruptions for prolonged periods was a reasonable guarantee that the operation of the computer was error free.

5. Results

5.1. Statistical Efficiency

Before presenting the main body of our results, we shall discuss the statistical accuracy of the Monte Carlo estimates in detail for a sample calculation based on 300 photon histories, pertaining to 1-Mev radiation incident normally on an iron barrier. In table 1 are listed, in addition to the estimated buildup factors and buildup factor ratios, other quantities of statistical interest including fractional standard deviations and correlation coefficients.

TABLE 1. *Statistical analysis of buildup factor estimates for 1-Mev radiation incident on an iron barrier*

$\mu_0 t$	$\overline{B}(0,t)$	$\frac{\sigma(0,t)}{\overline{B}(0,t)-1}$	$\overline{B}(t,t)$	$\frac{\sigma(t,t)}{\overline{B}(t,t)-1}$	$\overline{B}(t,\infty)$	$\frac{\sigma(t,\infty)}{\overline{B}(t,\infty)-1}$	$1-\rho$	k	$\frac{\sigma_k}{k}$	q
0.5	1.048	0.0586	1.40	0.61	1.53	0.43	9.2×10^{-2}	0.755	0.29	0.4
1.0	1.057	.0696	1.71	.73	1.89	.58	2.2×10^{-2}	.798	.20	.3
2.0	1.061	.0747	2.43	1.00	2.68	.89	6.5×10^{-3}	.851	.15	15.2
4.0	1.061	.0747	4.07	1.58	4.45	1.48	4.9×10^{-3}	.890	.18	43.6
8.0	1.061	.0747	7.80	2.90	8.60	2.68	3.4×10^{-3}	.895	.31	67.2
16.0	1.061	.0747	17.8	4.87	20.0	4.58	1.85×10^{-3}	.884	.41	115.0

Now let us see what the large amount of analysis introduced into the Monte Carlo calculation has accomplished. To estimate the transmission buildup factor for a barrier with thickness $\mu_0 t=16$ with a standard deviation amounting to 5 percent of the buildup factor would require on the order of 10^5 photon histories in an ordinary random sampling calculation. But according to table 1 the semi-analytical method requires only 8.5×10^3 histories. Taking into account the estimated increase in computation time per history required in the semi-analytical calculation, one finds that the effective reduction factor is $\approx$2,500. This is respectable but not quite good enough for a computer with the capabilities of SEAC. But one can do better still through the use of correlated sampling, i. e., by estimating the buildup factor ratio $k(t)$. It can be seen from table 1 that, in accordance with expectations, the correlation coefficient ρ is very close to unity, and the fractional standard deviation σ_k/k correspondingly small. A 5 percent standard deviation now only requires a sample of 67 histories. Taking into account the increased computation time per history, the reduction of effort is 80-fold. The over-all improvement factor is therefore $2{,}500\times80=200{,}000$.

The last column of table 1 lists the factor $q=[\sigma(t,t)/\overline{B}(t,t)]^2/[\sigma_k/k]^2$, by which the correlated sampling technique reduced the required sample size. Statistical analyses at other energies and for other scattering media yield over-all improvements in efficiency of about the same magnitude.

5.2. Buildup Factors

Reflection buildup factors for semi-infinite media are listed in table 2,a, for diverse conditions. The sample sizes were such that the quantities $\overline{B}(0,t)-1$, i. e., the increase of the flux due to reflection, had a statistical accuracy of 5 percent. It can be seen that energy reflection is appreciable only for low energies and low-Z materials. Table 2,b, shows the dependence of reflection on the barrier thickness for some typical cases. The outstanding feature of these results is the rapidity with which the reflection of energy assumes its maximum value. A barrier with a thickness of one, or at most two mean free paths of the source radiation is already equivalent to a semi-infinite medium.

TABLE 2. *Energy reflection*

a. Energy Reflection Buildup Factors for Semi-infinite Barriers

Energy	Water		Iron		Tin		Lead	
	ϑ_0							
	0°	60°	0°	60°	0°	60°	0°	60°
Mev.								
0.4	1.240	1.278	.....	.....	.....	.....	.....	.....
.66	1.148	1.189	.....	.....	.....	.....	.....	.....
1.0	1.081	1.153	1.061	1.142	1.022	1.086	1.009	1.042
4.0	1.012	1.035	1.011	.....	1.005	.....	1.001	.....
10.0	1.002	1.007	.....	.....	.....	.....	.....	.....

b. Dependence of Reflection on Barrier Thickness [a]

Material	Energy	ϑ_0	$\mu_0 t$		
			0.5	1	2
	Mev.				
Water	0.66	0°	0.65	0.88	0.99
Do	.66	60°	.61	.96	1.00
Iron	1.0	0°	.79	.93	1.00
Do	1.0	60°	.89	.98	1.00
Tin	1.0	0°	.95	.99	1.00
Lead	1.0	0°	.97	1.00	1.00

[a] Columns 4, 5, and 6 give the values of $k(0)=[\overline{B}(0,t)-1]/[\overline{B}(0,\infty)-1]$. $k(0)$ is a measure of the relative amount of reflected radiation from a finite barrier and from a semi-infinite medium.

Table 3 contains an extensive list of buildup factor ratios $k(t)$, for water at 0.66, 1, and 4 Mev, for iron, tin, and lead at 1, 4, and 10 Mev. Again, it can be seen that the boundary effect, indicated by deviations of $k(t)$ from unity, is appreciable only at low energies and for low-Z materials. It is significant that the ratios stay constant, within the limits of statistical error, as the barrier thickness is increased from $\mu_0 t=4$ to $\mu_0 t=16$. The physical reason for this constancy is the establishment of radiative near-equilibria in regions far from the source, which is well known from the diffusion theory for infinite media. Sufficiently deep in the material, both the energy spectrum and angular distribution of the radiation flux become very slowly varying functions of the penetration depth. Under these circumstances it is not surprising that the boundary effect, which depends on the characteristics of these distributions, likewise remains practically unchanged.

TABLE 3. *Buildup factor ratio* $k(t)=[\overline{B}(t,t)-1]/[\overline{B}(t,\infty)-1]$ *for comparing transmission of radiation through a finite barrier with penetration to an equal depth in a semi-infinite medium*

Material	Energy	$\mu_0 t$					
		*1.0	1.0	2.0	4.0	8.0	16.0
	Mev						
Water	0.66	0.601	0.663	0.713	0.783	0.785	0.784
	1	.661	.720	.754	.821	.828	.830
	4	.849	.885	.912	.920	.926	.933
Iron	1	.790	.798	.851	.890	.895	.894
	4	.890	.910	.923	.936	.932	.949
	10	.941	.959	.972	.974	.978	.977
Tin	1	.889	.911	.924	.935	.938	.946
	4	.941	.926	.955	.967	.974	.978
	10	.951	.960	.962	.973	.971	.969
Lead	1	.939	.951	.969	.975	.979	.982
	4	.941	.977	.982	.990	.992	.994
	10	.986	.990	.995	.992	.994	.995
Estimated accuracy (%)	.....	±5.0	±2.0	±1.5	±1.5	±2.0	±2.5

* Comparison of a barrier with an *infinite* medium.

TABLE 4. *Energy-transmission buildup factors*

Material	Energy *Mev*	$\mu_0 t$					
		0.5	1.0	2.0	4.0	8.0	16.0
Water	0.66	1.49	1.96	3.10	5.99	13.3	39.4
	1	1.40	1.80	2.72	5.01	10.5	25.7
	4	1.22	1.42	1.83	2.60	4.21	7.20
Iron	1	1.40	1.72	2.43	4.07	7.80	17.8
	4	1.20	1.36	1.72	2.56	4.17	7.45
	10	1.07	1.16	1.35	1.75	2.80	5.85
Tin	1	1.29	1.56	2.10	3.15	5.31	10.2
	4	1.16	1.31	1.63	2.35	4.12	9.41
	10	1.06	1.12	1.26	1.59	2.75	8.22
Lead	1	1.20	1.35	1.63	2.09	2.87	4.24
	4	1.11	1.23	1.44	1.98	3.28	7.46
	10	1.03	1.08	1.17	1.40	2.17	6.47

The results of table 3 pertain to a comparison of finite barriers with a semi-infinite medium. For distances $\mu_0 t \geq 4$, a comparison with an infinite medium would yield practically identical results. Column 3 shows the buildup factor ratios for $\mu_0 t = 1$ obtained by a Monte Carlo calculation for transmission and a moment-calculation for an *infinite* medium. It can be seen that these ratios are up to 10 percent lower than the corresponding ratios for a semi-infinite medium. For $\mu_0 t = 2$ there is a similar but extremely small reduction, but our data are insufficient for us to quote a value of the reduction.

Table 4 lists the transmission buildup factors for the same range of conditions as in table 3. For $\mu_0 t = 0.5$, 1, and 2, the results were obtained entirely by the Monte Carlo calculation. For greater barrier thicknesses the values quoted are the result of applying the correction factors of table 3 to an extensive set of calculations for an infinite medium [5]. The infinite-medium results are stated to be accurate to within 5 percent. The accuracy of the derived transmission buildup factors is therefore of the order of 6 to 7 percent. The direct Monte Carlo results for shallow penetration have about the same accuracy.

5.3. Application of the Monte Carlo Method to an Infinite-Medium Problem

For heavy elements the boundary effect is so small that the Monte Carlo method does not add much new knowledge. Yet it can be utilized as a convenient and laborsaving tool for the extension of available results. As an example of such an application we have considered the penetration of radiation from a plane monodirectional oblique source in an infinite medium. This problem can be handled by the moment-method, but requires much more work than the corresponding problem for plane monodirectional sources with zero obliquity, or plane isotropic sources. We considered a 4-Mev plane oblique source in lead. A set of 100 energy-angle histories were selected that yielded buildup factors in close agreement with those of a moment-calculation for a monodirectional zero obliquity source for penetrations up to $\mu_0 t = 16$. Then we performed a rotation of the angular part of these histories. Provision for doing this is built into the SEAC code for the computation of the G_n's. After rotation, these histories can then be used as input data for oblique source problems, and the results can be expected to be reliable, since the energy part of the histories, known to be properly representative,

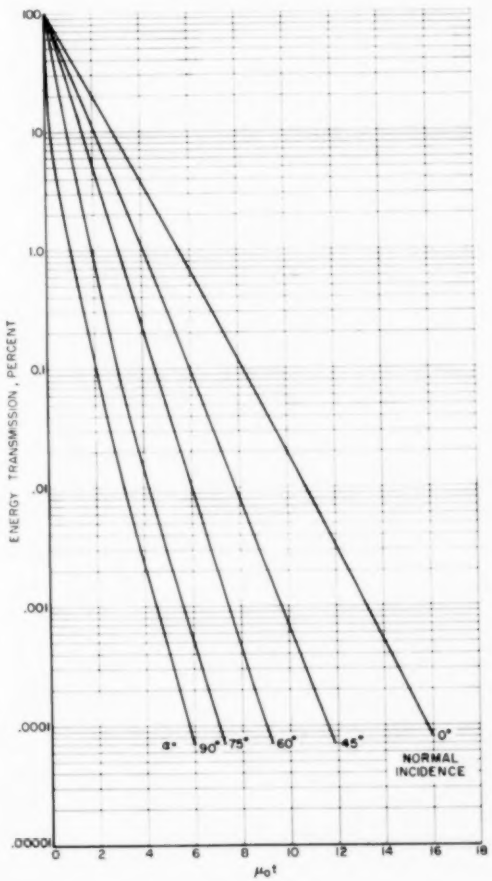

FIGURE 2. *Transmission of radiation from a 4-Mev plane monodirectional oblique source through a lead barrier.*

remained unchanged by the rotation. In this manner we have made quick calculations for obliquity angles $\theta_0=45°$, 60°, 75°, and 90°. As a final check, the fluxes from sources with different obliquities were summed so as to obtain the flux from a plane isotropic source. Again the agreement with a direct moment-calculation was close. Thus a fix on the accuracy of the Monte Carlo results was obtained at two points, and in spite of the small sample size the penetration of radiation to very great depths could be calculated with an accuracy which we estimate to be 5 to 7 percent. The results of the calculation are shown in figure 2 in the form of plots of the percent-energy-transmission (=buildup factor $\times$ $\exp(-\mu_0 t)$) versus $\mu_0 t$, for different obliquity angles.

5.4. Energy Spectra and Angular Distributions

In figure 3 we show for normally incident 0.66-Mev radiation the energy spectra of the scattered flux transmitted through water barriers with thicknesses $\mu_0 t=4$ and $\mu_0 t=8$. The corresponding energy spectra at the same depths in an infinite medium are also shown. (The histograms pertain to the Monte Carlo results, the curves to a moment-calculation.) The shaded areas between corresponding histograms for transmission and an infinite medium are a measure of the boundary effect. It can be seen that the presence of boundaries removes a large part of the low-energy end of the spectrum, but leaves spectral components near the source energy unchanged. It is noteworthy that the spectra are quite similar at both depths. This lends support to our argument that the constancy of the buildup factor ratios is connected with the occurrence of radiative equilibria.

Figure 4 pertains to the same conditions as figure 3, and shows the angular distribution of the scattered transmitted energy flux, and of the corresponding flux in an infinite medium. The shaded areas again indicate the boundary effect. The shaded areas for negative values of $\cos\theta$ represent photons which crossed the boundary 2, 4, 6, · · · times, while the areas for positive values of $\cos\theta$ represent photons which crossed the boundary 3, 5, 7, · · · times in an infinite medium. The relatively small number of photons in the latter group indicates that repeated crossings of any plane deep in an infinite medium are quite unlikely, so that it should be possible to calculate the boundary effect in reasonable approximation by infinite-medium theory, by setting the transmitted flux equal to the infinite-medium flux integrated over positive values of $\cos\theta$. The angular distributions are similar to the energy spectra in that they do not change their shape as

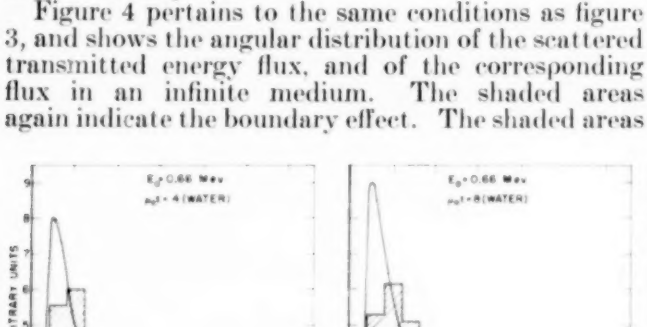

FIGURE 3. *Energy spectra of scattered radiation transmitted through water barriers of thickness $\mu_0 t=4$ and $\mu_0 t=8$, for normally incident beams of 0.66-Mev photons.*

The unshaded parts of the histograms pertain to penetration through a finite barrier, while the shaded areas indicate the additional radiation that would penetrate to a depth t in an infinitely extended medium. The curves accompanying the histograms represent the results of calculations by the moment-method for an infinite medium.

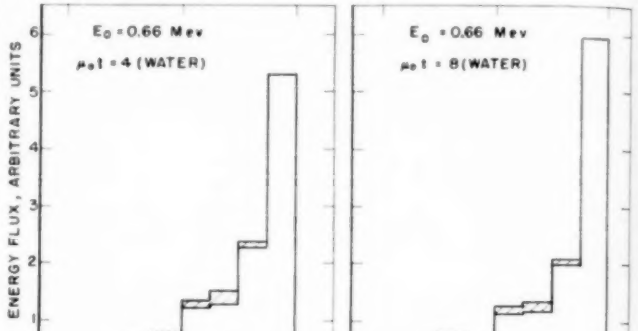

FIGURE 4. *Angular distributions of scattered radiation transmitted through water barriers of thickness $\mu_0 t=4$ and $\mu_0 t=8$, for normally incident beams of 0.66-Mev photons.*

The unshaded parts of the histograms pertain to penetration through a finite barrier, while the shaded areas indicate the additional radiation that would penetrate to a depth t in an infinitely extended medium. The angle θ measures the direction of the transmitted radiation with respect to the normal to the barrier face. Shaded areas for positive values of cos θ represent photons that would cross the boundry plane at least three times in an infinite medium.

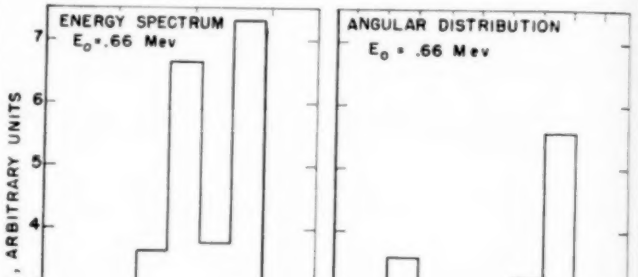

FIGURE 5. *Energy spectrum and angular distribution of radiation reflected from a semi-infinite water barrier, for a normally incident beam of 0.66-Mev photons.*

The angle θ indicates the direction between the direction of the reflected photons and the normal to the barrier face.

the barrier thickness is increased from $\mu_0 t=4$ to $\mu_0 t=8$.

Figure 5 shows the angular and energy distributions of reflected radiation due to 0.66-Mev photons incident normally on a semi-infinite water barrier. Both distributions have two distinct peaks. Their locations are such that they appear to imply the existence of two preferred modes of reflection, one associated with a first scattering through approximately 180°, the other with a first scattering through approximately 90°.

6. Discussion

6.1. Comparison with Experiments

A recent survey of experiments on the penetration and diffusion of γ-radiation [5] indicates that few experiments have been done for plane source radiation that are comparable with our calculations. Moreover, the uncertainty of the experimental results is usually at least of the order of magnitude of the boundary effect. It would seem that the boundary effect could best be checked by a differential experiment in which one measures the flux through a detector, both with and without backing material behind the detector.

The penetration of radiation with energies between 0.66 and 2.76 Mev through iron slabs has been measured by Beach et al. [7]. Their experimental values agree to within a few percent with the buildup factors listed in table 4. But the experimental results include large corrections for air-scattering, so that the evidence is not as conclusive as one might wish.

Kirn, Kennedy, and Wyckoff [8] measured the penetration of Co^{60} radiation (1.17 and 1.33 Mev) through concrete barriers. An attempt has been made to match their results by a calculation for an aluminum barrier with a concrete-equivalent electron density. (The photoelectric absorption cross section per electron is very nearly the same for concrete as for aluminum, except at extremely low energies.) The penetration in an infinite aluminum medium was found by interpolation from calculations of Goldstein and Wilkins [5]. These results were then corrected for the boundary effect with the use of table 3 of this paper. Finally, the predicted buildup factors were increased by small amounts (not more than 2%) to account for the energy response of the experimental detector. One more major adjustment must be made prior to a comparison of theory and experiment. The experimental cobalt source was 1 cm thick, so that there was an appreciable chance for Compton scattering and resultant energy degradation of the radiation in the source. The degraded radiation is absorbed much more strongly than the primary radiation while passing through the concrete barrier. When considering the attenuation at moderate and great depths one should renormalize the source strength so as to include only undegraded photons emerging from the source. An approximate single-scattering calculation leads to the estimate that the effective source strength is $.82 \pm .05$ times the nominal source strength. Table 5 shows the experimental and theoretical energy transmission (for normal incidence of the Co^{60} radiation on the concrete barrier). The agreement with the adjusted experimental values is good. Although the source strength correction constitutes a weakness of the comparison (at least insofar as verification of the boundary effect is concerned), it is significant that by adjusting a single normalization constant one can get agreement between theory and experiment over a wide range of barrier thicknesses.

TABLE 5. *Energy transmission by a concrete barrier*

Comparison of the experimental transmission found by Kirn et al. [8], and the predicted transmission. (Transmission=buildup factor×exp($-\mu_0 t$).)

	Energy transmission, in percent, with concrete barrier thickness of—			
	5.0 in.	10.0 in.	15.0 in.	17.5 in.
Experiment, uncorrected	39.0	11.0	2.80	1.40
Experiment, corrected for the degradation of radiation in the source	46.8	13.2	3.36	1.68
Theory	44.3	13.7	3.41	1.69

The experimental literature on the reflection of gamma radiation from barriers is even scarcer than that on transmission. We have learned of some unpublished measurements by Kirn, Kennedy, and Wyckoff [4] of the reflection of Co^{60} radiation from effectively semi-infinite concrete and lead barriers. (The lead barrier actually was a concrete block fronted by ¼ in. of lead, but this combination was in effect equivalent to a solid lead barrier.) By interpolation based on the results in table 2 we obtained reflection buildup factors which, according to the comparison in table 6, are in reasonably good agreement with the experimental values.

TABLE 6. *Energy-reflection buildup factors for Co^{60} radiation incident on semi-infinite barriers*

Comparison of the theory with the experiment of Kirn et al.

Material	Angle of incidence, θ_0	Experiment	Theory
	deg		
Concrete	0	1.063	1.065
	60	1.086	1.110
Lead	0	1.012	1.0095
	60	1.041	1.040

6.2 Comparison With Other Calculations

In table 7 a comparison is made for buildup factors for shallow and moderate penetration depths, pertaining to 0.66 Mev radiation incident on water barriers. The comparison includes the results of this paper, infinite-medium calculations by the moment-method [10] and the results of two other Monte Carlo calculations, one of them done by a direct stochastic analog method [9], the other

[4] H. O. Wyckoff, private communication.

TABLE 7. *Comparison of buildup factors obtained by various methods for 0.66-Mev radiation in water medium*

Method	Transmission, $\overline{B}(t,t)$			Penetration in semi-infinite medium, $\overline{B}(t,\infty)$			Reflection from semi-infinite medium, $\overline{B}(0,\infty)$	
	$\mu_0 t$							
	1	2	4	1	2	4	$\theta_0=0$	$\theta_0=60°$
Monte Carlo (this paper)	1.96	3.10	5.99	....	4.02	7.15	1.148	1.189
Monte Carlo (NBS) [6]	1.89	3.21	5.64	2.48	4.07	6.98	1.15	1.18
Monte Carlo (NRL) [9]	1.92	3.30	5.55	2.43	3.75	6.55	1.14	.....
Spencer-Fano moment-method [10]	.....	.....	.....	.....	3.89	7.37	.....	.....

based on an analytical integration over a sampled collision density [6]. The agreement of the various methods is on the whole satisfactory.

6.3. Comments

We have demonstrated the constancy of the boundary effect for thick barriers, and the resultant lack of necessity to do deep-penetration Monte Carlo calculations, only for plane geometry. But it appears plausible that a similar situation will also prevail in other geometries since the constancy of the boundary effect appears to be rooted in the occurrence of equilibrium spectra far from a radiation source.

The advantage of incorporating knowledge obtained from other sources into a Monte Carlo calculation through the technique of correlated sampling has been clearly demonstrated. In fact, it was only this technique which made it possible for us to survey the boundary effect for a variety of conditions without excessive computation.

The analytical treatment of the space variable likewise proved successful, but we feel that it may have been too much of a good thing. From the standpoint of computing efficiency, there is an optimum amount of analysis that should be put into a Monte Carlo calculation, which depends on the nature of the problem and the capabilities of the computing machine. It is questionable whether we operated near this optimum. If one is interested in the radiation intensity, it is not unreasonable to take, as we have done, relatively small samples and to analyze them exhaustively. But if energy spectra and angular distributions are desired, it is probably preferable to use larger and more representative samples of energy-angle histories and to analyze them less thoroughly. One possible compromise would be to confine the analytic treatment of the space variable to a limited number of collisions, and then to revert to a stochastic calculation.

The authors thank Anne Futterman for aid and advice in programing the problem for SEAC.

7. References

[1] L. V. Spencer and U. Fano, J. Research NBS **46,** 446 (1951) RP2213.
[2] L. V. Spencer, Phys, Rev. **88,** 793 (1952).
[3] G. H. Peebles, Rand Report R-240 (1952); J. Appl. Phys. **24,** 1272, 1437 (1953).
[4] H. Kahn, Nucleonics **6,** No. 6, 60 (1950); Applied Mathematics Series NBS (June 1951) AMS12.
[5] H. Goldstein and J. E. Wilkins, Jr., AEC Report NYO 3075 (June 1954).
[6] M. J. Berger, Reflection and transmission of γ-radiation by barriers: Monte Carlo calculation by the collision density method, J. Research NBS **55,** 343 (1955) RP2640.
[7] L. A. Beach, R. B. Theus, and W. R. Faust, Phys. Rev. **92,** 355 (1953).
[8] F. S. Kirn, R. J. Kennedy, and H. O. Wyckoff, Radiology **63,** 94 (1954).
[9] L. A. Beach, R. B. Theus, J. D. Plawchan, and W. R. Faust, NRL Report 4412 (April 1954).
[10] M. J. Berger, The penetration of γ-radiation from a plane monodirectional oblique source, J. Research NBS **56,** (1956) (in press).

WASHINGTON, September 1, 1955.

Journal of Research of the National Bureau of Standards Vol. 56, No. 2, February 1956 Research Paper 2654

An Examination of the Helium Vapor-Pressure Scale of Temperature Using a Magnetic Thermometer[1]

E. Ambler and R. P. Hudson

The variation of the mutual inductance of two coils surrounding a paramagnetic crystal has been measured as a function of the saturation vapor pressure of helium in the range 1.3° to 4.2° K. The fact that this quantity should vary inversely as the absolute temperature has been made use of to investigate the consistency of two recently proposed vapor-pressure temperature scales. The results suggest errors above 2° K in the empirical equation proposed by Clement, Logan, and Gaffney (in contrast to the experiences of Erickson and Roberts with a magnetic thermometer) and are in closer accord with the thermodynamic calculation of Van Dijk and Durieux.

1. Introduction

All practical thermometry in the "liquid-helium region" (that is, between 1° and 5.2° K) is dependent, directly or indirectly, upon a knowledge of the relation between the saturation vapor pressure of helium and the absolute temperature. Many investigators measure directly the pressure over the liquid-helium cryostat and derive T from p-T tables; others use the same procedure to calibrate a resistance thermometer or magnetic thermometer, etc. In this type of vapor-pressure measurement the accepted practice is to apply a depth correction ("hydrostatic head") to the measured value of p; this correction is, however, of somewhat doubtful validity and can be avoided by measuring the pressure in a vapor-pressure bulb that is in thermal equilibrium with the material under investigation (effectively zero immersion).

The p-T tables in general use at the present time comprise the "1948 scale" [1][2] and are based on the work of Schmidt and Keesom [2], Bleaney and Simon [3], and Kamerlingh Onnes and Weber [4]. Possible errors in the 1948 scale were admitted at the time of its preparation, notably in the 1.3° to 2.2° K region from consideration of the helium isotherm measurements of Kistemaker [5], and between the normal boiling point and the critical point due to the sparseness of the experimental data upon which the scale was based in the latter region. The investigations of Erickson and Roberts [6] with a magnetic thermometer for the region 1° to 4.2° K and those of Berman and Swenson [7] above 4.2° K with a gas thermometer provided a strong basis for a revision of the 1948 scale, and an empirical formula was developed by Clement and coworkers [8] from which a p-T table could be conveniently calculated to any desired precision, and which fitted the new data to within 0.002 deg throughout the entire range. A summary of the situation obtaining in October 1954, prior to the development of the Clement formula and the publication of the supporting evidence obtained by Corak et al. [9] from calorimetric work and by Keller [10] from He^4 and He^3 isotherm data, has been given by Hudson [11]. The latter report made reference to some preliminary magnetic thermometer investigations by Hudson and de Klerk (unpublished) that were in qualitative agreement with the findings of Erickson and Roberts [6] but suggested somewhat larger errors in the 1948 scale in the region of 3.5° K. These measurements have now been extended, using improved apparatus, and the results provide the subject of the present report. While this work was in progress, Keesom and Pearlman [12] reported that some anomalies in their calorimetric data could be removed upon reevaluating their data in terms of the Clement equation.

In summary, the evidence available in mid-1955 strongly supported the validity of the Clement equation. A revision of the 1948 scale, long overdue, therefore seemed feasible and the time opportune with the approach of the Fourth International Conference on Low Temperature Physics in Paris in September 1955. During this conference, however, the results of a new thermodynamic calculation of the p-T relation, which differs by several millidegrees from the Clement equation below 1.5° K and above 2.2° K, were announced by Van Dijk and Durieux.[3]

The first part of section 4 of this paper deals with an analysis of our data in terms of the Clement equation. In section 4.2 the same data are reanalyzed in terms of the Van Dijk-Durieux table.

2. Apparatus

To reduce uncertainties in the measurement of p, the saturation vapor pressure, occasioned by measurement of the bath-pressure and application of the hydrostatic-head correction, a vapor-pressure bulb was employed. A series of measurements was performed with the apparatus shown in figure 1, a.

The magnetic thermometer comprised a paramagnetic salt specimen, A (a 1-in. sphere ground from a large crystal of chromic methylammonium alum)[4]

[1] A brief account of this work was presented at the Fourth International Conference on Low Temperature Physics, Paris, August 30 to September 8, 1955.

[2] Figures in brackets indicate the literature references at the end of this paper.

[3] H. van Dijk and M. Durieux, paper presented at the Fourth International Conference on Low Temperature Physics, Paris Aug. 30 to Sept. 8, 1955. We are indebted to Dr. van Dijk for kindly providing us with advance information on this calculation.

[4] The choice of salt was based upon the requirements: Reproducible behavior, small crystal field splitting and dipole-dipole interaction, absence of direct exchange interaction, and ease of growth of large crystals.

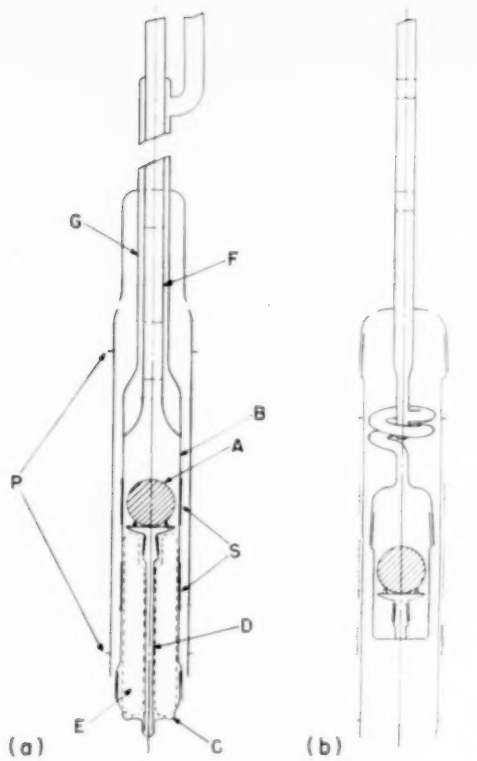

FIGURE 1. *Vapor-pressure bulb and magnetic thermometer.*

a, First apparatus, used in June 1955 measurements; b, modification as used in August 1955 measurements. For explanation of symbols, see text.

located within a mutual inductance, P-S, which was wound, in a rigid assembly, on concentric glass tubes. The latter was connected to an a-c mutual-inductance bridge [13]. For convenience of removal and inspection of the crystal, the bulb, B, was extended to project beyond the coil windings, and closed at the bottom by a ground-joint plug, C. A pedestal, D, supported the crystal, and the volume of the bulb was reduced by means of a hollow glass "filler", E. The tube, F, connected the bulb to the manometer system and was protected by a vacuum jacket, G. Sealed-in glass disks, each perforated by one small hole (about 2 mm in diameter), provided radiation shielding, and F and B were silvered internally.

The purpose of the jacket, G, was to avoid a "cold spot" on F: Due to the hydrostatic head effect, the liquid helium in the surrounding bath is coldest at the surface and, if the vapor in F comes to thermal equilibrium with the bath liquid at this point, the pressure indicated on the manometers will be that corresponding to the temperature at the liquid surface and not at the paramagnetic salt (but see below).

As the temperature of A changed with changing bath pressure, the variation in susceptibility was detected as a change in the bridge setting, n. Since the approximate calibration formula of the thermometer was $T=34/n$ and the precision of bridge setting was $\Delta n=0.001$, temperature changes could be observed as follows: At 4° K, 5×10^{-4} deg; at 3° K, 2.5×10^{-4} deg; at 2° K, 1.2×10^{-4} deg; at 1.3° K, 5×10^{-5} deg. This precision was not realized in practice because of small fluctuations at the lowest pressures and to the necessity for applying small corrections for the nonlinearity of the bridge, but the probable error due to such effects was less than 1 millidegree thoughout the range of measurement (1.3° to 4.2° K).

Subsequently the apparatus was redesigned, for reasons given below, and the second version is shown in figure 1, b In this modification there was no vacuum jacket shielding the tube, F, the vapor-pressure bulb was shortened considerably, and access to the latter was made possible by winding the coils of the mutual inductance on demountable formers. This assembly proved thoroughly satisfactory from the point of view of rigidity.

3. Experimental Procedure

With liquid helium in the cryostat, liquid helium was introduced into the vapor-pressure bulb by condensation of gas under a small overpressure. Prior to the silvering and final assembly, a test filling was carried out to determine the exact quantity of helium required to submerse the crystal, A, and to observe the change of liquid level within the bulb during continuous cooling of the bath. This level will tend to rise because of condensation of the helium gas in the manometer system and fall because of increased density of the liquid as the lambda point is approached. In the present apparatus, the former effect tended to outweigh the latter, and there resulted about a 3-mm submersion at the lambda point. As the precise depth varied with bath level (a large part of the dead-space gas is contained in the section of F that is immersed), the possible correction of 0.03 mm of Hg was not applied to the measured value of p. [The corresponding error in T is 3×10^{-4} deg at the lambda point and becomes progressively smaller as T increases; below the lambda point there is, of course, no depth correction.]

In an experimental determination of helium vapor pressure the most probable sources of error, i. e., extraneous heat influxes to the bulb, will lead to an overestimate of p. Apart from the more familiar radiation and conduction effects, there is one peculiar to low-temperature apparatus; viz., a heat influx due to oscillations in the gas column in a tube such as F. As a result of these heat leaks, the surface temperature of the bulb liquid will be raised, and temperature inhomogeneity will persist because of the low thermal conductivity of the liquid. A thermometer below the surface will therefore be at a lower temperature than that corresponding to the measured value of p. The paramagnetic salt is a much better heat conductor than liquid helium, but, even so, a very small heat influx (if all passes through the salt) will suffice to set up a differential of several millidegrees across a 1-in. sphere. (A rough calculation gives: at 4.2° K, 5×10^{-4} watt per millidegree; at 2.2° K, 10^{-4} watt per millidegree.) The employment of a vacuum jacket in order to

avoid a cold spot on tube F (fig. 1), was found to do more harm than good; heat flow along F from above is prevented from entering the bath-liquid, and the conduction heat leak into the vapor-pressure bulb is greatly intensified. A strong manifestation of this effect was observed in the first apparatus, and it was found necessary to admit "exchange gas" into the erstwhile vacuum space, G, in order to minimize this heat leak. [In fact, the "cold-spot hypothesis" appears, upon closer examination, to be invalid for liquid-helium vapor-pressure thermometry in a glass apparatus. This was not appreciated, however, at the time of designing the first apparatus. The hypothesis supposes that a pressure drop exists along the tube corresponding to the full hydrostatic head, which is, for example, 1 mm of Hg for a 10-cm depth. (This is equivalent to 1.5 millidegrees at 4° K, 3.7 millidegrees at 3° K.) Under such a Δp, there would be a very large flow of vapor up the tube, which, for the maintenance of the supposed conditions, must cool to the cold-spot temperature and then return downward by convection or condense and flow back as liquid. A rough calculation shows at once that in a tube of the size used (1-cm i. d.) the required heat transfer could not possibly take place through the wall and the process must be self-stifling.]

The presence of gas oscillations in the tube, F, was sought for by connecting a small oil manometer of 2-mm bore between F and the bath.[5] None could be detected with the arm connected to the bath closed off. (With this arm open, the oil meniscus oscillated with a period of some 15 sec and an amplitude of about 1 mm.) The same manometer could be used as a direct check on the hydrostatic-head effect. In the first apparatus, the hydrostatic head as measured in this way was always considerably higher than that computed from the level of the liquid in the bath. With the second apparatus, the two values always checked much more closely, which suggests that a heat leak was present in the first apparatus.

The second apparatus was accordingly built without the vacuum shield, G (fig. 1, a) and with smaller holes in the radiation shields (which were also increased in number and more closely spaced). Enough liquid was condensed to reach, initially, the equator of the sphere, A, to make better use of the thermal conductivity of the salt as opposed to that of liquid helium.

The manometers were of sufficiently large bore to obviate the necessity for meniscus-height corrections. Thermomolecular pressure effects, and the reflux of helium due to film flow in the He II region, were negligible for the 1-cm-diameter tube used. Pressures were measured to 0.01 mm by means of a Wild cathetometer and the readings corrected to standard gravity and 20° C. Pressures were stabilized through simultaneous adjustment of a fine-control pumping valve and the current through a small heating coil in the bottom of the cryostat.

[5] We are indebted to J. R. Clement for suggesting this procedure.

The bridge reading, n, is a linear function of the susceptibility of the paramagnetic salt specimen, χ, which varies as the inverse of the absolute temperature (Curie law). Departures from the Curie law due to the crystalline field splitting of the ground state spin-quadruplet are negligible down to 1.3° K, the lower limit of measurement [14]. The calibration formula actually has the form

$$n-B=A/T, \tag{1}$$

where A is proportional to the Curie constant of the material, and B is a second constant, equivalent to the bridge balance value at infinite temperature. In order to examine the over-all consistency of a given p-T relation the two constants A and B may be determined by plotting n as a function of $1/T$ and fitting a straight line to the data. Inserting these values into eq (1), magnetic temperatures, T_m, are then computed for each measured value of n, and the differences $\Delta T=T-T_m$ provide a measure of the "over-all validity" of the given p-T relation. [As the latter may be a priori in error in any part of the temperature range investigated, the correct values of A and B are, within limits, infinitely variable and the final choice correspondingly arbitrary. The two constants may be fixed by considering the scale to be correct at any two chosen points, preferably at opposite ends of the temperature interval (cf. Erickson and Roberts [6]).] Values of $\Delta T/T_m$ are then plotted against T_m for a more sensitive check of the quality of the above fit: for let us suppose that the derived ΔT's are entirely due to incorrect choices of the values for A and B. Then

$$\Delta T=T-T_m=\frac{\partial T_m}{\partial A}\Delta A+\frac{\partial T_m}{\partial B}\Delta B$$

$$=\frac{\Delta A}{A}T_m+\frac{\Delta B}{A}T_m^2, \tag{2}$$

and

$$\frac{\Delta T}{T_m}=\frac{\Delta A}{A}+\frac{\Delta B}{A}T_m. \tag{2a}$$

Bearing in mind that this type of plot will tend to exaggerate deviations at the lowest temperatures, the best straight line may now be drawn and the originally chosen values of A and B modified accordingly (see footnote 5). By such a procedure it was found possible to assign final values to A and B with confidence that any alternative choices that could be readily permitted would only affect the values of ΔT in a minor way and would not invalidate the general conclusions as to the over-all correctness of the scale. [This procedure becomes the more acceptable, the better is the p-T relation under examination. In the case of the 1948 Scale, for example, the errors are so large that the choice of B would have to be supported by an independent determination of this quantity from measurements at high temperatures; this was not possible in the present apparatus where the measuring coils were immersed in liquid helium.]

TABLE 1. *Corresponding values of pressure in millimeters of mercury, p (corrected to 20° C and standard gravity), and bridge dial-setting, n (corrected for nonlinearity in decade scale)*

June 7, 1955		June 8, 1955		June 16, 1955		June 17, 1955		August 17, 1955	
p	*n*	*p*	*n*	*p*	*n*	*p*	*p*	*p*	*n*
768.00	11.223$_1$	748.67	11.164	758.94	11.202$_0$	769.97	11.227$_3$	726.55	17.012$_1$
751.77	11.178$_5$	413.42	9.876$_3$	758.12	11.200$_5$	750.63	11.173$_5$	726.22	17.013$_2$
627.49	10.803$_9$	41.060	3.805$_8$	680.15	10.977$_8$	550.49	10.520$_8$	603.46	17.280$_8$
508.12	10.334$_1$	37.894	3.577$_9$	603.56	10.723$_2$	547.46	10.510$_3$	495.96	17.573$_7$
341.13	9.443$_7$	23.473	2.182$_7$	501.32	10.317$_4$	315.84	9.258$_5$	320.30	18.263$_1$
254.04	8.736$_3$	16.987	1.240$_4$	402.33	9.829$_5$	45.486	4.110$_3$	181.73	19.224$_2$
153.91	7.473$_0$	13.827	0.638$_8$	173.72	7.794$_0$	36.834	3.492$_2$	96.08	20.385$_0$
71.02	5.378$_0$	13.581	.585$_0$	88.05	5.992$_2$	21.691	1.959$_8$	24.595	23.100$_9$
70.71	5.376$_1$	8.526	−.795$_0$	87.81	5.984$_7$	8.576	−0.775$_2$	17.795	23.755$_2$
26.03	2.478$_3$	8.556	−.788$_3$	14.676	0.814$_7$	3.502	−3.515$_7$	13.126	24.371$_7$
25.80	2.451$_3$	6.415	−1.650$_3$	14.774	.836$_7$	.....	.....	9.367	25.070$_4$
.....	.....	3.907	−3.173$_0$	.....	.....	.....	.....	6.141	25.951$_0$
.....	.....	2.229	−4.927$_0$	.....	.....	.....	.....	3.770	27.003$_0$
.....	.....	1.263	−6.765$_7$	.....	.....	.....	.....	2.358	28.010$_9$

4. Results

The experimental data, i. e., corresponding values of pressure in millimeters of mercury (corrected to 20° C and standard gravity) and bridge reading (corrected for nonlinearity), are given in table 1.

4.1. Comparison With the Clement Equation

Four runs on different days were made with the first apparatus and the results could be harmonized, using slightly different values for the constants A and B, with a quite small scatter. This is shown in fig. 2,a.[6]

The signal feature of these results is a large positive deviation hump ($\Delta T \sim 5$ millidegrees) in the middle of the He I region. The deviations are very small in the He II region (less than 1 millidegree) and achieve significant negative values above 4°K. From what has been said in the preceding section, the good fit in the He II region could be fortuitous, and one might, for example, reassess the thermometer calibration to give a zero deviation in the region of the boiling point and again somewhere in the middle, say, of the He II region. This has been done in figure 2, b. The main effect is to exaggerate the 3°K "hump" while only slightly affecting the points below the lambda point.

On either assessment, however, the suggestion remains that the "Clement temperature" (T_{C1}) is too high by several millidegrees in the neighborhood of 3°K. Equally well, of course, the measured vapor pressures could be too high here due to errors of measurement, such as would be occasioned by extraneous heat influx to the bulb. All the data of figure 2 were obtained with exchange gas introduced into the jacket, G (fig. 1, a). Without exchange gas the 3°K hump became several times larger, and this finds a ready explanation in terms of heat conducted down tube F (fig. 1, a), as discussed in section 3. By the same token, the hump of figure 2 might be due to an ineradicable heating effect, and that it is partly so is supported by the data obtained with the second apparatus, shown in figure 3.

[6] The results as presented in figs. 2a and 3 were actually obtained using the same A, B values as finally chosen for the corresponding Van Dijk-Durieux evaluation (figs. 4 and 5, respectively). It so happens that these values provide as good a general fit as any others.

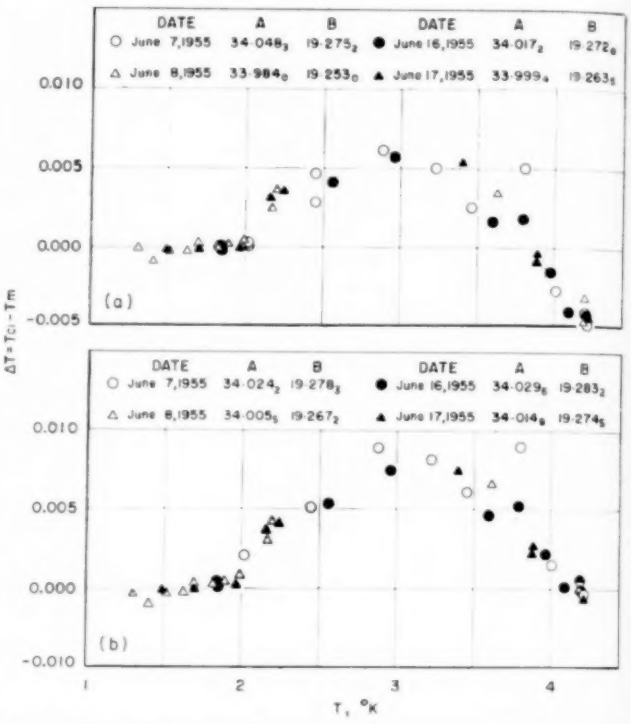

FIGURE 2. *Deviation of temperature as indicated by vapor pressure and Clement p-T relation (T_{C1}) from magnetic temperature (T_m) as a function of T.*

a, Results of June 1955; b, data reanalyzed with different values of constants A and B, equation (1), to give $\Delta T = 0$ at normal boiling point.

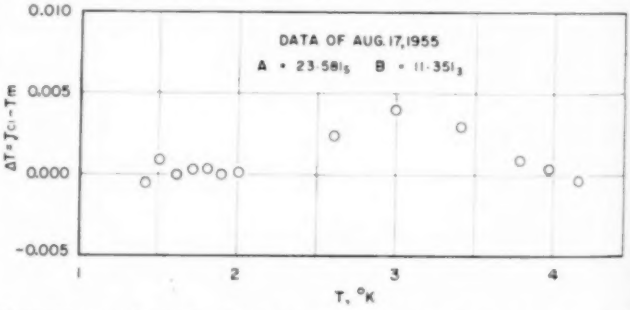

FIGURE 3. *Results of August 1955 analyzed in terms of Clement temperatures, corresponding to June data of figures 2a and 2b.*

Only one experiment was carried out with this apparatus, and the data are accordingly somewhat sparse. The thermometer calibration was quite different from the previous case, i. e., one was then operating upon a different section of the bridge windings, which is an advantage in checking the internal consistency of the bridge. The results are very similar to those of figure 2, b, but the hump in the He I region is much less pronounced (see footnote 6).

4.2. Comparison With the Van Dijk-Durieux Table

Recently Van Dijk and Durieux (see footnote 3) have recalculated the p-T relation for helium, making a reassessment of the best available thermodynamic data. Their results are not in exact accord with the Clement equation and, in fact, deviate from it in the He I region after the manner of the points in figure 3, with a ΔT_{max} of 3.6 millidegrees at 2.9°K. In the He II region, $\Delta T(=T_{C1}-T_{VDD})$ increases steadily from −0.001 deg at 1.9°K to +0.0016 deg at 1.0°K.

In consequence, the magnetic thermometer data of this report can be fitted somewhat more closely to the Van Dijk-Durieux table than to the Clement equation. Figure 3 has been obtained in a rather subjective manner, with an eye to the general features of a plot of $T_{C1}-T_{VDD}$ versus T.

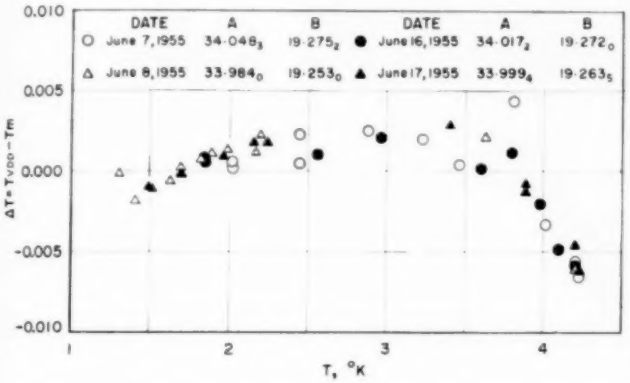

FIGURE 4. *Deviation of temperature as indicated by vapor pressure and Van Dijk-Durieux p-T relation (T_{VDD}) from magnetic temperature, T_m, as a function of T.*

Results of June 1955.

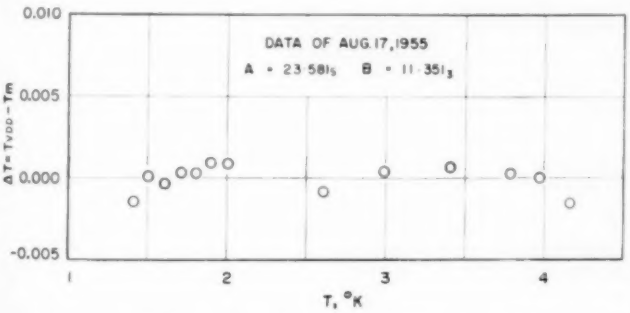

FIGURE 5. *Results of August 1955 analyzed in terms of "Van Dijk-Durieux temperatures," corresponding to June data of figure 4.*

(Compare fig. 3.)

The latter [not shown] shows zero deviation at 1.7°K and a minimum deviation at about 3.8°K; these features have been used as a guide in obtaining the calibration curves from which figure 4 is derived. It can be seen that a two-point tie-down is forced on one here, as it is impossible to choose values of A and B (eq (1)) that will give effectively zero ΔT over a significantly large temperature interval without causing unduly large deviations elsewhere. Thus one may keep the magnitude of $\Delta T(=T_{VDD}-T_m$ small throughout the entire range of measurement but then one also obtains a systematic deviation in the He II region.

The August data are plotted in figure 5, which is to be compared with figure 3. Figure 5 was obtained as the best fit throughout the entire range of measurement, and it, too, has the feature of practically zero deviation at 1.7° and 3.8° K. The magnitude of ΔT now lies within $\pm$1.5 millidegrees throughout the range of measurement.

5. Discussion

The two sets of data, viz., the June results with the first apparatus and the August results with the second, do not agree quantitatively but do show qualitatively the same behavior. It is felt that the August data are the more valid (smaller heat leaks into vapor-pressure bulb), and these agree very closely with the Van Dijk-Durieux calculated p-T table. Both Van Dijk and Clement have recently made significant modifications to their respective p-T tabulations. In a subsequent report the present authors will reevaluate the above data together with the results of a new series of measurements.

None of the present measurements can be brought into very close accord with the Clement equation, in contrast to the results of Erickson and Roberts [6]. The greater part of the latter data was obtained from bath-pressures plus hydrostatic-head correction, which might account for the discrepancy, since the conditions necessary for the exact validity of applying such a correction are impossible to achieve in practice.

The significant differences among the data of Erickson and Roberts and the first and second series reported here point up a major problem in vapor-pressure thermometry in the liquid-helium region, viz., the difficulty of reproducing results from one apparatus to another and of checking any p-T relation to the desirable accuracy of 1 millidegree. From the practical point of view, one desires to obtain accurate values of absolute temperature from simply performed measurements of vapor pressure, the latter being an essentially minor part of any given investigation. It is not entirely unreasonable to seek a solution in the direction of making rigid stipulations concerning the technique of vapor-pressure measurement and to evolve a "practical p-T relation" that is different from that calculated on a thermodynamic basis.

On the other hand, it is true that the differences between the Clement equation and the Van Dijk-

Durieux table are never greater than a few millidegrees. Allowing a 2-millidegree precision for the latter table (as its authors claim), a "Clement temperature" should have a maximum deviation from the thermodynamic temperature of 5.6 millidegrees at 2.9° K, a probable error that is tolerable for many of the common research problems in this region. Experiments demanding a knowledge of dT/dp (e. g., specific-heat determinations) are, of course, most sensitive to deficiencies in the temperature scale.

The authors are greatly indebted to J. R. Clement of the U. S. Naval Research Laboratory for many stimulating discussions and helpful suggestions. It is a pleasure to acknowledge the further benefit derived from general discussions of the problem with R. A. Erickson (Ohio State University), M. P. Garfunkel (Westinghouse), P. H. Keesom (Purdue University), W. E. Keller (Los Alamos), L. D. Roberts (Oak Ridge), C. A. Swenson (Iowa State College); and with H. van Dijk, D. de Klerk, and M. P. Durieux (Kamerlingh Onnes Laboratory).

6. References

[1] H. van Dijk and D. Shoenberg, Nature **164,** 151 (1949).
[2] G. Schmidt and W. H. Keesom, Physica **4,** 963, 971 (1937).
[3] B. Bleaney and F. Simon, Trans. Faraday Soc. **35,** 1205 (1939).
[4] H. Kamerlingh Onnes and S. Weber, Leiden Commun. 147b (1915).
[5] J. Kistemaker, Physica **12,** 272 (1946).
[6] R. A. Erickson and L. D. Roberts, Phys. Rev. **93,** 957 (1954).
[7] R. Berman and C. A. Swenson, Phys. Rev. **95,** 311 (1954).
[8] J. R. Clement, J. K. Logan, and J. Gaffney, Phys. Rev. **100,** 743 (1955).
[9] W. S. Corak, M. P. Garfunkel, C. B. Satterthwaite, and A. Wexler, Phys. Rev. **98,** 1699 (1955).
[10] W. E. Keller, Phys. Rev. **97,** 1 (1955); **98,** 1571 (1955).
[11] R. P. Hudson, "Temperature, its measurement and control in science and industry," vol. II, p. 185 (Rheinhold Publishing Corp., New York, N. Y., 1935).
[12] P. H. Keesom and N. Pearlman, Phys. Rev. **98,** 548 (1955).
[13] D. de Klerk and R. P. Hudson, J. Research NBS **53,** 173 (1954) RP 2530.
[14] R. P. Hudson, Phys. Rev. **88,** 570 (1952).

Washington, November 22, 1955.

Journal of Research of the National Bureau of Standards Vol. 56, No. 2, February 1956 Research Paper 2655

Calculation of Thermodynamic Functions for Polyatomic Molecules[1]

Harold W. Woolley

Formulas are given from which the thermodynamic functions may be obtained for polyatomic molecules not exhibiting special phenomena, such as internal rotation. The effects of first and second order anharmonicities and rotational-vibrational interaction are treated in detail, as also are the angular momentum effects of doubly degenerate vibrations in linear molecules. This paper presents formulas for the corrections carried to higher order than has hitherto been available.

1. Introduction

There is occasionally need for accurate thermodynamic functions for polyatomic molecules. A definite calculating procedure exists for approximate calculations via the rigid-rotator harmonic oscillator treatment, with small corrections for effects of anharmonicity, stretching, etc.

This paper presents formulas for the corrections carried to higher order than has hitherto been available. Calculations can thus be made via the approximation formulas with accuracy probably comparable with that of the direct summation method using extrapolated formulas for the energy levels, aside from effects related to vibrational and rotational cut-off, which have been omitted.

2. Nonlinear Polyatomic Molecules

The partition function for the internal molecular energy states may be written as

$$Q=Q_R Q_{Rc} Q_{H.O.} Q_c. \tag{1}$$

For nonlinear molecules,

$$Q_R=(1/\gamma)\sqrt{(\pi/A_0B_0C_0)(kT/hc)^3} \tag{2}$$

is the rigid rotator partition function for the lowest vibrational energy state, where A_0, B_0, and C_0 are the rotational constants for the ground vibrational state, and γ is the symmetry number. $Q_{H.O.}$ is the partition function for vibrational levels of harmonic oscillators. Q_{Rc} is a correction factor including (1) a factor $1+\rho T. \ . \ .$ for rotational stretching, as shown by Wilson [1][2] and (2) a factor $1+\theta_1/T+\theta_2/T^2$ for a low temperature quantum correction for rotation as shown by Stripp and Kirkwood [2].[3] Q_c is a factor including rotational-vibrational interaction and the anharmonicity corrections, now to be treated in detail.

The rotational-vibrational interaction in its simple form arises from the vibrational dependence of the analogue of eq (2) for higher vibrational states. Before summation over vibrational quantum numbers, the dependence is introduced by including the factor

$$R_v=\exp[\Sigma a_i v_i+\Sigma a_{ii} v_i^2+\Sigma a_{ij} v_i v_j+\Sigma a_{iii} v_i^3+\Sigma a_{iij} v_i^2 v_j+\Sigma a_{ijk} v_i v_j v_k], \tag{3}$$

equivalent to a form introduced by Benedict [3].[4] With his formulation, the constants in the factor R_v come from sums of corresponding constants for A_v, B_v, and C_v. A summation procedure adequate to treat this with the anharmonicity effects follows, extending the latter beyond the linear terms of Stockmayer, Kavanagh, and Mickley [4].

[1] Related to a thesis submitted to the Graduate School of the University of Michigan in partial fulfillment of the requirements for the Ph. D. degree in Physics.

[2] Figures in brackets indicate the literature references at the end of this paper.

[3] Expressions representing the T^2 rotational stretching effect and the T^{-3} low temperature correction as well as a low temperature correction for symmetry effects for different classes of rotational levels for the asymmetric rotator are included in the thesis.

[4] An equivalent representation in slightly different form is given in the thesis.

For a given vibrational level, specified by vibrational quantum numbers v_i, $1 \leq i \leq n$, the statistical weight is the product of the n quantities

$$p_i = (v_i + d_i - 1)!/[v_i!(d_i - 1)!], \tag{4}$$

where d_i is the degeneracy associated with the ith fundamental frequency.

The summation over the vibrational levels may be indicated as

$$Q = Q_R Q_{Rc} \sum_{\substack{r \\ v_i s}} R_v \exp[-hcG_v/kT] \prod_i p_i \tag{5}$$

with the vibrational energy in wave numbers given by

$$G_v = \Sigma \omega_i v_i + \Sigma x_{ii} v_i (v_i - 1) + \Sigma x_{ij} v_i v_j + \Sigma y_{iii} v_i (v_i - 1)(v_i - 2) + \Sigma y_{iij} v_i (v_i - 1) v_j + \Sigma y_{ijk} v_i v_j v_k. \tag{6}$$

The relations between these constants and the more usual ones are indicated in appendix 1.

The Boltzmann factor is separated into two factors, one for harmonic oscillators fitting the lowest levels and a second giving the alteration due to anharmonicity

$$\exp[-hcG_v/kT] = \exp[-hc\Sigma \omega_i v_i/kT] \exp[-hc(G_v - \Sigma \omega_i v_i)/kT]. \tag{7}$$

Q_{vc}, the product of the second factor on the right hand side of (7) with R_v, is expanded into a power series whose terms are polynomials in the v's. Defining a function

$$f_i(Z) = v_i!/(v_i - Z)! \tag{8}$$

it can be shown that[5]

$$\sum_{v_i=0}^{\infty} p_i e^{-u_i v_i} = (1 - e^{-u_i})^{-d_i}, \tag{9}$$

where $u_i = hc\omega_i/kT$, and that

$$\sum_{v_i=0}^{\infty} f_i(Z) p_i e^{-u_i v_i} = [(d_i + Z - 1)!/(d_i - 1)!] \cdot [e^{-Zu_i}/(1 - e^{-u_i})^{d_i + Z}]. \tag{10}$$

The factor Q_{vc} can be expressed as a sum of terms, each linear in whatever f_i's it contains.[6] The results of multiple summation over all v_i's follow by application of eq (10). If the right-hand side of eq (10) be designated by $f_i^*(Z)$, one has $\Sigma_v Q_v Q_{vc} = Q_{H.O.} Q_c$, where $Q_v = \exp[-\Sigma_i u_i v_i]$ $Q_{H.O.} = \Sigma_v Q_v$ and where Q_c is the same function of $f_i^*(Z)$ as Q_{vc} was of $f_i(Z)$. Thus eq (1) has been evaluated, $Q_{H.O.}$ being given by

$$Q_{H.O.} = \prod_i (1 - e^{-u_i})^{-d_i}. \tag{11}$$

There is some advantage in using the logarithm of the partition function from this point on because of analytic cancellations of some higher order terms. The terms removed are cross products without linkage in the subscripts, such as $x_{ij}x_{kl}$, $x_{ii}x_{jk}$, and $a_i x_{jj}^2$, for example.

The contribution to ln Q_c due to x_{ii} and x_{ij} terms, with $r_i = e^{-u_i}$ and $s_i = (1 - e^{-u_i})^{-1}$ is

$$\begin{aligned} -(hc/kT) \sum \{ x_{ii} d_i (d_i + 1) r_i^2 s_i^2 + x_{ij} d_i d_j r_i r_j s_i s_j \} + \tfrac{1}{2} (hc/kT)^2 \sum \{ 2x_{ii}^2 d_i (d_i + 1) r_i^2 [1 + 2(d_i + 1) r_i] s_i^4 \\ + x_{ij}^2 d_i d_j r_i r_j [1 + d_i r_i + d_j r_j] s_i^2 s_j^2 + 2x_{ij} x_{ik} d_i d_j d_k r_i r_j r_k s_i^2 s_j s_k + 4 x_{ii} x_{ij} d_i (d_i + 1) d_j r_i^2 r_j s_i^3 s_j \}, \end{aligned} \tag{12}$$

with terms of higher order for this and other contributions listed in appendix 4. At high temperature the first term varies as T and the second as T^2. The terms in the appendix are higher than T^2 in principal dependence at high temperature.

[5] See appendix 2.

[6] Relations giving the simpler polynomials in terms of the f's will be found in appendix 3.

Similarly, the contribution of higher order anharmonic terms is

$$-(hc/kT)\sum\{y_{iii}d_i(d_i+1)(d_i+2)r_i^3s_i^3+y_{iij}d_i(d_i+1)d_jr_i^2r_js_i^2s_j+y_{ijk}d_id_jd_kr_ir_jr_ks_is_js_k\}. \quad (13)$$

The contribution due to rotational-vibrational interaction is

$$\sum\{a_id_ir_is_i+a_{ii}d_ir_i(1+d_ir_i)s_i^2+a_{ij}d_id_jr_ir_js_is_j+\tfrac{1}{2}a_i^2d_ir_is_i^2\} \quad (14)$$

as far as a's alone are concerned, while their mixing with anharmonicities gives

$$-(hc/kT)\sum\{2a_ix_{ii}d_i(d_i+1)r_i^2s_i^3+a_ix_{ij}d_id_jr_ir_js_i^2s_j\}. \quad (15)$$

In all of these (multiple) summations, if the terms are completely symmetric in the indices that are present, such as i, j, etc., the symmetric indices are to progress in size as with $i<j<k$, and so forth. For terms not completely symmetric in the indices, the indices not symmetric are simply not to be equal, thus $i\neq j\neq k$, and so forth.[7]

3. Linear Molecules

There is an additional kind of vibrational-rotational interaction, concerning vibrational angular momentum, which is important for linear molecules. When doubly degenerate vibrations occur, the vibrational energy, eq (6), contains an additional term $g=\sum_{i\leq j} g_{ij}l_il_j$. For linear molecules, in addition, there is dependence of the rotational energy upon l where $l=\Sigma l_i$, giving for the two together

$$F(J,\,l)=g+B_v[J(J+1)-l^2]-D_v[J(J+1)-l^2]^2, \quad (16)$$

where $J=l,\,l+1,\,l+2$ . . ., with double degeneracy for $|l|>0$.

The sum over the rotational levels for $J\geq|l|$ follows from a half integer summation formula of the Euler-Maclaurin type [5]

$$\sum_{n=n_1}^{\infty} f(n)=\int_{n_1-\frac{1}{2}}^{\infty} f(n)dn+(1/24)f'(n_1-\tfrac{1}{2})-(7/5760)f'''(n_1-\tfrac{1}{2})+(31/967680)f^{(5)}(n_1-\tfrac{1}{2}) \ . \ . \ ., \quad (17)$$

giving

$$\sum_{J=|l|}^{\infty}(2J+1)\exp hcB[J(J+1)-l^2]/kT=kT/hcB+1/3+ \ . \ . \ . \quad (18)$$

and

$$Q=\sum_{J=|l|}^{\infty}(2J+1)e^{-hcF/kT}=(1/\gamma)[kT/hcB+1/3+2(kT/hcB)^2D/B]\cdot e^{-hcg/kT}. \quad (19)$$

The exponential in g is expanded as a power series and the summations made with v_i increasing by steps of two from l_i to ∞, then summing l_i from $-\infty$ to $+\infty$. If g is extended to include possible contributions to ln Q_e varying as T^2 at high temperature, while retaining the g_{ij} term needed for nonlinear molecules, as in

$$g=\sum_i g_{ii}l_i^2+\sum_{i<j}g_{ij}l_il_j+\sum g_{iii}l_i^2v_i+\sum g_{iik}l_i^2v_k, \quad (20)$$

the contribution of g to ln Q_e becomes

$$-2(hc/kT)\Sigma\{g_{ii}r_is_i^2+g_{iii}r_i(1+3r_i)s_i^3+g_{iik}d_kr_ir_ks_i^2s_k-2g_{ii}a_ir_i^2s_i^3\}+(hc/kT)^2\Sigma\{g_{ii}^2(r_i+8r_i^2$$
$$+r_i^3)s_i^4+2g_{ij}^2r_ir_js_i^2s_j^2+4g_{ii}x_{ii}r_i^2(4+3r_i)s_i^4+2g_{ii}x_{ik}r_ir_k(1+r_i)s_i^3s_k\}. \quad (21)$$

[7] For a case with 3 frequencies, for example, $x_{11}x_{ij}$ which is not completely symmetric in the indices would include $x_{11}x_{13}$ and also $x_{33}x_{31}$. But $x_{ii}x_{jj}x_{ij}$ has complete symmetry in the indices, and $x_{33}x_{11}x_{13}$ is sufficient without $x_{33}x_{11}x_{31}$ also.

Constants of the latter two types in eq (20) are not experimentally available at present. For a linear molecule, when there is only one doubly degenerate frequency, with $l=l_2$, the $-P_t l^2$ term of eq (16) is commonly absorbed into the $g_{22}l_2^2$ term. In that case, g_{tt} of eq (21) represents $g_{22}+B_v$ of the spectroscopist.

The free energy function for a mole of a substance in the standard ideal gas state is given by

$$-(F^\circ-E_0^\circ)/RT=\ln Q+(5/2)\ln T+(3/2)\ln M+\ln (2\pi/N)^{3/2}k^{5/2}/h^3P_0,$$

P_0 being atmospheric pressure, M the molecular weight, and the others known physical constants. The other functions follow by differentiation as given in appendix 5.

A tabulation by Pennington and Kobe [6] may also be used for convenient evaluation of the more important of the contribution here treated.

4. References

[1] E. B. Wilson, Jr., J. Chem. Phys. **4,** 525 (1936).
[2] K. F. Stripp and J. G. Kirkwood, J. Chem. Phys. **19,** 1131 (1951).
[3] W. S. Benedict (with A. M. Bass), unpublished data.
[4] W. H. Stockmayer, G. M. Kavanagh, and H. S. Mickley, J. Chem. Phys. **12,** 408 (1944).
[5] L. M. Milne-Thompson, The calculus of finite differences (Macmillan and Co., Ltd., London, 1933).
[6] R. E. Pennington and K. A. Kobe, J. Chem. Phys. **22,** 1442 (1954).

5. Appendices

5.1. Appendix 1

The relation of the constants of eq (6) with those in

$$G_v=\sum\bar{\omega}_t(v_t+d_t/2)+\sum\bar{x}_{tt}(v_t+d_t/2)^2+\sum_{t<j}\bar{x}_{tj}(v_t+d_t/2)(v_j+d_j/2)+\sum\bar{y}_{ttt}(v_t+\bar{d}_t/2)^3$$
$$+\sum_{t\neq j}\bar{y}_{ttj}(v_t+d_t/2)^2(v_j+d_j/2)+\sum_{t<j<k}\bar{y}_{tjk}(v_t+d_t/2)(v_j+d_j/2)(v_k+d_k/2)$$

is

$$\omega_t=\bar{\omega}_t+(d_t+1)\bar{x}_{tt}+\sum_j\tfrac{1}{2}d_j\bar{x}_{tj}+(1/4)(3d_t^2+6d_t+4)\bar{y}_{ttt}$$
$$+\sum_j(\tfrac{1}{2})(d_t+1)d_j\bar{y}_{ttj}+\sum_j(d_t^2/4)\bar{y}_{tjj}+\sum_{j<k}\sum(d_jd_k/4)\bar{y}_{tjk}$$

$$x_{tt}=\bar{x}_{tt}+(\tfrac{1}{2})(3d_t+6)\bar{y}_{ttt}+\sum_j(d_j/2)\bar{y}_{ttj}$$

$$x_{tj}=\bar{x}_{tj}+(d_t+1)\bar{y}_{ttj}+(d_j+1)\bar{y}_{tjj}+\sum_k(d_k/2)\bar{y}_{tjk}$$

$$y_{ttt}=\bar{y}_{ttt},\ y_{ttj}=\bar{y}_{ttj}\text{ and }y_{tjk}=\bar{y}_{tjk}.$$

5.2. Appendix 2

To obtain eq (9) and (10), begin with the identity

$$\sum_{v=0}^{\infty}x^{-v}=(1-x^{-1})^{-1}.$$

Multiply by x^{Z-1} and differentiate n times with respect to x, getting

$$\sum_{v=0}(-1)^n\frac{(v+n-Z)!}{(v-Z)!}x^{-v-1+Z-n}=\frac{d^n}{dx^n}[x^Z(x-1)^{-1}].$$

For the second member of the identity, let $x-1=t$, giving

$$\frac{d^n}{dt^n}\,[(t+1)^Z t^{-1}] \qquad \text{or} \qquad \frac{d^n}{dt^n}\left[\sum_{r=0}^{r=Z}\frac{Z!}{(Z-r)!r!}\,t^{Z-r-1}\right].$$

For $n>Z-1$, the only contribution is from the one term with $r=Z$, giving $\dfrac{d^n}{dt^n}\,t^{-1}$ or $(-1)^n n!$ $(x-1)^{-1-n}$. Multiplying both members of the identity by $(-1)^n\,\dfrac{x^{1-Z+n}}{(n-Z)!}$, one has

$$\sum_{v=0}\frac{(v+n-Z)!\,x^{-v}}{(v-Z)!\,(n-Z)!}=\frac{n!}{(n-Z)!}\,x^{-Z}(1-x^{-1})^{-1-n}.$$

Inserting e^{-u_i} for x, one may obtain eq (10) by using $n=Z+d_i-1$, with eq (9) as the special case given by $Z=0$.

5.3. Appendix 3

Functions of v in terms of $(f(s)=v!/(v-s)!$:

$$v=f(1)$$

$$v^2=f(2)+f(1)$$

$$v^3=f(3)+3f(2)+f(1)$$

$$v^4=f(4)+6f(3)+7f(2)+f(1)$$

$$v^5=f(5)+10f(4)+25f(3)+15f(2)+f(1)$$

$$v^6=f(6)+15f(5)+65f(4)+90f(3)+31f(2)+f(1)$$

$$v^3-v^2=f(3)+2f(2)$$

$$v^4-v^3=f(4)+5f(3)+4f(2)$$

$$v^4-2v^3+v^2=f(4)+4f(3)+2f(2)$$

$$v^5-2v^4+v^3=f(5)+8f(4)+14f(3)+4f(2).$$

5.4. Appendix 4

Additional terms in the formulas given earlier are as follows:

Equation (12):

$$-(1/6)(hc/kT)^3\sum\{4x_{ii}^3d_i(d_i+1)r_i^2[1+(8d_i+12)r_i+(8d_i^2+22d_i+15)r_i^2+(2d_i^2+4d_i+2)r_i^3]s_i^6$$
$$+x_{ii}^3d_id_jr_ir_j[1+(3d_i+1)r_i+(3d_j+1)r_j+d_i^2r_i^2+d_j^2r_j^2+(6d_id_j+3d_i+3d_j+1)r_ir_j+d_i^2r_i^2r_j$$
$$+d_j^2r_ir_j^2]s_i^3s_j^3+12x_{ii}^2x_{ij}d_i(d_i+1)d_jr_i^2r_j[1+(3d_i+4)r_i+(d_i+1)r_i^2]s_i^5s_j+6x_{ii}x_{ij}^2d_i(d_i+1)d_jr_i^2r_j[2$$
$$+(2d_i+1)r_i+2d_jr_j+d_jr_ir_j]s_i^4s_j^2+3x_{ii}^2x_{ik}d_id_jd_kr_ir_jr_k[1+(2d_i+1)r_i+d_jr_j+d_jr_ir_j]s_i^3s_j^2s_k$$
$$+24x_{ii}x_{ij}x_{ij}d_i(d_i+1)d_j(d_j+1)r_i^2r_j^2s_i^3s_j^3+12x_{ii}x_{ij}x_{ik}d_i(d_i+1)d_jd_kr_i^2r_jr_k(2+r_i)s_i^4s_js_k$$
$$+12x_{ii}x_{ij}x_{jk}d_i(d_i+1)d_jd_kr_i^2r_jr_ks_i^3s_j^2s_k+6x_{ij}x_{ik}x_{il}d_id_jd_kd_lr_ir_jr_kr_l(1+r_i)s_i^3s_js_ks_l$$
$$+6x_{ij}x_{ik}x_{jl}d_id_jd_kd_lr_ir_jr_kr_ls_i^2s_j^2s_ks_l+6x_{ij}x_{ik}x_{jk}d_id_jd_kr_ir_jr_k(1+d_ir_i+d_jr_j+d_kr_k)s_i^2s_j^2s_k^2\}$$

Equation (13):

$$-(hc/kT)\sum\{z_{iiii}d_i(d_i+1)(d_i+2)(d_i+3)r_i^4s_i^4+z_{iiij}d_i(d_i+1)(d_i+2)d_jr_i^3r_js_i^3s_j$$
$$+z_{iijj}d_i(d_i+1)d_jd_kr_i^2r_jr_ks_i^2s_js_k+z_{iijj}d_i(d_i+1)d_j(d_j+1)r_i^2r_j^2s_i^2s_j^2+z_{ijkl}d_id_jd_kd_lr_ir_jr_kr_ls_is_js_ks_l\}$$
$$+(1/2)(hc/kT)^2\sum\{12x_{ii}y_{iii}d_i(d_i+1)(d_i+2)r_i^3[1+(d_i+1)r_i]s_i^5+4x_{ii}y_{iij}d_i(d_i+1)d_jr_i^2r_j[1$$
$$+2(d_i+1)r_i]s_i^4s_j+4x_{ii}y_{jjj}d_i(d_i+1)d_j(d_j+1)r_i^2r_j^2s_i^3s_j^2+4x_{ii}y_{ijk}d_i(d_i+1)d_jd_kr_i^2r_jr_ks_i^3s_js_k$$
$$+6x_{ij}y_{iii}d_i(d_i+1)(d_i+2)d_jr_i^3r_js_i^4s_j+2x_{ij}y_{iij}d_i(d_i+1)d_jr_i^2r_j[2+d_ir_i+2d_jr_j]s_i^3s_j^2$$
$$+4x_{ij}y_{iik}d_i(d_i+1)d_jd_kr_i^2r_jr_ks_i^3s_js_k+2x_{ij}y_{kkl}d_id_jd_k(d_k+1)r_ir_jr_k^2s_i^2s_js_k^2+2x_{ij}y_{ikl}d_id_jd_kd_lr_ir_jr_kr_ls_i^2$$
$$s_js_ks_l+2x_{ij}y_{ijk}d_id_jd_kr_ir_jr_k(1+d_jr_i+d_jr_j)s_i^2s_j^2s_k\}$$

Equation (14):

$$\Sigma\{a_ia_{ii}d_ir_i[1+(1+2d_i)r_i]s_i^3+a_ia_{ij}d_id_jr_ir_js_i^2s_j+(1/6)a_i^3d_ir_i(1+r_i)s_i^3+a_{iii}d_ir_i[1+(1+3d_i)r_i$$
$$+d_i^2r_i^2]s_i^3+a_{iij}d_id_jr_ir_j(1+d_ir_i)s_i^2s_j+a_{ijk}d_id_jd_kr_ir_jr_ks_is_js_k\}$$

Equation (15):

$$-(hc/kT)\Sigma\{a_{ii}x_{ii}d_i(d_i+1)r_i^2[4+(4d_i+2)r_i]s_i^4+2a_{ij}x_{ii}d_i(d_i+1)r_i^2r_js_i^3s_j+a_{ii}x_{ij}d_id_jr_ir_j[1$$
$$+(2d_i+1)r_i]s_i^3s_j+a_{ij}x_{ij}d_id_jr_ir_j[1+d_ir_i+d_jr_j]s_i^2s_i^2+a_{ij}x_{kj}d_id_jd_kr_ir_jr_ks_is_i^2s_k\}$$
$$+\tfrac{1}{2}(hc/kT)^2\Sigma\{4a_{ii}x_{ii}^2d_i(d_i+1)r_i^2[1+(3d_i+4)r_i+(d_i+1)r_i^2+(d_i^2+d_i)r_i^3]s_i^5+a_{ii}x_{ij}^2d_id_jr_ir_j[1$$
$$+(2d_i+1)r_i+d_jr_j+d_jr_ir_j]s_i^3s_j^2+4a_{ii}x_{ii}x_{ij}d_i(d_i+1)d_jr_i^2r_j(2+r_i)s_i^4s_i+4a_{jj}x_{ii}x_{ij}d_i(d_i$$
$$+1)d_jr_i^2r_js_i^3s_j^2+2a_{ii}x_{ij}x_{ik}d_id_jd_kr_ir_jr_k(1+r_i)s_i^3s_js_k+2a_{jj}x_{ij}x_{ik}d_id_jd_kr_ir_jr_ks_i^2s_j^2s_k\}$$

Equation (21):

$$-(1/3)(hc/kT)^3\sum\{g_{ii}^3(r_i+50r_i^2+194r_i^3+50r_i^4+r_i^5)s_i^6+6x_{ii}g_{ii}^2r_i^2(16+99r_i+70r_i^2+3r_i^3)s_i^6$$
$$+3x_{ij}g_{ii}^2d_jr_ir_j(1+19r_i+19r_i^2+r_i^3)s_i^5s_j+12x_{ij}g_{ii}g_{jj}r_ir_j(1+r_i)(1+r_j)s_i^3s_j^3$$
$$+12x_{ii}^2g_{ii}r_i^2(4+55r_i+70r_i^2+9r_i^3)s_i^6+12x_{ii}x_{ij}g_{ii}d_jr_i^2r_j(8+17r_i+3r_i^2)s_i^5s_j$$
$$+3x_{ij}^2g_{ii}d_jr_ir_j[1+8r_i+5r_i^2+d_j(r_j+4r_ir_j+r_i^2r_j)]s_i^4s_j^2+12x_{ij}x_{jj}g_{ii}d_j(d_j+1)r_ir_j^2(1+r_i)s_i^3s_j^3$$
$$+6x_{ij}x_{ik}g_{ii}d_jd_kr_ir_jr_k(1+4r_i+r_i^2)s_i^4s_js_k+6x_{ij}x_{jk}g_{ii}d_jd_kr_ir_jr_k(1+r_i)s_i^3s_j^2s_k\}$$

5.5. Appendix 5

For a term of ln Q of the form

$$z=xu^pf_1\prod_i r_i^{m_i}s_i^{n_i}=Wf_1,$$

with $f_1=1+\sum_i t_ir_i^{q_i}$ and $u=hc/kT$ and with x, p, m_i, n_i, t_i, and q_i constants, the contributions to the various thermodynamic functions are: For $-(F^\circ-E_0^\circ)/RT$, $z=Wf_1$; for $(H^\circ-E_0^\circ)/RT$, $-udz/du=Wh_2$; for C_p°/R, $u^2d^2z/du^2=Wh_3$; with $h_2=f_1g_1+f_2$, $h_3=f_1g_2+2f_2g_1+f_3$, where

$$f_2=\sum_i t_iq_iu_ir_i^{q_i}$$
$$f_3=\sum_i t_iq_i^2u_i^2r_i^{q_i}$$
$$g_1=-p+\sum_i n_iu_ir_is_i+\sum m_iu_i$$
$$g_2=-p+\sum_i n_iu_i^2r_is_i^2+g_1^2.$$

WASHINGTON, January 11, 1956.

U. S. GOVERNMENT PRINTING OFFICE: 1956

Recent Publications of the National Bureau of Standards

Journal of Research of the National Bureau of Standards, volume 55, No. 6, December 1955 (RP2633 to RP2640 incl.). Annual subscription $4.00.

Technical News Bulletin, volume 39, No. 12, December 1955. 10 cents. Annual subscription $1.00.

Basic Radio Propagation Predictions for March 1956. Three months in advance. CRPL 136. Issued December 1955. 10 cents. Annual subscription $1.00.

Research Papers

Journal of Research, volume 55, number 6, December 1955. Single copies of the Journal vary in price. Single copies of Research Papers appearing in the Journal are not available for sale. The Superintendent of Documents, U. S. Government Printing Office, Washington 25, D. C., will reprint 100 or more copies of a Research Paper. Request for the purchase price should be mailed promptly to that office.

RP2633. First spectrum of barium, Ba I. Henry Norris Russell and Charlotte E. Moore.

RP2634. Compressibilities of long-chain normal hydrocarbons. C. E. Weir and J. D. Hoffman.

RP2635. Absolute calibration of the National Bureau of Standards photoneutron standard: II. Absorption in manganese sulfate. James De Juren and Jack Chin.

RP2636. A new Bunsen-type calorimeter. Ralph S. Jessup.

RP2637. Mass spectra of thermal degradation products of polymers. Paul Bradt and Fred L. Mohler.

RP2638. Heats of combustion of liquid *n*-hexadecane, 1-hexadecene, *n*-decylbenzene, *n*-decylcyclohexane, *n*-decylcyclopentane, and the variation of heat of combustion with chain length. Frances Maron Fraser and Edward J. Prosen.

RP2639. Computation of atomic energy levels: Spectrum of singly-ionized tantalum. R. E. Trees, W. F. Cahill, and P. Rabinowitz.

RP2640. Reflection and transmission of gamma radiation by barriers: Monte Carlo calculation by a collision-density method. Martin J. Berger.

Applied Mathematics Series

AM845. Table of hyperbolic sines and cosines. 55 cents.

AM846. Table of the descending exponential. 50 cents.

Circulars

C539. Standard X-ray diffraction powder patterns. Howard E. Swanson, Nancy T. Gilfrich, and George M. Ugrinic. 45 cents.

C553. The ISCC–NBS method of designating colors and a dictionary of color names. Kenneth L. Kelly and Deane B. Judd. $2.00.

Handbooks

H60. X-ray protection. 20 cents.

H61. Regulation of radiation exposure by legislative means. 25 cents.

Publications in Other Journals

The development of some infrared transmitting glasses. G. W. Cleek and E. H. Hamilton. Proc. Conference on Infrared Optical Materials, Filters and Films, held at the Engr. Research and Development Laboratories, Fort Belvoir, Va. (Feb. 1955).

Manganese thermal neutron activation cross section. J. De Juren and J. Chin. Phys. Rev. (57 E. 55th St., New York 22, N. Y.) **99**, No. 1, 191 (July 1955).

The spectral radiant energy from the sun through varying degrees of smog at Los Angeles. Ralph Stair. Proc. Third National Air Pollution Symposium (612 S. Flower St., Suite 332, Los Angeles 14, Calif.) 48 (April 1955).

Instrumentation research at the National Bureau of Standards. William A. Wildhack. Ann. N. Y. Acad. Sci. (2 E. 63d St., New York 21, N. Y.) **63**, 309 (April 1955).

Generation of Coulomb wave functions by means of recurrence relations. Irene A. Stegun and Milton Abramowitz. Phys. Rev. (57 E. 55th St., New York 22, N. Y.) **98**, No. 6, 1851 (June 1955).

Stress-strain relationships in yarns subjected to rapid impact loading. Part II. Breaking velocities, strain energies, and theory neglecting wave propagation. Frank L. McCrackin, Herbert F. Schiefer, Jack C. Smith, and Walter K. Stone. Textile Research J. (10 E. 40th St., New York 16, N. Y.) **25**, No. 6, 529 (June 1955).

Publications for which a price is indicated are available only from the Superintendent of Documents, U. S. Government Printing Office, Washington 25, D. C. (foreign postage, one-third additional). Reprints from outside journals are not available from the National Bureau of Standards but can often be obtained from the publishers.

UNITED STATES
GOVERNMENT PRINTING OFFICE
DIVISION OF PUBLIC DOCUMENTS
WASHINGTON 25, D. C.

OFFICIAL BUSINESS

PENALTY FOR PRIVATE USE TO AVOID PAYMENT OF POSTAGE, $300

Journal of Research of the National Bureau of Standards Vol. 56, No. 2 February 1

Contents

		Page
Residual entropy of linear polymers. H. N. V. Temperley.	RP2648	55
Molecular weights of thermally degraded polymethyl methacrylate. Victor E. Hart.	RP2649	67
Thermal expansion of binary alkaline-earth borate glasses. Herman F. Shermer.	RP2650	73
Dielectric relaxation for a three-dimensional rotator in a crystalline field: theory for a general six-site model. Benjamin M. Axilrod.	RP2651	81
A matrix with real characteristic roots. Karl Goldberg.	RP2652	87
Reflection and transmission of gamma radiation by barriers: semi-analytic Monte Carlo calculation. Martin J. Berger and John Doggett.	RP2653	89
An examination of the helium vapor-pressure scale of temperature using a magnetic thermometer. E. Ambler and R. P. Hudson.	RP2654	99
Calculation of thermodynamic functions for polyatomic molecules. Harold W. Woolley.	RP2655	105

Single copies of the above Research Papers are not available for sale, but the Superintendent of Documents, U. S. Government Printing Office, Washington 25, D. C., will reprint 100 or more copies, and request for the purchase price should be mailed promptly to that Office.

[A list of recent NBS publications is given on page 3 of the cover.]

For sale by the Superintendent of Documents, U. S. Government Printing Office, Washington 25, D. C. Price 60¢ (single co
Subscription price: $6 a year; $1.25 additional for foreign mailing. Single copies vary in price.

UNITED STATES GOVERNMENT PRINTING OFFICE, WASHINGTON : 1956